

Finite-temperature many-body perturbation theory for electrons: Algebraic recursive definitions, second-quantized derivation, linked-diagram theorem, general-order algorithms, grand canonical and canonical ensembles

So Hirata^{1, a)}

Department of Chemistry, University of Illinois at Urbana-Champaign, Urbana, Illinois 61801, United States

(Dated: 11 August 2021)

A comprehensive and detailed account is presented for the finite-temperature many-body perturbation theory for electrons that expands in power series all thermodynamic functions on an equal footing. Algebraic recursions in the style of the Rayleigh–Schrödinger perturbation theory are derived for the grand potential, chemical potential, internal energy, and entropy in the grand canonical ensemble and for the Helmholtz energy, internal energy, and entropy in the canonical ensemble, leading to their sum-over-states analytical formulas at any arbitrary order. For the grand canonical ensemble, these sum-over-states formulas are systematically transformed to sum-over-orbitals reduced analytical formulas by the quantum-field-theoretical techniques of normal-ordered second quantization and Feynman diagrams extended to finite temperature. It is found that the perturbation corrections to energies entering the recursions have to be treated as a nondiagonal matrix, whose off-diagonal elements are generally nonzero within a subspace spanned by degenerate Slater determinants. They give rise to a unique set of linked diagrams—renormalization diagrams—whose resolvent lines are displaced upwards, which are distinct from the well-known anomalous diagrams of which one or more resolvent lines are erased. A linked-diagram theorem is introduced that proves the size-consistency of the finite-temperature many-body perturbation theory at any order. General-order algorithms implementing the recursions establish the convergence of the perturbation series towards the finite-temperature full-configuration-interaction limit unless the series diverges. Normal-ordered Hamiltonian at finite temperature sheds light on the relationship between the finite-temperature Hartree–Fock and first-order many-body perturbation theories.

I. INTRODUCTION

Strong electron correlation^{1–13} is said to occur in systems with many low-lying excited states, rendering their ground states quasidegenerate. Not only are they difficult to characterize theoretically and therefore a worthy computational challenge,^{14,15} but they are also technologically important, serving as a basis of useful materials whose structures and properties can change dramatically upon external stimuli. Electronic excitations, phase transitions, and crossovers underlying these large, abrupt changes may also occur thermally, giving rise to such fascinating phenomena as Mott transitions,^{16,17} Peierls distortion,^{18–20} and high- T_c superconductivity.^{16,17,20–23}

It can be imagined that in such systems, thermally averaged properties are more accurately computable than are the zero-temperature properties of a minimum-energy state, whose mean-field wave function tends to be unstable.^{24–27} It may even be argued that a finite-temperature treatment is more realistic and meaningful for systems whose very attractiveness derives from its large response to perturbations including temperature variations. For these and other reasons, there has been a surge of interest in finite-temperature electron-correlation theories recently.^{28–41}

Despite being a cornerstone of finite-temperature electron-correlation theories,^{42–45} many-body perturbation theory (MBPT) in the grand canonical ensemble^{46–52} has not been

fully developed, having gaps in its details: The grand potentials and chemical potentials are treated differently⁵³ with no analytical formulas available for the lowest-order corrections to the chemical potential, internal energy, or entropy for a long time.^{54,55} The time-dependent, diagrammatic formulation exploiting the isomorphism of the Schrödinger and Bloch equations is elegant at the outset,^{46–52} but it becomes quickly inscrutable with the exhaustiveness of diagram enumeration being uncertain. Convergence of the finite-temperature MBPT to the well-established zero-temperature MBPT has been suspect,^{48,49,56} compelling Kohn and Luttinger⁴⁸ to conclude at one point that the theory “is in general not correct.”⁴⁸ Convergence towards the exact, i.e., full-configuration-interaction (FCI) limit at finite temperature⁵⁷ is also unverifiable either numerically or analytically because of the lack of a Rayleigh–Schrödinger-type recursion. The relationship between the widely used finite-temperature Hartree–Fock (HF) theory⁵⁸ and finite-temperature MBPT is tenuous, and the physical meaning⁵⁹ of their orbital energies and thus (quasiparticle) energy bands is still unknown.⁶⁰

We recently introduced^{54,55} a new finite-temperature MBPT in the grand canonical ensemble, which expands in power series the grand potential, chemical potential, internal energy, and entropy on an equal footing. We obtained sum-over-states and sum-over-orbitals analytical formulas for the first- and second-order perturbation corrections to these thermodynamic functions in a transparent algebraic derivation involving only the combinatorial identities and the energy sum rules of the Hirschfelder–Certain degenerate perturbation theory (HCPT).⁶¹ Sum-over-states formulas in the canonical ensemble were also reported up to the third order.⁶² These for-

^{a)}Email: sohirata@illinois.edu

mulas were verified by the exact numerical agreement with the benchmark data computed as the λ -derivatives of the finite-temperature FCI (Ref. 57) (where λ is the dimensionless perturbation strength). Using these analytical formulas, we elucidated⁵⁶ the root cause of the nonconvergence at the correct zero-temperature limit,⁴⁸ which has to do with the non-analytic nature of the Boltzmann factor and thus plagues most any finite-temperature MBPT.

This article is a comprehensive account of this new finite-temperature MBPT that expands all thermodynamic functions in uniform perturbation series. We introduce algebraic recursions in the style of the Rayleigh–Schrödinger perturbation theory,⁶³ generating sum-over-states analytical formulas at any arbitrary order for both grand canonical and canonical ensembles. They are implemented into general-order algorithms that compute the perturbation corrections at any arbitrary order, demonstrating their convergence towards the exact (i.e., finite-temperature FCI) limits.⁵⁷ For the grand canonical ensemble, we introduce systematic methods of converting them into sum-over-orbitals reduced analytical formulas, which will be useful for actual condensed-matter applications. One of the conversion methods is the normal-ordered second quantization,^{28,42} which is fully developed in this study, and the other is the Feynman diagrams,^{44,47,50,51} the rules of which are stipulated not just for the grand potential, but also for the chemical potential and entropy. The second-quantization rules shed light on the relationship between the finite-temperature HF and first-order MBPT.

To derive the correct reduced analytical formulas, it has been found that the perturbation energies entering the recursions have to be treated as a nondiagonal matrix (not as scalars). Off-diagonal elements of this matrix, which are in general nonzero within a subspace spanned by degenerate Slater determinants, are shown to give rise to the renormalization terms⁶³ of the Rayleigh–Schrödinger perturbation equations that are not necessarily unlinked. They are responsible for a unique set of linked diagrams whose resolvent lines (i.e., factors of the energy denominators) are shifted, but not erased (the existence of ‘anomalous’ diagrams^{48,52} with one or more resolvent lines erased is well known). Since such ‘renormalization’ diagrams originate from the degenerate perturbation theory and occur for the first time at the third order, it is unclear whether the time-dependent, diagrammatic derivation^{46–51} or density-matrix formulation⁵² correctly take them into account.

We furthermore prove the linked-diagram theorem of the finite-temperature MBPT, which asserts that all thermodynamic functions in the grand canonical ensemble are diagrammatically linked and therefore size-consistent (size-extensive)⁶⁴ at any perturbation order. The proof is based on the zero-temperature linked-diagram theorem^{65–70} (see also Refs. 59, 63, and 71) and the systematic cancellation of unlinked anomalous diagrams. Finally, we document the numerical results of the perturbation corrections to the thermodynamic functions in both ensembles in a wide range of temperatures.

II. ALGEBRAIC RECURSIVE DEFINITIONS

In this section are presented the Rayleigh–Schrödinger-like algebraic recursion relationships of the sum-over-states analytical formulas for the perturbation corrections to all thermodynamic functions for electrons in the grand canonical ensemble. Those for the canonical ensemble are readily inferred from these by restricting the summations to \bar{N} -electron states and setting all chemical potentials to zero. They are relegated to Appendix A. The sum-over-states analytical formulas have limited practical utility except to produce benchmark data. They nevertheless serve as a mathematical basis of second-quantized and diagrammatic derivations of reduced (sum-over-orbitals) analytical formulas expressed in terms of molecular integrals, which are the foci of Secs. III and IV. They also lead to the linked-diagram theorem proven in Sec. V. Translational, rotational, and vibrational degrees of freedom are suppressed.

A. Grand canonical ensemble

The grand partition function for electrons is given by⁵⁷

$$\Xi = \sum_I e^{-\beta E_I + \beta \mu N_I}, \quad (1)$$

where I runs over all states, E_I is the exact (FCI) energy of the I th state, N_I is the number of electrons of the same state, and $\beta = (k_B T)^{-1}$ (k_B is the Boltzmann constant and T is the temperature). The exact chemical potential, μ , is the one that keeps the average number of electrons at \bar{N} , the value ensuring the electroneutrality of the system. It is the root of the following equation:

$$\bar{N} = \frac{1}{\beta} \frac{\partial}{\partial \mu} \ln \Xi. \quad (2)$$

The exact thermodynamic functions such as grand potential (Ω), internal energy (U), and entropy (S) are derived from Ξ .

$$\Omega = -\frac{1}{\beta} \ln \Xi, \quad (3)$$

$$U = -\frac{\partial}{\partial \beta} \ln \Xi + \mu \bar{N}, \quad (4)$$

$$S = k_B \beta^2 \frac{\partial \Omega}{\partial \beta}. \quad (5)$$

They bear the following well-known relationship:

$$\Omega = U - \mu \bar{N} - TS. \quad (6)$$

B. Recursion for $\Omega^{(n)}$

The n th-order perturbation correction to any thermodynamic function X ($X = \Xi, \mu, \Omega, U, \text{ or } S$) is given by^{53,59}

$$X^{(n)} = \frac{1}{n!} \left. \frac{\partial^n X(\lambda)}{\partial \lambda^n} \right|_{\lambda=0}, \quad (7)$$

where $X(\lambda)$ is defined exactly by the finite-temperature FCI (Ref. 57) with a perturbation-scaled Hamiltonian, $\hat{H} = \hat{H}_0 + \lambda\hat{V}$, with λ being the dimensionless perturbation strength.

Using the Taylor expansions of exponential and logarithm,

$$e^{a+b} = e^a + be^a + \frac{b^2}{2!}e^a + \frac{b^3}{3!}e^a + \dots, \quad (8)$$

$$\ln(a+b) = \ln a + \frac{b}{a} - \frac{b^2}{2a^2} + \frac{b^3}{3a^3} - \dots, \quad (9)$$

which are rapidly convergent when $a \gg b$, and defining

$$D_I^{(n)} = E_I^{(n)} - \mu^{(n)}N_I \quad (10)$$

to minimize clutter, we obtain the recursion for $\Xi^{(n)}$ ($n \geq 1$) as

$$\begin{aligned} \frac{\Xi^{(n)}}{\Xi^{(0)}} &= (-\beta)\langle D_I^{(n)} \rangle + \frac{(-\beta)^2}{2!} \sum_{i=1}^{n-1} \langle D_I^{(i)} D_I^{(n-i)} \rangle \\ &+ \frac{(-\beta)^3}{3!} \sum_{i=1}^{n-2} \sum_{j=1}^{n-i-1} \langle D_I^{(i)} D_I^{(j)} D_I^{(n-i-j)} \rangle \\ &+ \dots + \frac{(-\beta)^n}{n!} \langle (D_I^{(1)})^n \rangle, \end{aligned} \quad (11)$$

where the bracket denotes a zeroth-order thermal average:

$$\langle X_I \rangle \equiv \frac{\sum_I X_I e^{-\beta E_I^{(0)} + \beta \mu^{(0)} N_I}}{\sum_I e^{-\beta E_I^{(0)} + \beta \mu^{(0)} N_I}} = \frac{\sum_I X_I e^{-\beta D_I^{(0)}}}{\sum_I e^{-\beta D_I^{(0)}}}. \quad (12)$$

State index I is shown explicitly in the bracket to distinguish it from other state indexes that can coappear in the summand, as in Eq. (28). A double bracket denotes a thermal average of a Dirac bracket; see, e.g., Eq. (46). In Eq. (119), a Brueckner bracket is represented by the same symbol, but this is appropriate since it too stands for a thermal average.

Postponing until Sec. II C the important discussion of $E_I^{(n)}$, we can use Eq. (9) to arrive at the following recursion for $\Omega^{(n)}$, which in turn depends on the above recursion for $\Xi^{(n)}$:

$$\begin{aligned} -\beta\Omega^{(n)} &= \frac{\Xi^{(n)}}{\Xi^{(0)}} - \frac{1}{2} \sum_{i=1}^{n-1} \frac{\Xi^{(i)}}{\Xi^{(0)}} \frac{\Xi^{(n-i)}}{\Xi^{(0)}} \\ &+ \frac{1}{3} \sum_{i=1}^{n-2} \sum_{j=1}^{n-i-1} \frac{\Xi^{(i)}}{\Xi^{(0)}} \frac{\Xi^{(j)}}{\Xi^{(0)}} \frac{\Xi^{(n-i-j)}}{\Xi^{(0)}} \\ &- \dots - \frac{(-1)^n}{n} \left(\frac{\Xi^{(1)}}{\Xi^{(0)}} \right)^n \end{aligned} \quad (13)$$

for $n \geq 1$. Although nontrivial, we can rewrite the above as

$$\begin{aligned} -\beta\Omega^{(n)} &= \frac{\Xi^{(n)}}{\Xi^{(0)}} - \frac{(-\beta)^2}{2!} \sum_{i=1}^{n-1} \Omega^{(i)} \Omega^{(n-i)} \\ &- \frac{(-\beta)^3}{3!} \sum_{i=1}^{n-2} \sum_{j=1}^{n-i-1} \Omega^{(i)} \Omega^{(j)} \Omega^{(n-i-j)} \\ &- \dots - \frac{(-\beta)^n}{n!} (\Omega^{(1)})^n. \end{aligned} \quad (14)$$

A proof of the equivalence of Eqs. (13) and (14) is given in Appendix B. This is further simplified to a form that does not depend on $\Xi^{(n)}$:

$$\begin{aligned} \Omega^{(n)} &= \langle D_I^{(n)} \rangle + \frac{(-\beta)}{2!} \sum_{i=1}^{n-1} (\langle D_I^{(i)} D_I^{(n-i)} \rangle - \Omega^{(i)} \Omega^{(n-i)}) \\ &+ \frac{(-\beta)^2}{3!} \sum_{i=1}^{n-2} \sum_{j=1}^{n-i-1} (\langle D_I^{(i)} D_I^{(j)} D_I^{(n-i-j)} \rangle - \Omega^{(i)} \Omega^{(j)} \Omega^{(n-i-j)}) \\ &+ \dots + \frac{(-\beta)^{n-1}}{n!} \{ \langle (D_I^{(1)})^n \rangle - (\Omega^{(1)})^n \} \end{aligned} \quad (15)$$

for $n \geq 1$.

Next, we describe how $\langle E_I^{(n)} \rangle$, $\langle E_I^{(i)} E_I^{(n-i)} \rangle$, etc., can be evaluated so that the above recursion for $\Omega^{(n)}$ can be executed. See Sec. II D for the recursion for $\mu^{(n)}$, which is also needed. The above recursion is tantalizing with the linked-diagram theorem of $\Omega^{(n)}$, which will be discussed in Sec. V.

C. Recursion for $\langle E_I^{(n)} \rangle$

The perturbation corrections to energy, $E_I^{(i)}$ ($1 \leq i \leq n$), and their thermal averages, $\langle E_I^{(i)} \rangle$, are crucial quantities entering the recursion for $\Omega^{(n)}$. They are identified as those defined by the Hirschfelder–Certain degenerate perturbation theory (HCPT).⁶¹ The more familiar Møller–Plesset perturbation theory (MPPT)⁷² will not suffice here because a finite-temperature MBPT accesses all states, many of whose zeroth-order energies are exactly degenerate. Other degenerate or quasidegenerate perturbation theories may also fall short because HCPT is the proper Rayleigh–Schrödinger perturbation theory for degenerate and nondegenerate reference states, complying with the canonical definition of perturbation theory, i.e., Eq. (7), although there are equivalent degenerate perturbation theories under different names.⁷³

For a nondegenerate reference state,⁶³ HCPT reduces to MPPT. The Schrödinger equation may be written with perturbatively expanded energy and wave function as

$$\begin{aligned} (\hat{H}_0 + \lambda\hat{V})(\Phi_I^{(0)} + \lambda\Phi_I^{(1)} + \lambda^2\Phi_I^{(2)} + \dots) \\ = (E_I^{(0)} + \lambda E_I^{(1)} + \lambda^2 E_I^{(2)} + \dots)(\Phi_I^{(0)} + \lambda\Phi_I^{(1)} + \lambda^2\Phi_I^{(2)} + \dots) \end{aligned} \quad (16)$$

with intermediate normalization $\langle \Phi_I^{(0)} | \Phi_I^{(n)} \rangle = \delta_{n0}$, where $\Phi_I^{(0)}$ is the nondegenerate reference (zeroth-order) wave function of the I th state, which is a single Slater determinant. Expanding and equating terms carrying the n th power of λ , we obtain the recursion for the n th-order correction to the wave function, $\Phi_I^{(n)}$, as

$$(E_I^{(0)} - \hat{H}_0)\Phi_I^{(n)} = \hat{V}\Phi_I^{(n-1)} - \sum_{i=1}^n E_I^{(i)}\Phi_I^{(n-i)} \quad (17)$$

or

$$\Phi_I^{(n)} = \hat{R}_I \left(\hat{V}\Phi_I^{(n-1)} - \sum_{i=1}^{n-1} E_I^{(i)}\Phi_I^{(n-i)} \right), \quad (18)$$

where \hat{R}_I is the resolvent operator:

$$\hat{R}_I = \sum_A^{\text{denom.} \neq 0} \frac{|\Phi_A^{(0)}\rangle\langle\Phi_A^{(0)}|}{E_I^{(0)} - E_A^{(0)}}. \quad (19)$$

Here, “denom. $\neq 0$ ” limits the summation to just over the states $\Phi_A^{(0)}$ that are not degenerate with the I th state, and therefore to the cases where $E_I^{(0)} - E_A^{(0)} \neq 0$. The second term in the right-hand side of Eq. (17) is known as the renormalization term,⁶³ which is entirely diagrammatically unlinked (non-size-consistent) in MPPT. It vanishes exactly by cancelling out

the unlinked contribution of the same magnitude in the first term, leaving only the linked (size-consistent) contribution as the perturbation correction to the wave function. Multiplying Eq. (17) by $\Phi_I^{(0)*}$ from left and integrating, we have

$$E_I^{(n)} = \langle\Phi_I^{(0)}|\hat{V}|\Phi_I^{(n-1)}\rangle, \quad (20)$$

defining the n th-order energy correction according to MPPT.

For M -tuply degenerate reference states ($M \geq 2$),⁶¹ HCPT and MPPT differ from each other materially. The perturbation expansion of the Schrödinger equation now becomes a M -by- M matrix equation of the form,

$$\begin{aligned} & (\hat{H}_0 + \lambda\hat{V}) \left\{ \begin{pmatrix} \Phi_1^{(0)} \\ \vdots \\ \Phi_M^{(0)} \end{pmatrix} + \lambda \begin{pmatrix} \Phi_1^{(1)} \\ \vdots \\ \Phi_M^{(1)} \end{pmatrix} + \lambda^2 \begin{pmatrix} \Phi_1^{(2)} \\ \vdots \\ \Phi_M^{(2)} \end{pmatrix} + \dots \right\} \\ & = \left\{ \begin{pmatrix} E_{11}^{(0)} & \dots & E_{M1}^{(0)} \\ \vdots & & \vdots \\ E_{1M}^{(0)} & \dots & E_{MM}^{(0)} \end{pmatrix} + \lambda \begin{pmatrix} E_{11}^{(1)} & \dots & E_{M1}^{(1)} \\ \vdots & & \vdots \\ E_{1M}^{(1)} & \dots & E_{MM}^{(1)} \end{pmatrix} + \lambda^2 \begin{pmatrix} E_{11}^{(2)} & \dots & E_{M1}^{(2)} \\ \vdots & & \vdots \\ E_{1M}^{(2)} & \dots & E_{MM}^{(2)} \end{pmatrix} + \dots \right\} \left\{ \begin{pmatrix} \Phi_1^{(0)} \\ \vdots \\ \Phi_M^{(0)} \end{pmatrix} + \lambda \begin{pmatrix} \Phi_1^{(1)} \\ \vdots \\ \Phi_M^{(1)} \end{pmatrix} + \lambda^2 \begin{pmatrix} \Phi_1^{(2)} \\ \vdots \\ \Phi_M^{(2)} \end{pmatrix} + \dots \right\}, \end{aligned} \quad (21)$$

where all M zeroth-order states, $\{\Phi_I^{(0)}\}$ ($1 \leq I \leq M$), are degenerate, and therefore $E_{IJ}^{(0)} = E_I^{(0)}\delta_{IJ}$. Collecting terms that are proportional to λ^n , we obtain

$$\begin{pmatrix} (E_I^{(0)} - \hat{H}_0)\Phi_1^{(n)} \\ \vdots \\ (E_I^{(0)} - \hat{H}_0)\Phi_M^{(n)} \end{pmatrix} = \begin{pmatrix} \hat{V}\Phi_1^{(n-1)} \\ \vdots \\ \hat{V}\Phi_M^{(n-1)} \end{pmatrix} - \sum_{i=1}^n \begin{pmatrix} E_{11}^{(i)} & \dots & E_{M1}^{(i)} \\ \vdots & & \vdots \\ E_{1M}^{(i)} & \dots & E_{MM}^{(i)} \end{pmatrix} \begin{pmatrix} \Phi_1^{(n-i)} \\ \vdots \\ \Phi_M^{(n-i)} \end{pmatrix} \quad (22)$$

or

$$\begin{pmatrix} \Phi_1^{(n)} \\ \vdots \\ \Phi_M^{(n)} \end{pmatrix} = \hat{R}_I \left\{ \begin{pmatrix} \hat{V}\Phi_1^{(n-1)} \\ \vdots \\ \hat{V}\Phi_M^{(n-1)} \end{pmatrix} - \sum_{i=1}^{n-1} \begin{pmatrix} E_{11}^{(i)} & \dots & E_{M1}^{(i)} \\ \vdots & & \vdots \\ E_{1M}^{(i)} & \dots & E_{MM}^{(i)} \end{pmatrix} \begin{pmatrix} \Phi_1^{(n-i)} \\ \vdots \\ \Phi_M^{(n-i)} \end{pmatrix} \right\}, \quad (23)$$

where the definition of \hat{R}_I remains unchanged [Eq. (19)]. Multiplying the J th row of Eq. (22) by $\Phi_I^{(0)*}$ from the left and integrating for all I and J ($1 \leq I, J \leq M$), we have for $n \geq 1$,

$$\mathbf{E}^{(n)} \equiv \begin{pmatrix} E_{11}^{(n)} & \dots & E_{1M}^{(n)} \\ \vdots & & \vdots \\ E_{M1}^{(n)} & \dots & E_{MM}^{(n)} \end{pmatrix} = \begin{pmatrix} \langle\Phi_1^{(0)}|\hat{V}|\Phi_1^{(n-1)}\rangle & \dots & \langle\Phi_1^{(0)}|\hat{V}|\Phi_M^{(n-1)}\rangle \\ \vdots & & \vdots \\ \langle\Phi_M^{(0)}|\hat{V}|\Phi_1^{(n-1)}\rangle & \dots & \langle\Phi_M^{(0)}|\hat{V}|\Phi_M^{(n-1)}\rangle \end{pmatrix}, \quad (24)$$

which is Hermitian.⁶¹ Owing to the degeneracy, $\Phi_1^{(0)}$ through $\Phi_M^{(0)}$ can mix with one another and remain as valid zeroth-order references insofar as they are orthonormal. We seek a unique (up to a phase) set of the zeroth-order wave functions that brings $\mathbf{E}^{(1)}$ through $\mathbf{E}^{(n)}$ into a diagonal form, so that the above M -fold coupled Schrödinger equation [Eq. (21)] is separated into M independent Schrödinger equations of the form of Eq. (16). The eigenvalues of $\mathbf{E}^{(n)}$ are then identified as the n th-order HCPT energy corrections,⁶¹ although the foregoing formulation is considerably simpler than that of Ref. 61. Given above is an abridged version that has just enough

details to make the recursion for $\Omega^{(n)}$ self-contained.

At this point, it may appear hopeless to try to derive compact analytical formulas of $\langle E_I^{(n)} \rangle$ written in terms of molecular integrals because eigenvalues are only procedurally defined and cannot be written in a closed form (for $M \geq 5$ according to the Abel–Ruffini theorem). Fortunately, however, we can still derive analytical formulas without knowing the eigenvalues.^{54,55} Since these energy corrections are thermally averaged [Eq. (12)] with the same Boltzmann weight within each degenerate subspace, we only need the sum of the eigenvalues (not the individual eigenvalues) in order to calculate

the thermal average correctly. This sum is equal to the sum of diagonal elements owing to the trace invariance for a cyclic permutation of a matrix product,

$$\text{Tr } U^{-1} \mathbf{E}^{(i)} U = \text{Tr } \mathbf{E}^{(i)}, \quad (25)$$

$$\text{Tr } U^{-1} \mathbf{E}^{(i)} U U^{-1} \mathbf{E}^{(j)} U = \text{Tr } \mathbf{E}^{(i)} \mathbf{E}^{(j)}, \quad (26)$$

etc., where U is the unitary matrix that brings all of $\mathbf{E}^{(i)}$ ($1 \leq i \leq n$) into a diagonal form. Each matrix element (before diagonalization) can be written in a closed form, lending the trace and thus thermal average to analytical expressions.

In our previous studies,^{54,55} we used the Slater–Condon rules⁷⁴ to evaluate these matrix elements and derived compact analytical formulas for the thermal averages with custom-made combinatorial identities. Such an order-by-order approach reaches an impasse at higher orders, and hence, in this study, we switch to second-quantized and diagrammatic formulations expounded on in the subsequent sections. For the sum-over-states recursion and general-order algorithm based on it, we can still diagonalize $\mathbf{E}^{(i)}$ and use its eigenvalues in principle, but we elect to leave $\mathbf{E}^{(i)}$ undiagonalized because the diagonalization step is simply superfluous.

The foregoing argument must not be misconstrued to mean that only diagonal elements of $\mathbf{E}^{(i)}$ matter. As we demonstrate in Sec. III, off-diagonal elements of $\mathbf{E}^{(i)}$ enter thermal averages via the renormalization term [the second term of Eq. (22) or (23)], giving rise to unique diagrams—the renormalization diagrams with displaced resolvent lines (distinguished from the anomalous diagrams with missing resolvents) appearing for the first time at the third order.

To summarize, $\langle E^{(n)} \rangle$, $\langle E^{(i)} E^{(n-i)} \rangle$, etc. are evaluated by thermally averaging the traces of $\mathbf{E}^{(i)}$, $\mathbf{E}^{(i)} \mathbf{E}^{(n-i)}$, etc. using the energy recursion [Eq. (24)], which in turn depends on the recursion for wave functions [Eq. (23)]. In other words, for the purpose of executing the recursions, we may use the following substitutions, where $E_I^{(i)}$ is the I th eigenvalue, whereas $E_{IJ}^{(i)}$ is the IJ th element of the matrix $\mathbf{E}^{(i)}$:

$$\langle E_I^{(i)} \rangle = \langle E_{II}^{(i)} \rangle, \quad (27)$$

$$\langle E_I^{(i)} E_I^{(j)} \rangle = \langle E_{IJ}^{(i)} \hat{P}_I E_{JI}^{(j)} \rangle, \quad (28)$$

etc., where the inner projector, \hat{P}_I , restricts the summation over J (whose summation symbol is suppressed according to Einstein's convention) to determinants within the degenerate subspace of I . It is not only advantageous, but also necessary to treat the energy corrections that enter the recursions as a nondiagonal matrix rather than scalars.

D. Recursion for $\mu^{(n)}$

The recursion for $\mu^{(n)}$ comes from⁵⁵

$$\left(\frac{\partial \Omega^{(n)}}{\partial \mu^{(0)}} \right)_{\mu^{(1)}, \dots, \mu^{(n)}} = 0. \quad (29)$$

Substituting this to Eq. (14), we have

$$\frac{\partial}{\partial \mu^{(0)}} \frac{\Xi^{(n)}}{\Xi^{(0)}} = 0. \quad (30)$$

Using the recursion for $\Xi^{(n)}/\Xi^{(0)}$ [Eq. (11)] in the above, we arrive at the following recursion for $\mu^{(n)}$ ($n \geq 1$):

$$\begin{aligned} \mu^{(n)} \langle N_I^2 - \bar{N}^2 \rangle &= \langle E_I^{(n)} (N_I - \bar{N}) \rangle \\ &+ \frac{(-\beta)}{2!} \sum_{i=1}^{n-1} \langle D_I^{(i)} D_I^{(n-i)} (N_I - \bar{N}) \rangle \\ &+ \frac{(-\beta)^2}{3!} \sum_{i=1}^{n-2} \sum_{j=1}^{n-i-1} \langle D_I^{(i)} D_I^{(j)} D_I^{(n-i-j)} (N_I - \bar{N}) \rangle \\ &+ \dots + \frac{(-\beta)^{n-1}}{n!} \langle (D_I^{(1)})^n (N_I - \bar{N}) \rangle, \end{aligned} \quad (31)$$

where we used the identity,

$$\frac{\partial}{\partial \mu^{(0)}} \langle X_I \rangle = \langle X_I N_I \rangle - \langle X_I \rangle \langle N_I \rangle. \quad (32)$$

Its application to the first term of Eq. (11) leads to

$$\frac{\partial}{\partial \mu^{(0)}} \langle D_I^{(n)} \rangle = \langle E_I^{(n)} (N_I - \bar{N}) \rangle - \mu^{(n)} \langle N_I^2 - \bar{N}^2 \rangle, \quad (33)$$

which was also used in Eq. (31).

E. Recursion for $U^{(n)}$

Differentiating Eq. (4) n times with λ , we obtain

$$U^{(n)} - \mu^{(n)} \bar{N} = \left(\frac{\partial(-\beta \Omega^{(n)})}{\partial(-\beta)} \right)_{\mu^{(0)}, \dots, \mu^{(n)}}. \quad (34)$$

Substituting Eq. (14) into this, we arrive at

$$\begin{aligned} U^{(n)} - \mu^{(n)} \bar{N} &= \frac{\partial}{\partial(-\beta)} \frac{\Xi^{(n)}}{\Xi^{(0)}} - (-\beta) \sum_{i=1}^{n-1} (U^{(i)} - \mu^{(i)} \bar{N}) \Omega^{(n-i)} \\ &- \frac{(-\beta)^2}{2!} \sum_{i=1}^{n-2} \sum_{j=1}^{n-i-1} (U^{(i)} - \mu^{(i)} \bar{N}) \Omega^{(j)} \Omega^{(n-i-j)} \\ &- \dots - \frac{(-\beta)^{n-1}}{(n-1)!} (U^{(1)} - \mu^{(1)} \bar{N}) (\Omega^{(1)})^{n-1}. \end{aligned} \quad (35)$$

The first term can be expanded as

$$\begin{aligned} \frac{\partial}{\partial(-\beta)} \frac{\Xi^{(n)}}{\Xi^{(0)}} &= \langle D_I^{(n)} \rangle - (-\beta) \langle D_I^{(n)} \rangle \langle D_I^{(0)} \rangle + (-\beta) \sum_{i=1}^n \langle D_I^{(i)} D_I^{(n-i)} \rangle \\ &\quad - \frac{(-\beta)^2}{2!} \sum_{i=1}^{n-1} \langle D_I^{(i)} D_I^{(n-i)} \rangle \langle D_I^{(0)} \rangle \\ &\quad + \frac{(-\beta)^2}{2!} \sum_{i=1}^{n-1} \sum_{j=1}^{n-i} \langle D_I^{(i)} D_I^{(j)} D_I^{(n-i-j)} \rangle \\ &\quad - \frac{(-\beta)^3}{3!} \sum_{i=1}^{n-2} \sum_{j=1}^{n-i-1} \langle D_I^{(i)} D_I^{(j)} D_I^{(n-i-j)} \rangle \langle D_I^{(0)} \rangle \\ &\quad + \frac{(-\beta)^3}{3!} \sum_{i=1}^{n-2} \sum_{j=1}^{n-i-1} \sum_{k=1}^{n-i-j} \langle D_I^{(i)} D_I^{(j)} D_I^{(k)} D_I^{(n-i-j-k)} \rangle \\ &\quad - \dots - \frac{(-\beta)^n}{n!} \langle (D_I^{(1)})^n \rangle \langle D_I^{(0)} \rangle \\ &\quad + \frac{(-\beta)^n}{n!} \langle (D_I^{(1)})^n D_I^{(0)} \rangle, \end{aligned} \quad (36)$$

where we used Eq. (11) and

$$\frac{\partial}{\partial(-\beta)} \langle X_I \rangle = \langle X_I D_I^{(0)} \rangle - \langle X_I \rangle \langle D_I^{(0)} \rangle. \quad (37)$$

Therefore, the recursion for $U^{(n)}$ ($n \geq 1$) is given by

$$\begin{aligned} U^{(n)} &= \langle E_I^{(n)} \rangle + (-\beta) \sum_{i=1}^n \langle D_I^{(i)} D_I^{(n-i)} \rangle \\ &\quad - (-\beta) \sum_{i=1}^n \Omega^{(i)} (U^{(n-i)} - \mu^{(n-i)} \bar{N}) \\ &\quad + \frac{(-\beta)^2}{2!} \sum_{i=1}^{n-1} \sum_{j=1}^{n-i} \langle D_I^{(i)} D_I^{(j)} D_I^{(n-i-j)} \rangle \\ &\quad - \frac{(-\beta)^2}{2!} \sum_{i=1}^{n-1} \sum_{j=1}^{n-i} \Omega^{(i)} \Omega^{(j)} (U^{(n-i-j)} - \mu^{(n-i-j)} \bar{N}) \\ &\quad + \dots + \frac{(-\beta)^n}{n!} \langle (D_I^{(1)})^n D_I^{(0)} \rangle \\ &\quad - \frac{(-\beta)^n}{n!} (\Omega^{(1)})^n (U^{(0)} - \mu^{(0)} \bar{N}), \end{aligned} \quad (38)$$

where we used $\langle D_I^{(0)} \rangle = U^{(0)} - \mu^{(0)} \bar{N}$.

F. Recursion for $S^{(n)}$

The recursion for $S^{(n)}$ is a concatenation of the recursions for $\Omega^{(n)}$, $\mu^{(n)}$, and $U^{(n)}$ given above because

$$S^{(n)} = k_B \beta (U^{(n)} - \mu^{(n)} \bar{N} - \Omega^{(n)}). \quad (39)$$

III. SECOND-QUANTIZED DERIVATION

In this section, we derive the reduced analytical formulas of $\Omega^{(n)}$ and $\mu^{(n)}$ for the few lowest n 's,^{54,55} starting from the sum-over-states analytical formulas obtained from the recursions.

We rely on the rules of normal-ordered second quantization at finite temperature,^{28,42} expounded on in Appendix C. Second-quantized derivations of $U^{(n)}$ and $S^{(n)}$ follow essentially the same procedure and will not be repeated.

A. Zeroth order

The zeroth-order formulas initiate the recursions. They correspond to the Fermi–Dirac theory discussed in many textbooks.^{42–45} We therefore only document the results:^{54,55,57}

$$\Omega^{(0)} = E_{\text{nuc.}} + \frac{1}{\beta} \sum_p \ln f_p^+, \quad (40)$$

$$U^{(0)} = E_{\text{nuc.}} + \sum_p \epsilon_p f_p^-, \quad (41)$$

$$S^{(0)} = -k_B \sum_p (f_p^- \ln f_p^- + f_p^+ \ln f_p^+), \quad (42)$$

where $E_{\text{nuc.}}$ is the nucleus-nucleus repulsion energy, and f_p^- (f_p^+) is the Fermi–Dirac occupancy (vacancy) function for the p th spinorbital given by

$$f_p^- = \frac{1}{1 + e^{\beta(\epsilon_p - \mu^{(0)})}}, \quad (43)$$

$$f_p^+ = \frac{e^{\beta(\epsilon_p - \mu^{(0)})}}{1 + e^{\beta(\epsilon_p - \mu^{(0)})}}. \quad (44)$$

Lastly, $\mu^{(0)}$ is the root of the following equation embodying the zeroth-order electroneutrality condition:

$$\bar{N} = \sum_p f_p^-. \quad (45)$$

B. First order

According to the recursion for $\Omega^{(n)}$ [Eq. (15)], using Einstein's convention inside thermal averages $\langle \dots \rangle$, we can write $\Omega^{(1)}$ as

$$\Omega^{(1)} = \langle D_I^{(1)} \rangle = \langle \langle I | \hat{V} | I \rangle \rangle - \mu^{(1)} \langle \langle I | \hat{N} | I \rangle \rangle, \quad (46)$$

where $\langle \langle I | \hat{V} | I \rangle \rangle$ is the thermal average of $\langle I | \hat{V} | I \rangle$ and I stands for $\Phi_I^{(0)}$. Consulting with Appendix C, we can evaluate this using the normal-ordered second quantization as

$$\begin{aligned} \Omega^{(1)} &= \langle \langle I | \langle E_I^{(1)} \rangle + F_{pq} \{ \hat{p}^\dagger \hat{q} \} + (1/4) \langle pq || rs \rangle \{ \hat{p}^\dagger \hat{q}^\dagger \hat{s} \hat{r} \} | I \rangle \rangle \\ &\quad - \mu^{(1)} \langle \langle I | \bar{N} + \{ \hat{p}^\dagger \hat{p} \} | I \rangle \rangle \end{aligned} \quad (47)$$

$$= \langle E_I^{(1)} \rangle - \mu^{(1)} \bar{N} \quad (48)$$

$$= \sum_p F_{pp} f_p^- - \frac{1}{2} \sum_{p,q} \langle pq || pq \rangle f_p^- f_q^- - \mu^{(1)} \bar{N} \quad (49)$$

$$\equiv \langle D_I^{(1)} \rangle_L. \quad (50)$$

In Eq. (47), we substituted the normal-ordered perturbation operator [Eq. (C41)] and number operator [Eq. (C29)] derived in Appendix C 3. Going from Eq. (47) to (48), we invoked

the rule that the thermal average of a normal-ordered product of operators is always zero, allowing only the constant terms in \hat{V} and \hat{N} to survive. In Eq. (49), $\langle E_I^{(1)} \rangle$ is defined by Eq. (C36) and F_{pq} by Eq. (C37), whereas $\langle pq||rs \rangle$ is an antisymmetrized two-electron integral, and $\mu^{(1)}$ will be considered below. Therefore, as in the zero-temperature normal ordering,⁶³ an effort has been prepaid to derive the analytical formula for $\langle E_I^{(1)} \rangle$ during the derivation of the normal-ordered form of \hat{V} . The end result [Eq. (49)] is recognized as diagrammatically linked and thus size-consistent,^{63,64} and can be symbolically written as Eq. (50) with subscript “L” standing for “linked.” Algebraically, a linked term is the one that is not a simple product of two or more extensive quantities ($\mu^{(n)}$, f_p^\pm , and F_{pq} are intensive, while $\langle E_I^{(n)} \rangle$ and \bar{N} are extensive).

We start with the sum-over-states formula of $\mu^{(1)}$ [Eq. (31)], which reads

$$\mu^{(1)} \langle N_I^2 - \bar{N}^2 \rangle = \langle E_I^{(1)} (N_I - \bar{N}) \rangle. \quad (51)$$

The thermal average in the left-hand side is evaluated as

$$\begin{aligned} \langle N_I^2 - \bar{N}^2 \rangle &= \langle \langle I | \hat{N}^2 - \bar{N}^2 | I \rangle \rangle \\ &= \langle \langle I | (\bar{N} + \{\hat{p}^\dagger \hat{p}\}) (\bar{N} + \{\hat{q}^\dagger \hat{q}\}) | I \rangle \rangle - \bar{N}^2 \\ &= \bar{N}^2 + \langle \langle I | \{\hat{p}^\dagger \hat{p}\} \{\hat{q}^\dagger \hat{q}\} | I \rangle \rangle - \bar{N}^2 \\ &= \sum_p f_p^- f_p^+ \equiv \langle N_I^2 - \bar{N}^2 \rangle_L, \end{aligned} \quad (52)$$

which is linked owing to the cancellation of the unlinked terms, \bar{N}^2 . The right-hand side of Eq. (51) is evaluated as

$$\begin{aligned} &\langle E_I^{(1)} (N_I - \bar{N}) \rangle \\ &= \langle E_{II}^{(1)} (N_I - \bar{N}) \rangle \\ &= \langle \langle I | \hat{V} (\hat{N} - \bar{N}) | I \rangle \rangle \\ &= \langle \langle I | (\langle E_I^{(1)} \rangle + F_{pq} \{\hat{p}^\dagger \hat{q}\} + (1/4) \langle pq||rs \rangle \{\hat{p}^\dagger \hat{q}^\dagger \hat{s} \hat{r}\}) (\{\hat{r}^\dagger \hat{t}\}) | I \rangle \rangle \\ &= \langle \langle I | F_{pq} \{\hat{p}^\dagger \hat{q}\} \{\hat{r}^\dagger \hat{t}\} | I \rangle \rangle \\ &= \sum_p F_{pp} f_p^- f_p^+ \equiv \langle E_I^{(1)} (N_I - \bar{N}) \rangle_L, \end{aligned} \quad (53)$$

which is also linked. Taken together, Eq. (51) can be symbolically rewritten as

$$\mu^{(1)} \langle N_I^2 - \bar{N}^2 \rangle_L = \langle E_I^{(1)} (N_I - \bar{N}) \rangle_L, \quad (54)$$

which reduces to

$$\mu^{(1)} \sum_p f_p^- f_p^+ = \sum_p F_{pp} f_p^- f_p^+. \quad (55)$$

For both $\Omega^{(1)}$ and $\mu^{(1)}$, we recover the reduced analytical formulas reported earlier.^{54,55}

C. Second order

From the $\Omega^{(n)}$ recursion [Eq. (15)], we have

$$\Omega^{(2)} = \langle D_I^{(2)} \rangle + \frac{(-\beta)}{2!} (\langle D_I^{(1)} D_I^{(1)} \rangle - \Omega^{(1)} \Omega^{(1)}), \quad (56)$$

whose components are expanded by using the $\langle E_I^{(n)} \rangle$ recursions [Eqs. (23) and (24)] as

$$\begin{aligned} \langle D_I^{(2)} \rangle &= \langle E_I^{(2)} \rangle - \mu^{(2)} \langle N_I \rangle \\ &= \langle E_{II}^{(2)} \rangle - \mu^{(2)} \langle \langle I | \hat{N} | I \rangle \rangle \\ &= \langle \langle I | \hat{V} \hat{R}_I \hat{V} | I \rangle \rangle - \mu^{(2)} \bar{N} \end{aligned} \quad (57)$$

and

$$\begin{aligned} \langle D_I^{(1)} D_I^{(1)} \rangle &= \langle E_I^{(1)} E_I^{(1)} \rangle - 2\mu^{(1)} \langle E_I^{(1)} N_I \rangle + (\mu^{(1)})^2 \langle N_I^2 \rangle \\ &= \langle E_{II}^{(1)} \hat{P}_I E_{II}^{(1)} \rangle - 2\mu^{(1)} \langle E_I^{(1)} (N_I - \bar{N}) \rangle \\ &\quad - 2\mu^{(1)} \langle E_I^{(1)} \rangle \bar{N} + (\mu^{(1)})^2 \langle N_I^2 - \bar{N}^2 \rangle + (\mu^{(1)})^2 \bar{N}^2 \\ &= \langle \langle I | \hat{V} \hat{P}_I \hat{V} | I \rangle \rangle - 2\mu^{(1)} \sum_p F_{pp} f_p^- f_p^+ \\ &\quad + (\mu^{(1)})^2 \sum_p f_p^- f_p^+ - 2\mu^{(1)} \langle E_I^{(1)} \rangle \bar{N} + (\mu^{(1)})^2 \bar{N}^2, \end{aligned} \quad (58)$$

where Eqs. (52) and (53) were used. The last two terms of Eq. (58) are unlinked, growing quadratically with size, which are, however, easily seen to be cancelled by the corresponding contributions in the $\Omega^{(1)} \Omega^{(1)}$ term of Eq. (56).

Let us evaluate $\langle E_I^{(2)} \rangle$ using the normal-ordered second-quantization rules for resolvent operators described in Appendix C 4. Using Einstein’s convention of implied summations, we write

$$\begin{aligned} \langle E_I^{(2)} \rangle &= \langle \langle I | \hat{V} \hat{R}_I \hat{V} | I \rangle \rangle \\ &= \langle \langle I | F_{pq} \{\hat{p}^\dagger \hat{q}\} \{\hat{a}^\dagger \hat{t}\} | I \rangle (\epsilon_i - \epsilon_a)^{-1} \langle I | \{\hat{t}^\dagger \hat{a}\} \{\hat{r}^\dagger \hat{s}\} F_{rs} | I \rangle \rangle \\ &\quad + \left(\frac{1}{4}\right)^3 \langle \langle I | \langle pq||rs \rangle \{\hat{p}^\dagger \hat{q}^\dagger \hat{s} \hat{r}\} \{\hat{a}^\dagger \hat{b}^\dagger \hat{j} \hat{i}\} | I \rangle (\epsilon_i + \epsilon_j - \epsilon_a - \epsilon_b)^{-1} \langle I | \{\hat{t}^\dagger \hat{j}^\dagger \hat{b}\} \{\hat{r}^\dagger \hat{u}^\dagger \hat{w} \hat{v}\} \langle tu||vw \rangle | I \rangle \rangle \times 16 \\ &= \sum_{p,q}^{\text{denom.} \neq 0} \frac{|F_{pq}|^2 f_p^- f_q^+}{\epsilon_p - \epsilon_q} + \frac{1}{4} \sum_{p,q,r,s}^{\text{denom.} \neq 0} \frac{|\langle pq||rs \rangle|^2 f_p^- f_q^- f_r^+ f_s^+}{\epsilon_p + \epsilon_q - \epsilon_r - \epsilon_s} \equiv \langle E_I^{(2)} \rangle_L, \end{aligned} \quad (59)$$

where i, j, a, b as well as p through w run over all spinor-

bitals and “ $\times 16$ ” means that there are 16 distinct, equal-

valued full contraction patterns. The constant term $\langle E_I^{(1)} \rangle$ in \hat{V} [see Eq. (C41)] does not contribute because the resolvent \hat{R}_I erases all determinants in the degenerate subspace of I (see Appendix C 4). The latter is also responsible for the restriction (“denom. $\neq 0$ ”) of the summations to nonzero denominators.

Although we did not examine the linkedness of the second-order HCPT energy corrections (be they eigenvalues or the trace of $E^{(2)}$), we could nonetheless establish the linkedness of their thermal average, $\langle E_I^{(2)} \rangle$.

Next, we evaluate $\langle E_I^{(1)} E_I^{(1)} \rangle$, recalling the rules for the inner projector \hat{P}_I (see Appendix C 4).

$$\begin{aligned}
 \langle E_I^{(1)} E_I^{(1)} \rangle &= \langle \langle I | \hat{V} \hat{P}_I \hat{V} | I \rangle \rangle \\
 &= \langle E_I^{(1)} \rangle \langle E_I^{(1)} \rangle + \langle \langle I | F_{pq} \{ \hat{p}^\dagger \hat{q} \} \{ \hat{a}^\dagger \hat{i} \} | I \rangle \langle I | \{ \hat{i}^\dagger \hat{a} \} \{ \hat{r}^\dagger \hat{s} \} F_{rs} | I \rangle \rangle \\
 &\quad + \left(\frac{1}{4} \right)^3 \langle \langle I | \langle pq || rs \rangle \{ \hat{p}^\dagger \hat{q}^\dagger \hat{s} \hat{r} \} \{ \hat{a}^\dagger \hat{b}^\dagger \hat{j} \hat{i} \} | I \rangle \langle I | \{ \hat{i}^\dagger \hat{j}^\dagger \hat{b} \hat{a} \} \{ \hat{r}^\dagger \hat{u}^\dagger \hat{w} \hat{v} \} | I \rangle \rangle \times 16 \\
 &= \langle E_I^{(1)} \rangle \langle E_I^{(1)} \rangle + \sum_{p,q}^{\text{denom.}=0} |F_{pq}|^2 f_p^- f_q^+ + \frac{1}{4} \sum_{p,q,r,s}^{\text{denom.}=0} |\langle pq || rs \rangle|^2 f_p^- f_q^- f_r^+ f_s^+ \equiv \langle E_I^{(1)} \rangle_L \langle E_I^{(1)} \rangle_L + \langle E_I^{(1)} E_I^{(1)} \rangle_L. \quad (60)
 \end{aligned}$$

Unlike in $\langle E_I^{(2)} \rangle$, the inner projector \hat{P}_I allows the constant part $\langle E_I^{(1)} \rangle$ of \hat{V} to survive, resulting in the unlinked contribution $\langle E_I^{(1)} \rangle_L \langle E_I^{(1)} \rangle_L$, which is cancelled by the corresponding contribution in the $\Omega^{(1)} \Omega^{(1)}$ term of Eq. (56). It is also responsible for the restrictions (“denom. = 0”) to the summations to the cases whose fictitious denominator factor ($\epsilon_p - \epsilon_q$ in the first sum or $\epsilon_p + \epsilon_q - \epsilon_r - \epsilon_s$ in the second sum) is zero. See the discussion regarding Eq. (28) and Appendix C 4 for the justification of this rule.

reduced analytical formula reported earlier:⁵⁵

$$\begin{aligned}
 \Omega^{(2)} &= \sum_{p,q}^{\text{denom.} \neq 0} \frac{|F_{pq}|^2 f_p^- f_q^+}{\epsilon_p - \epsilon_q} + \frac{1}{4} \sum_{p,q,r,s}^{\text{denom.} \neq 0} \frac{|\langle pq || rs \rangle|^2 f_p^- f_q^- f_r^+ f_s^+}{\epsilon_p + \epsilon_q - \epsilon_r - \epsilon_s} \\
 &\quad - \frac{\beta}{2} \sum_{p,q}^{\text{denom.}=0} |F_{pq}|^2 f_p^- f_q^+ - \frac{\beta}{8} \sum_{p,q,r,s}^{\text{denom.}=0} |\langle pq || rs \rangle|^2 f_p^- f_q^- f_r^+ f_s^+ \\
 &\quad + \beta \mu^{(1)} \sum_p F_{pp} f_p^- f_p^+ - \frac{\beta}{2} (\mu^{(1)})^2 \sum_p f_p^- f_p^+ - \mu^{(2)} \bar{N} \quad (61)
 \end{aligned}$$

$$\equiv \langle D_I^{(2)} \rangle_L + \frac{(-\beta)}{2!} \langle D_I^{(1)} D_I^{(1)} \rangle_L, \quad (62)$$

which is linked.

As per the $\mu^{(n)}$ recursion [Eq. (31)], we have

$$\begin{aligned}
 \mu^{(2)} \langle N_I^2 - \bar{N}^2 \rangle &= \langle E_I^{(2)} (N_I - \bar{N}) \rangle \\
 &\quad + \frac{(-\beta)}{2!} \langle D_I^{(1)} D_I^{(1)} (N_I - \bar{N}) \rangle, \quad (63)
 \end{aligned}$$

of which the left-hand side has already been evaluated in Eq. (52). The second term in the right-hand side is further expanded as

$$\begin{aligned}
 \langle D_I^{(1)} D_I^{(1)} (N_I - \bar{N}) \rangle &= \langle E_I^{(1)} E_I^{(1)} (N_I - \bar{N}) \rangle \\
 &\quad - 2\mu^{(1)} \langle E_I^{(1)} N_I (N_I - \bar{N}) \rangle \\
 &\quad + (\mu^{(1)})^2 \langle N_I N_I (N_I - \bar{N}) \rangle. \quad (64)
 \end{aligned}$$

The first term of Eq. (63) is evaluated as

Substituting all these results into Eq. (56), we observe exact mutual cancellations of all unlinked terms, reproducing the

$$\begin{aligned}
\langle E_I^{(2)}(N_I - \bar{N}) \rangle &= \langle \langle I | \hat{V} \hat{R}_I \hat{V} (\hat{N} - \bar{N}) | I \rangle \rangle \\
&= \langle \langle I | F_{pq} \{ \hat{p}^\dagger \hat{q} \} \{ \hat{a}^\dagger \hat{i} \} | I \rangle \langle \epsilon_i - \epsilon_a \rangle^{-1} \langle I | \{ \hat{i}^\dagger \hat{a} \} \{ \hat{r}^\dagger \hat{s} \} F_{rs} \{ \hat{r}^\dagger \hat{i} \} | I \rangle \rangle + \langle \langle I | F_{pq} \{ \hat{p}^\dagger \hat{q} \} \{ \hat{a}^\dagger \hat{i} \} | I \rangle \langle \epsilon_i - \epsilon_a \rangle^{-1} \langle I | \{ \hat{i}^\dagger \hat{a} \} \{ \hat{r}^\dagger \hat{s} \} F_{rs} \{ \hat{r}^\dagger \hat{i} \} | I \rangle \rangle \\
&\quad + \frac{1}{4} \langle \langle I | F_{pq} \{ \hat{p}^\dagger \hat{q} \} \{ \hat{a}^\dagger \hat{i} \} | I \rangle \langle \epsilon_i - \epsilon_a \rangle^{-1} \langle I | \{ \hat{i}^\dagger \hat{a} \} \{ \hat{r}^\dagger \hat{s} \} \hat{u} \hat{t} \langle rs \| tu \rangle \{ \hat{v}^\dagger \hat{v} \} | I \rangle \rangle \times 4 \\
&\quad + \left(\frac{1}{4} \right)^2 \langle \langle I | \langle pq \| rs \rangle \{ \hat{p}^\dagger \hat{q} \} \{ \hat{r}^\dagger \hat{s} \} \{ \hat{a}^\dagger \hat{b}^\dagger \} \{ \hat{j} \hat{i} \} | I \rangle \langle \epsilon_i + \epsilon_j - \epsilon_a - \epsilon_b \rangle^{-1} \langle I | \{ \hat{i}^\dagger \hat{a} \} \{ \hat{r}^\dagger \hat{s} \} \{ \hat{t}^\dagger \hat{u} \} F_{tu} \{ \hat{v}^\dagger \hat{v} \} | I \rangle \rangle \times 16 \\
&\quad + \left(\frac{1}{4} \right)^3 \langle \langle I | \langle pq \| rs \rangle \{ \hat{p}^\dagger \hat{q} \} \{ \hat{r}^\dagger \hat{s} \} \{ \hat{a}^\dagger \hat{b}^\dagger \} \{ \hat{j} \hat{i} \} | I \rangle \langle \epsilon_i + \epsilon_j - \epsilon_a - \epsilon_b \rangle^{-1} \langle I | \{ \hat{i}^\dagger \hat{a} \} \{ \hat{r}^\dagger \hat{s} \} \{ \hat{t}^\dagger \hat{u} \} \hat{w} \hat{v} \langle tu \| vw \rangle \{ \hat{x}^\dagger \hat{x} \} | I \rangle \rangle \times 32 \\
&\quad + \left(\frac{1}{4} \right)^3 \langle \langle I | \langle pq \| rs \rangle \{ \hat{p}^\dagger \hat{q} \} \{ \hat{r}^\dagger \hat{s} \} \{ \hat{a}^\dagger \hat{b}^\dagger \} \{ \hat{j} \hat{i} \} | I \rangle \langle \epsilon_i + \epsilon_j - \epsilon_a - \epsilon_b \rangle^{-1} \langle I | \{ \hat{i}^\dagger \hat{a} \} \{ \hat{r}^\dagger \hat{s} \} \{ \hat{t}^\dagger \hat{u} \} \hat{w} \hat{v} \langle tu \| vw \rangle \{ \hat{x}^\dagger \hat{x} \} | I \rangle \rangle \times 32 \quad (65) \\
&= \sum_{p,q}^{\text{denom.} \neq 0} \frac{|F_{pq}|^2 f_p^- f_q^+ f_p^+}{\epsilon_p - \epsilon_q} - \sum_{p,q}^{\text{denom.} \neq 0} \frac{|F_{pq}|^2 f_p^- f_q^+ f_q^-}{\epsilon_p - \epsilon_q} \\
&\quad + \sum_{p,q,s}^{\text{denom.} \neq 0} \frac{F_{pq} \langle qs \| ps \rangle f_p^- f_q^+ f_s^- f_s^+}{\epsilon_p - \epsilon_q} + \sum_{p,q,r}^{\text{denom.} \neq 0} \frac{\langle pq \| rq \rangle F_{rp} f_p^- f_q^- f_q^+ f_r^+}{\epsilon_p - \epsilon_r} \\
&\quad + \frac{1}{2} \sum_{p,q,r,s}^{\text{denom.} \neq 0} \frac{|\langle pq \| rs \rangle|^2 f_p^- f_q^- f_r^+ f_s^+ f_p^+}{\epsilon_p + \epsilon_q - \epsilon_r - \epsilon_s} - \frac{1}{2} \sum_{p,q,r,s}^{\text{denom.} \neq 0} \frac{|\langle pq \| rs \rangle|^2 f_p^- f_q^- f_r^+ f_s^+ f_r^-}{\epsilon_p + \epsilon_q - \epsilon_r - \epsilon_s} \quad (66) \\
&\equiv \langle E_I^{(2)}(N_I - \bar{N}) \rangle_L. \quad (67)
\end{aligned}$$

The constant part [Eq. (C41)] in the first \hat{V} vanishes because the resolvent \hat{R}_I annihilates it. The constant part in the second \hat{V} does not contribute, either, because it cannot form a valid contraction with $\hat{N} - \bar{N} = \{ \hat{p}^\dagger \hat{p} \}$. As a result, the above thermal average is linked. The first term of Eq. (64) is evaluated similarly as

$$\begin{aligned}
\langle E_I^{(1)} E_I^{(1)}(N_I - \bar{N}) \rangle &= \langle \langle I | \hat{V} \hat{P}_I \hat{V} (\hat{N} - \bar{N}) | I \rangle \rangle \\
&= \langle \langle I | \langle E_I^{(1)} \rangle | I \rangle \langle I | F_{pq} \{ \hat{p}^\dagger \hat{q} \} \{ \hat{r}^\dagger \hat{r} \} | I \rangle \rangle + \langle \langle I | F_{pq} \{ \hat{p}^\dagger \hat{q} \} \{ \hat{a}^\dagger \hat{i} \} | I \rangle \langle I | \{ \hat{i}^\dagger \hat{a} \} \langle E_I^{(1)} \rangle \{ \hat{r}^\dagger \hat{r} \} | I \rangle \rangle \\
&\quad + \langle \langle I | F_{pq} \{ \hat{p}^\dagger \hat{q} \} \{ \hat{a}^\dagger \hat{i} \} | I \rangle \langle I | \{ \hat{i}^\dagger \hat{a} \} \{ \hat{r}^\dagger \hat{s} \} F_{rs} \{ \hat{r}^\dagger \hat{i} \} | I \rangle \rangle + \langle \langle I | F_{pq} \{ \hat{p}^\dagger \hat{q} \} \{ \hat{a}^\dagger \hat{i} \} | I \rangle \langle I | \{ \hat{i}^\dagger \hat{a} \} \{ \hat{r}^\dagger \hat{s} \} F_{rs} \{ \hat{r}^\dagger \hat{i} \} | I \rangle \rangle \\
&\quad + \frac{1}{4} \langle \langle I | F_{pq} \{ \hat{p}^\dagger \hat{q} \} \{ \hat{a}^\dagger \hat{i} \} | I \rangle \langle I | \{ \hat{i}^\dagger \hat{a} \} \{ \hat{r}^\dagger \hat{s} \} \hat{u} \hat{t} \langle rs \| tu \rangle \{ \hat{v}^\dagger \hat{v} \} | I \rangle \rangle \times 4 \\
&\quad + \left(\frac{1}{4} \right)^2 \langle \langle I | \langle pq \| rs \rangle \{ \hat{p}^\dagger \hat{q} \} \{ \hat{r}^\dagger \hat{s} \} \{ \hat{a}^\dagger \hat{b}^\dagger \} \{ \hat{j} \hat{i} \} | I \rangle \langle I | \{ \hat{i}^\dagger \hat{a} \} \{ \hat{r}^\dagger \hat{s} \} \{ \hat{t}^\dagger \hat{u} \} F_{tu} \{ \hat{v}^\dagger \hat{v} \} | I \rangle \rangle \times 16 \\
&\quad + \left(\frac{1}{4} \right)^3 \langle \langle I | \langle pq \| rs \rangle \{ \hat{p}^\dagger \hat{q} \} \{ \hat{r}^\dagger \hat{s} \} \{ \hat{a}^\dagger \hat{b}^\dagger \} \{ \hat{j} \hat{i} \} | I \rangle \langle I | \{ \hat{i}^\dagger \hat{a} \} \{ \hat{r}^\dagger \hat{s} \} \{ \hat{t}^\dagger \hat{u} \} \hat{w} \hat{v} \langle tu \| vw \rangle \{ \hat{x}^\dagger \hat{x} \} | I \rangle \rangle \times 32 \\
&\quad + \left(\frac{1}{4} \right)^3 \langle \langle I | \langle pq \| rs \rangle \{ \hat{p}^\dagger \hat{q} \} \{ \hat{r}^\dagger \hat{s} \} \{ \hat{a}^\dagger \hat{b}^\dagger \} \{ \hat{j} \hat{i} \} | I \rangle \langle I | \{ \hat{i}^\dagger \hat{a} \} \{ \hat{r}^\dagger \hat{s} \} \{ \hat{t}^\dagger \hat{u} \} \hat{w} \hat{v} \langle tu \| vw \rangle \{ \hat{x}^\dagger \hat{x} \} | I \rangle \rangle \times 32 \quad (68) \\
&= 2 \langle E_I^{(1)} \rangle \sum_p F_{pp} f_p^- f_p^+ + \sum_{p,q}^{\text{denom.}=0} |F_{pq}|^2 f_p^- f_q^+ f_p^+ - \sum_{p,q}^{\text{denom.}=0} |F_{pq}|^2 f_p^- f_q^+ f_q^- \\
&\quad + \sum_{p,q,s}^{\text{denom.}=0} F_{pq} \langle qs \| ps \rangle f_p^- f_q^+ f_s^- f_s^+ + \sum_{p,q,r}^{\text{denom.}=0} \langle pq \| rq \rangle F_{rp} f_p^- f_q^- f_q^+ f_r^+ \\
&\quad + \frac{1}{2} \sum_{p,q,r,s}^{\text{denom.}=0} |\langle pq \| rs \rangle|^2 f_p^- f_q^- f_r^+ f_s^+ f_p^+ - \frac{1}{2} \sum_{p,q,r,s}^{\text{denom.}=0} |\langle pq \| rs \rangle|^2 f_p^- f_q^- f_r^+ f_s^+ f_r^- \\
&\equiv 2 \langle E_I^{(1)} \rangle_L \langle E_I^{(1)}(N_I - \bar{N}) \rangle_L + \langle E_I^{(1)} E_I^{(1)}(N_I - \bar{N}) \rangle_L. \quad (70)
\end{aligned}$$

The first term is unlinked, as each factor is extensive, making the product grow quadratically with size. This unlinked term will be cancelled exactly (see below).

Likewise, the thermal average in the second term of Eq. (64) is evaluated as

$$\begin{aligned} & \langle E_I^{(1)} N_I (N_I - \bar{N}) \rangle \\ &= \langle \langle I | \hat{V} \hat{N} (\hat{N} - \bar{N}) | I \rangle \rangle \\ &= \langle \langle I | \langle E_I^{(1)} \rangle \{ \hat{p}^\dagger \hat{p} \} \{ \hat{q}^\dagger \hat{q} \} | I \rangle \rangle + \langle \langle I | F_{pq} \{ \hat{p}^\dagger \hat{q} \} \bar{N} \{ \hat{r}^\dagger \hat{r} \} | I \rangle \rangle \\ &+ \langle \langle I | F_{pq} \{ \hat{p}^\dagger \hat{q} \} \{ \hat{r}^\dagger \hat{r} \} \{ \hat{s}^\dagger \hat{s} \} | I \rangle \rangle + \langle \langle I | F_{pq} \{ \hat{p}^\dagger \hat{q} \} \{ \hat{r}^\dagger \hat{r} \} \{ \hat{s}^\dagger \hat{s} \} | I \rangle \rangle \\ &+ \frac{1}{4} \langle \langle I | \langle pq || rs \rangle \{ \hat{p}^\dagger \hat{q}^\dagger \hat{s} \hat{r} \} \{ \hat{r}^\dagger \hat{t} \} \{ \hat{u}^\dagger \hat{u} \} | I \rangle \rangle \times 4 \\ &= \langle E_I^{(1)} \rangle \sum_p f_p^- f_p^+ + \bar{N} \sum_p F_{pp} f_p^- f_p^+ + \sum_p F_{pp} f_p^- f_p^+ f_p^+ \\ &- \sum_p F_{pp} f_p^- f_p^+ f_p^- + \sum_{p,q} \langle pq || pq \rangle f_p^- f_p^+ f_q^- f_q^+ \end{aligned} \quad (71)$$

$$\begin{aligned} & \equiv \langle E_I^{(1)} \rangle_L \langle N_I^2 - \bar{N}^2 \rangle_L + \bar{N} \langle E_I^{(1)} (N_I - \bar{N}) \rangle_L \\ & + \langle E_I^{(1)} N_I (N_I - \bar{N}) \rangle_L. \end{aligned} \quad (72)$$

The first two terms are unlinked.

The thermal average in the third term of Eq. (64) becomes

$$\begin{aligned} & \langle N_I N_I (N_I - \bar{N}) \rangle \\ &= \langle \langle I | \hat{N} \hat{N} (\hat{N} - \bar{N}) | I \rangle \rangle \\ &= \langle \langle I | \bar{N} \{ \hat{p}^\dagger \hat{p} \} \{ \hat{q}^\dagger \hat{q} \} | I \rangle \rangle + \langle \langle I | \{ \hat{p}^\dagger \hat{p} \} \bar{N} \{ \hat{q}^\dagger \hat{q} \} | I \rangle \rangle \\ &+ \langle \langle I | \{ \hat{p}^\dagger \hat{q} \} \{ \hat{r}^\dagger \hat{r} \} \{ \hat{s}^\dagger \hat{s} \} | I \rangle \rangle + \langle \langle I | \{ \hat{p}^\dagger \hat{q} \} \{ \hat{r}^\dagger \hat{r} \} \{ \hat{s}^\dagger \hat{s} \} | I \rangle \rangle \\ &= 2\bar{N} \sum_p f_p^- f_p^+ + \sum_p f_p^- f_p^+ f_p^+ - \sum_p f_p^- f_p^+ f_p^- \end{aligned} \quad (73)$$

$$\equiv 2\bar{N} \langle N_I^2 - \bar{N}^2 \rangle_L + \langle N_I N_I (N_I - \bar{N}) \rangle_L. \quad (74)$$

The first term is unlinked.

Substituting these into Eq. (63), we again observe systematic cancellations of unlinked terms with the aid of Eq. (54), leaving

$$\begin{aligned} & \mu^{(2)} \langle N_I^2 - \bar{N}^2 \rangle_L \\ &= \langle E_I^{(2)} (N_I - \bar{N}) \rangle_L + \frac{(-\beta)}{2!} \langle E_I^{(1)} E_I^{(1)} (N_I - \bar{N}) \rangle_L \\ &+ \beta \mu^{(1)} \langle E_I^{(1)} N_I (N_I - \bar{N}) \rangle_L + \frac{(-\beta)}{2!} (\mu^{(1)})^2 \langle N_I N_I (N_I - \bar{N}) \rangle_L \\ &= \langle E_I^{(2)} (N_I - \bar{N}) \rangle_L + \frac{(-\beta)}{2!} \langle D_I^{(1)} D_I^{(1)} (N_I - \bar{N}) \rangle_L, \end{aligned} \quad (75)$$

which translates to

$$\begin{aligned} & \mu^{(2)} \sum_p f_p^- f_p^+ \\ &= \sum_{p,q}^{\text{denom.} \neq 0} \frac{|F_{pq}|^2 f_p^- f_q^+ (f_p^+ - f_q^-)}{\epsilon_p - \epsilon_q} \\ &+ \sum_{p,q,r}^{\text{denom.} \neq 0} \frac{(F_{pq} \langle qr || pr \rangle + \langle pr || qr \rangle F_{qp}) f_p^- f_q^- f_r^- f_r^+}{\epsilon_p - \epsilon_q} \\ &+ \frac{1}{4} \sum_{p,q,r,s}^{\text{denom.} \neq 0} \frac{|(pq || rs)|^2 f_p^- f_q^- f_r^+ f_s^+ (f_p^+ + f_q^+ - f_r^- - f_s^-)}{\epsilon_p + \epsilon_q - \epsilon_r - \epsilon_s} \\ &- \frac{\beta}{2} \sum_{p,q}^{\text{denom.} = 0} |F_{pq}|^2 f_p^- f_q^+ (f_p^+ - f_q^-) \\ &- \frac{\beta}{2} \sum_{p,q,r}^{\text{denom.} = 0} (F_{pq} \langle qr || pr \rangle + \langle pr || qr \rangle F_{qp}) f_p^- f_q^- f_r^- f_r^+ \\ &- \frac{\beta}{8} \sum_{p,q,r,s}^{\text{denom.} = 0} |(pq || rs)|^2 f_p^- f_q^- f_r^+ f_s^+ (f_p^+ + f_q^+ - f_r^- - f_s^-) \\ &+ \beta \mu^{(1)} \sum_p F_{pp} f_p^- f_p^+ (f_p^+ - f_p^-) + \beta \mu^{(1)} \sum_{p,q} \langle pq || pq \rangle f_p^- f_p^+ f_q^- f_q^+ \\ &- \frac{\beta}{2} (\mu^{(1)})^2 \sum_p f_p^- f_p^+ (f_p^+ - f_p^-). \end{aligned} \quad (76)$$

This is identified as Eq. (69) of Ref. 55.

D. Third order

We shall derive the reduced analytical formulas for $\Omega^{(3)}$ using diagrams in Sec. IV. Here, we focus on its most important contribution, $\langle E^{(3)} \rangle$, since this is where linked renormalization terms appear for the first time, giving rise to a new, unique class of the renormalization diagrams.

According to Eq. (24), the third-order correction to the energy matrix of HCPT is written as

$$E_{IJ}^{(3)} = \langle I | \hat{V} \hat{R}_I \hat{V} \hat{R}_I \hat{V} | J \rangle - \sum_K \langle I | \hat{V} \hat{R}_I \hat{R}_I \hat{V} | K \rangle E_{KJ}^{(1)}, \quad (77)$$

where K runs over all states that are degenerate with I and J . The second term is the renormalization term of the Rayleigh-Schrödinger perturbation theory.⁶³

If I is nondegenerate, HCPT reduces to MPPT, and therefore $I = J = K$. The first term then consists of the linked and unlinked contributions, and is written as

$$\begin{aligned} \langle I | \hat{V} \hat{R}_I \hat{V} \hat{R}_I \hat{V} | I \rangle &= \langle I | \hat{V} \hat{R}_I \hat{V} \hat{R}_I \hat{V} | I \rangle_L \\ &+ \langle I | \hat{V} \hat{R}_I \hat{R}_I \hat{V} | I \rangle_L E_I^{(1)}, \end{aligned} \quad (78)$$

with the unlinked (second) term cancelling exactly the renormalization term [the second term of Eq. (77)], leaving

$$E_I^{(3)} = \langle I | \hat{V} \hat{R}_I \hat{V} \hat{R}_I \hat{V} | I \rangle_L. \quad (79)$$

When I is degenerate, the cancellation of unlinked terms may or may not be as straightforward in individual matrix elements, $E_{IJ}^{(3)}$. However, the cancellation occurs completely analogously and straightforwardly in the thermal average, $\langle E_I^{(3)} \rangle$. Using the trace invariance of $E^{(3)}$, we have

$$\begin{aligned} \langle E_I^{(3)} \rangle &= \langle E_{II}^{(3)} \rangle \\ &= \langle \langle I | \hat{V} \hat{R}_I \hat{V} \hat{R}_I \hat{V} | I \rangle \rangle - \langle \langle I | \hat{V} \hat{R}_I \hat{R}_I \hat{V} | K \rangle \rangle E_{KI}^{(1)} \\ &= \langle \langle I | \hat{V} \hat{R}_I \hat{V} \hat{R}_I \hat{V} | I \rangle \rangle - \langle \langle I | \hat{V} \hat{R}_I \hat{R}_I \hat{V} | K \rangle \rangle \langle K | \hat{V} | I \rangle \\ &= \langle \langle I | \hat{V} \hat{R}_I \hat{V} \hat{R}_I \hat{V} | I \rangle \rangle - \langle \langle I | \hat{V} \hat{R}_I \hat{R}_I \hat{V} \hat{P}_I \hat{V} | I \rangle \rangle, \end{aligned} \quad (80)$$

where summation symbols are again suppressed. Each term of the last line is then decomposed into linked and unlinked contributions. Recalling the normal-ordered form of \hat{V} [Eq. (C41)], we can decompose each term as

$$\begin{aligned} \langle \langle I | \hat{V} \hat{R}_I \hat{V} \hat{R}_I \hat{V} | I \rangle \rangle &= \langle \langle I | \hat{V} \hat{R}_I \hat{V} \hat{R}_I \hat{V} | I \rangle \rangle_L \\ &\quad + \langle \langle I | \hat{V} \hat{R}_I \hat{V} \hat{R}_I \hat{V} | I \rangle \rangle_{\text{unlinked}}, \quad (81) \\ \langle \langle I | \hat{V} \hat{R}_I \hat{R}_I \hat{V} \hat{P}_I \hat{V} | I \rangle \rangle &= \langle \langle I | \hat{V} \hat{R}_I \hat{R}_I \hat{V} \hat{P}_I \hat{V} | I \rangle \rangle_L \\ &\quad + \langle \langle I | \hat{V} \hat{R}_I \hat{R}_I \hat{V} \hat{P}_I \hat{V} | I \rangle \rangle_{\text{unlinked}}, \quad (82) \end{aligned}$$

where the unlinked contraction patterns are indicated by the staple symbols in the second terms, which can be seen to have an equal value. They therefore cancel each other in Eq. (80), leaving linked $\langle E^{(3)} \rangle$:

$$\langle E_I^{(3)} \rangle = \langle \langle I | \hat{V} \hat{R}_I \hat{V} \hat{R}_I \hat{V} | I \rangle \rangle_L - \langle \langle I | \hat{V} \hat{R}_I \hat{R}_I \hat{V} \hat{P}_I \hat{V} | I \rangle \rangle_L. \quad (83)$$

Unlike in MPPT, the renormalization term in HCPT has both unlinked and linked contributions with the former cancelling exactly the unlinked contribution in the parent term, while the latter is nonzero and therefore should not be overlooked or neglected. In the above example, this linked renormalized contribution has one resolvent (\hat{R}_I) operator shifted from in between the last two \hat{V} operators to in between the first two \hat{V} operators. Diagrammatically, it will correspond to a closed, connected diagram with no resolvent line between a pair of adjacent vertexes but with two resolvent lines crammed in between the other pair of adjacent vertexes (see Sec. IV C). This unusual diagram with a displaced resolvent occurs at $T > 0$, and should be distinguished from the anomalous diagrams^{48,52} with missing resolvents. In the next section, we will document the reduced analytical formula of $\langle E_I^{(3)} \rangle$ obtained with diagrams.

IV. FEYNMAN DIAGRAMS

The diagrammatic rules are obtained by a systematic modification of the zero-temperature counterpart^{42,44,63} and justified by the one-to-many correspondence with the foregoing normal-ordered second-quantization logic at finite temperature. The rules to generate diagrams and to interpret them algebraically are given in Tables I and II, respectively.

Each vertex graphically represents a matrix element of the normal-ordered Hamiltonian or number operator. Each line

TABLE I. Rules to generate all $\Omega^{(n)}$ diagrams in the Hugenholtz style ($n \geq 2$). See the text for generating diagrammatic equations for $\mu^{(n)}$, and $S^{(n)}$ from the $\Omega^{(n)}$ equation.

- (1) Place n vertexes in an unambiguous vertical order, using three types of vertexes: filled-circle two-line (F_{pq}) vertex, numbered two-line (μ) vertex, and filled-circle four-line ($\langle pq||rs \rangle$) vertex. Count an $\mu^{(m)}$ vertex as m vertexes.
- (2) Connect all vertexes with lines to form a closed connected diagram in all topologically distinct manner. Each two-line (four-line) vertex should be connected with one outgoing and one incoming (two outgoing and two incoming) lines.
- (3) Insert zero through $n - 1$ resolvent (wiggly) lines into the diagram in all 2^{n-1} ways with either zero or one resolvent in between each pair of adjacent vertexes. Call the diagram with $n - 1$ resolvents a normal diagram and the one with $n - 2$ or less resolvents an anomalous diagram.
- (4) Starting with the normal diagram, shift upwards one through $n - 2$ resolvents in all possible ways. Call the diagram with at least one shifted resolvent a renormalization diagram.

$$\begin{aligned} \Omega^{(1)} &= \begin{array}{ccc} \text{p} & \text{p} & \text{p} \\ \text{q} & \text{q} & \text{q} \\ \text{p} & \text{p} & \text{p} \\ \text{q} & \text{q} & \text{q} \end{array} \\ &= \begin{array}{ccc} \text{p} & \text{p} & \text{p} \\ \text{q} & \text{q} & \text{q} \\ \text{p} & \text{p} & \text{p} \\ \text{q} & \text{q} & \text{q} \end{array} \end{aligned}$$

FIG. 1. Diagrammatic equations of $\Omega^{(1)}$.

(edge) connecting two vertexes corresponds to a Wick contraction. That only full contractions yield a nonzero thermal average translates to the diagrammatic rule that all lines must be terminated by vertexes at both ends in order to form a closed diagram (no dangling line). An internal contraction is depicted as a ‘bubble,’ i.e., a contraction of a vertex with itself forming a short loop. In a $\Omega^{(n)}$ diagram, the bubbles are seen only as a part of the normal-ordered Hamiltonian or number operator such as $\langle E_I^{(1)} \rangle$, F_{pq} , and \bar{N} . This is because outside of these operator definitions, internal contractions are zero in a thermal average (see Appendix C). An unlinked diagram (‘unlinked’ is synonymous with ‘disconnected’ for a closed diagram) corresponds to a full contraction pattern that results in a product of two or more scalars with no shared summation index [e.g., the second terms of Eqs. (81) and (82)]. Section V proves that all thermodynamic functions of the finite-temperature MBPT are represented by linked diagrams only.

A. First order

The diagrammatic rules are not so helpful at the zeroth and first orders, but for the sake of completeness, we show in Fig. 1 the diagrammatic formulation of $\Omega^{(1)}$. Figure 2 defines the relevant vertexes.

Using the interpretation rules in Table II, we can transform

TABLE II. Rules to transform an $\Omega^{(n)}$, $\mu^{(n)}$, or $S^{(n)}$ diagram in the Hugenoltz style to an algebraic formula ($n \geq 1$).

- (1) Label lines with indexes p, q, r, s , etc.
- (2) Associate each filled-circle two-line vertex with F_{pq} , where p (q) is the outgoing (incoming) line label.
- (3) Associate each vertex with number n with $-\mu^{(n)}\delta_{pq}$, where p (q) is the outgoing (incoming) line label.
- (4) The F_{pq} and $\mu^{(1)}$ vertexes can be consolidated into a shaded two-line vertex to reduce the number of diagrams. If this simplification is used, associate the vertex with $F_{pq} - \mu^{(1)}\delta_{pq}$.
- (5) Associate each filled-circle four-line vertex with $\langle pq||rs \rangle$, where p, q, r , and s are the left-outgoing, right-outgoing, left-incoming, and right-incoming line labels, respectively.
- (6) Associate a downgoing (upgoing) line with f_p^- (f_p^+). The directionality of a bubble is judged at the farthest point from the vertex or from its point of contact.
- (7) Associate each dashed bubble with $\beta(\epsilon_p - \mu^{(0)})$ additionally.
- (8) Associate each resolvent line with $1/(\epsilon_p + \epsilon_q \cdots - \epsilon_r - \epsilon_s \cdots)$, where p, q, \dots (r, s, \dots) are the labels of the downgoing (upgoing) lines intersecting the resolvent line.
- (9) Sum over all line indexes. Restrict the summations to cases that existing denominator factors are nonzero and fictitious (due to missing resolvents) denominator factors are zero.
- (10) Multiply $1/n!$ for each set of n equivalent lines. Two lines are equivalent when they start from a same vertex and end at a same vertex as well as have the identical line directions. Ignore attached bubbles when judging the equivalence.
- (11) Multiply $(-1)^{h+l}$ to the diagram with h downgoing lines and l loops. A bubble counts as a loop.
- (12) Multiply $(-\beta)^n/(n+1)!$ to the diagram with n missing resolvents. Further multiply with n to an $S^{(n)}$ diagram with no dashed bubble.
- (13) Multiply $(-1)^n$ to the diagram with n shifted resolvents.

$$F_{pq} = h_{pq} - \epsilon_p \delta_{pq} + \sum_r \langle pr||qr \rangle f_r^-$$

FIG. 2. Definitions of vertexes. See also Appendix C 3.

each diagram in Fig. 1 as

$$\Omega 1a = (-1)^{1+1} \sum_p F_{pp} f_p^-, \quad (84)$$

$$\Omega 1b = (-1)^{2+2} \left(\frac{1}{2}\right)^1 \sum_{p,q} \langle pq||pq \rangle f_p^- f_q^-, \quad (85)$$

$$\Omega 1c = (-1)^{1+1} \sum_p (-\mu^{(1)}) f_p^- = -\mu^{(1)} \bar{N}. \quad (86)$$

Summing them with the signs indicated in the figure, we recover the reduced analytical formula of $\Omega^{(1)}$ [Eq. (49)].

We can rewrite the diagrammatic equation in the first line of Fig. 1 into the second line, which will turn out to be more convenient for the diagrammatic derivation of $\mu^{(1)}$ and $S^{(1)}$ (see below). An open-circle, two-line vertex stands for h_{pq} -

$$0 = \mu 1a + \mu 1b + \mu 1c + \mu 1d$$

FIG. 3. Diagrammatic equation of $\mu^{(1)}$.

$$TS^{(1)} = S1a + S1b + S1c + S1d$$

FIG. 4. Diagrammatic equation of $TS^{(1)}$.

$\epsilon_p \delta_{pq}$. The algebraic interpretation of $\Omega 1d$ is then

$$\Omega 1d = (-1)^{1+1} \sum_p (h_{pp} - \epsilon_p) f_p^-, \quad (87)$$

leading to the same reduced analytical formula of $\Omega^{(1)}$.

The diagrammatic rules for $\mu^{(n)}$ are based on Eq. (29) with

$$\frac{\partial f_p^\pm}{\partial \mu^{(0)}} = \mp \beta f_p^- f_p^+. \quad (88)$$

The diagrammatic equation for $\mu^{(n)}$ is therefore obtained by ‘differentiating’ each line in the diagrammatic equation of $\Omega^{(n)}$ with respect to $\mu^{(0)}$. In view of Eq. (88), this process can be represented as attaching to each line a bubble with the opposite directionality (which is judged at the farthest point from its contact with the line). Note that the point of contact of the bubble is not a vertex, and therefore the bubble and line share the same spinorbital index.

Figure 3 is the diagrammatic equation for $\mu^{(1)}$. It is based on the second line of Fig. 1 rather than on the first line. This is because the latter may hide the fact that F_{pq} contains $\langle pr||qr \rangle$ that also needs to be differentiated with $\mu^{(0)}$. Each diagram is algebraically interpreted by the same rules of Table II as

$$\mu 1a = (-1)^{1+2} \sum_p (h_{pp} - \epsilon_p) f_p^- f_p^+, \quad (89)$$

$$\mu 1b = (-1)^{2+3} \left(\frac{1}{2}\right)^1 \sum_{p,q} \langle pq||pq \rangle f_p^- f_q^-, \quad (90)$$

$$\mu 1c = (-1)^{2+3} \left(\frac{1}{2}\right)^1 \sum_{p,q} \langle pq||pq \rangle f_p^- f_q^-, \quad (91)$$

$$\mu 1d = (-\mu^{(1)}) (-1)^{1+2} \sum_p f_p^- f_p^+. \quad (92)$$

They lead to the same reduced analytical equation for $\mu^{(1)}$ as Eq. (55).

The diagrammatic equation for $S^{(n)}$ utilizes the following identity obtained by differentiating Eq. (5) with λn times:

$$TS^{(n)} = \beta \left(\frac{\partial \Omega^{(n)}}{\partial \beta} \right)_{\mu^{(0)}, \dots, \mu^{(n)}} \quad (93)$$

with

$$\beta \frac{\partial f_p^\pm}{\partial \beta} = \pm \beta (\epsilon_p - \mu^{(0)}) f_p^- f_p^+. \quad (94)$$

Therefore, the diagrammatic rules for $S^{(n)}$ can be obtained by ‘differentiating’ the $\Omega^{(n)}$ diagram equation with β , keeping in mind that anomalous diagrams also carry a power of β . A β -differentiation of a line is diagrammatically depicted as attaching to the line a dashed-bubble with the opposite directionality.

At the first order, $\Omega^{(1)}$ does not have anomalous diagrams and so only lines (or more precisely their f_p^- factors) need to be differentiated with β . The diagrammatic equation for $S^{(1)}$ is drawn in Fig. 4. Each diagram is interpreted according to Table II as

$$S1a = (-1)^{1+2} \sum_p (h_{pp} - \epsilon_p) \beta (\epsilon_p - \mu^{(0)}) f_p^- f_p^+, \quad (95)$$

$$S1b = (-1)^{2+3} \left(\frac{1}{2}\right)^1 \sum_{p,q} \langle pq||pq \rangle f_p^- f_q^- \beta (\epsilon_q - \mu^{(0)}) f_q^+, \quad (96)$$

$$S1c = (-1)^{2+3} \left(\frac{1}{2}\right)^1 \sum_{p,q} \langle pq||pq \rangle f_p^- f_q^- \beta (\epsilon_p - \mu^{(0)}) f_p^+, \quad (97)$$

$$S1d = (-\mu^{(1)}) (-1)^{1+2} \sum_p f_p^- \beta (\epsilon_p - \mu^{(0)}) f_p^+, \quad (98)$$

leading to

$$TS^{(1)} = -\beta \sum_p (F_{pp} - \mu^{(1)}) (\epsilon_p - \mu^{(0)}) f_p^- f_p^+ \quad (99)$$

$$= -\beta \sum_p (F_{pp} - \mu^{(1)}) \epsilon_p f_p^- f_p^+. \quad (100)$$

The second equality follows from Eq. (55). In general, for the purpose of deriving the correct $S^{(n)}$ formulas, $\mu^{(0)}$ in Eq. (94) can be replaced by any constant (such as zero) by virtue of Eq. (29).

The diagrammatic equation and rules for $U^{(n)}$ are a concatenation of those for $\Omega^{(n)}$, $\mu^{(n)}$, and $S^{(n)}$ given above because

$$U^{(n)} = \Omega^{(n)} + \mu^{(n)} \bar{N} + TS^{(n)}. \quad (101)$$

The $U^{(1)}$ formula obtained as a combination of Eqs. (49) and (100) is the same as Eq. (61) of Ref. 55.

B. Second order

Following the rules in Table I, we obtain eight diagrams that consist in $\Omega^{(2)}$, which are shown in Fig. 5. They are interpreted algebraically according to Table II, leading to the same result as Eq. (61).

The first two ($\Omega2a$ and $\Omega2b$) are isomorphic to the usual MBPT(2) energy diagrams ($\Omega2b$ being the non-HF term⁶³) with exactly one resolvent (wiggly) line in between the pair of vertexes. The third and fourth ($\Omega2c$ and $\Omega2d$) are the corresponding anomalous diagrams,^{48,52} whose resolvent line is missing. In these diagrams, the summations over spinorbital indexes are limited to those cases whose fictitious denominators are zero. Instead of being divided by the energy denominators, they are divided by $2k_B T$ to restore the dimension of energy.

Diagrams $\Omega2e$ through $\Omega2g$ are also unique to the finite-temperature MBPT. The absence of a resolvent line implies that they are technically counted as anomalous diagrams. The summations in these diagrams are therefore also limited to zero fictitious denominators, but this restriction is automatically fulfilled because the $\mu^{(n)}$ vertex is zero whenever $p \neq q$.

We can compress the diagrammatic equations of $\Omega^{(n)}$ by introducing skeleton diagrams⁶³ and a modified Fock operator defined in Fig. 6. A skeleton diagram is the one that is stripped of line directions, line labels, and resolvents. Single skeleton diagram $\Omega2A$ in Fig. 7 stands for $\Omega2a$ plus $\Omega2c$, which differ from each other by the presence and absence of the resolvent. Skeleton diagram $\Omega2B$ in Fig. 8 is the sum of five diagrams. A replacement of the F_{pq} vertex by the $F_{pq} - \mu^{(1)} \delta_{pq}$ vertex has no effect on the normal diagram ($\Omega2b$) because its summation is limited to $p \neq q$, but it consolidates the remaining four anomalous diagrams into one. This process is closely related to the Luttinger–Ward prescription⁴⁹ for the Kohn–Luttinger conundrum.^{48,56} Together, we can simplify the diagrammatic equation of $\Omega^{(2)}$ into Fig. 9.

The diagrammatic equation of $\mu^{(2)}$ is drawn in Fig. 10. Translating them into algebraic formulas using the rules in Table II, we arrive at the same reduced analytical formula of $\mu^{(2)}$ as Eq. (69) of Ref. 55.

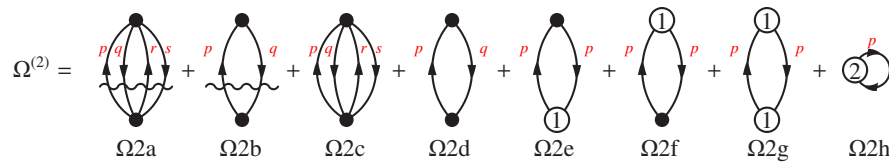
The diagrams defining $S^{(2)}$ are shown in Fig. 11. Evaluating them according to the rules in Table II, we obtain the reduced analytical formula that is consistent with the $U^{(2)}$ formula, i.e., Eq. (74) of Ref. 55. Note that the evaluation rules are slightly different between diagrams $S2a$ and $S2f$ and diagrams $\Omega2c$ and $\Omega2d$ – $\Omega2g$ (cf. Rule 12 of Table II) despite their identical appearances. Care must be exercised when combining diagrammatic equations of $\Omega^{(n)}$ and $S^{(n)}$ to form a concatenated equation of $U^{(n)}$.

C. Third order

The diagrammatic equation of $\Omega^{(3)}$ is given in Fig. 12. It is the sum of eight skeleton diagrams [cf. the zero-temperature MBPT(3) diagrams in page 133 of Shavitt and Bartlett⁶³] plus two anomalous diagrams involving $\mu^{(2)}$ and a bubble diagram of $\mu^{(3)}$. Each skeleton diagram in turn consists of five to fifteen diagrams differing from one another in line direction and/or placement of the resolvents, shown in Figs. 13 through 18. In each row of the right-hand sides of these diagram equations, the first diagram ($\Omega3x1$) is the normal (parent) diagram. The second diagram ($\Omega3x2$) is the renormalization diagram with a resolvent shifted upwards. The third through fifth diagrams are an anomalous diagram with one or two missing resolvents.

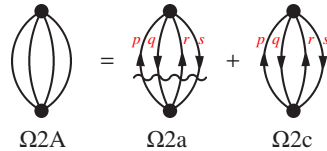
The diagrams in the first row of the right-hand side of Fig. 13 are interpreted algebraically as

$$\Omega3a1 = (-1)^{2+2} \left(\frac{1}{2}\right)^3 \times \sum_{p,q,r,s,t,u}^{\text{denom.1}\neq 0, \text{denom.2}\neq 0} \frac{\langle ps||qr \rangle \langle qr||tu \rangle \langle tu||ps \rangle f_p^- f_q^+ f_r^+ f_s^- f_t^+ f_u^+}{(\epsilon_p + \epsilon_s - \epsilon_q - \epsilon_r)(\epsilon_p + \epsilon_s - \epsilon_t - \epsilon_u)}, \quad (102)$$

FIG. 5. Diagrammatic equation of $\Omega^{(2)}$.

$$\tilde{F}_{pq} = F_{pq} - \mu^{(1)} \delta_{pq}$$

FIG. 6. Definitions of vertexes.

FIG. 7. A skeleton diagram of $\Omega^{(2)}$.

$$\Omega_{3a2} = (-1)^1 (-1)^{2+2} \left(\frac{1}{2}\right)^3 \times \sum_{p,q,r,s,t,u}^{\text{denom.1} \neq 0, \text{denom.2} = 0} \frac{\langle ps||qr \rangle \langle qr||tu \rangle \langle tu||ps \rangle f_p^- f_q^+ f_r^+ f_s^- f_t^+ f_u^+}{(\epsilon_p + \epsilon_s - \epsilon_q - \epsilon_r)^2}, \quad (103)$$

$$\Omega_{3a3} = \frac{(-\beta)}{2!} (-1)^{2+2} \left(\frac{1}{2}\right)^3 \times \sum_{p,q,r,s,t,u}^{\text{denom.1} = 0, \text{denom.2} \neq 0} \frac{\langle ps||qr \rangle \langle qr||tu \rangle \langle tu||ps \rangle f_p^- f_q^+ f_r^+ f_s^- f_t^+ f_u^+}{(\epsilon_p + \epsilon_s - \epsilon_t - \epsilon_u)}, \quad (104)$$

$$\Omega_{3a4} = \frac{(-\beta)}{2!} (-1)^{2+2} \left(\frac{1}{2}\right)^3 \times \sum_{p,q,r,s,t,u}^{\text{denom.1} \neq 0, \text{denom.2} = 0} \frac{\langle ps||qr \rangle \langle qr||tu \rangle \langle tu||ps \rangle f_p^- f_q^+ f_r^+ f_s^- f_t^+ f_u^+}{(\epsilon_p + \epsilon_s - \epsilon_q - \epsilon_r)}, \quad (105)$$

and

$$\Omega_{3a5} = \frac{(-\beta)^2}{3!} (-1)^{2+2} \left(\frac{1}{2}\right)^3 \times \sum_{p,q,r,s,t,u}^{\text{denom.1} = 0, \text{denom.2} = 0} \langle ps||qr \rangle \langle qr||tu \rangle \langle tu||ps \rangle f_p^- f_q^+ f_r^+ f_s^- f_t^+ f_u^+, \quad (106)$$

where ‘denom.1’ and ‘denom.2’ denote the first and second denominator factors, respectively, of the normal diagram [Eq. (102)]. Owing to this provision, none of the above summations encounters a division by zero.

Unlike in the zero-temperature MBPT, where the renormalization term vanishes upon cancelling unlinked contribution

in the parent diagram, in the finite-temperature MBPT, it has both linked and unlinked contributions, the latter cancelling exactly the unlinked contribution in the parent diagram, while the former persists as the renormalization diagram Ω_{3a2} [Eq. (103)] with its resolvent shifted upwards. Unlike in anomalous diagrams, no resolvent is deleted in a renormalization diagram and therefore it does not have to be divided by $k_B T$ to restore the correct dimension of energy. Instead, it is multiplied by the parity of (-1) raised to the power of the number/nestedness of diagram insertions.⁶³ It is not clear if the time-dependent, diagrammatic derivation^{46–51} or the density-matrix formulation⁵² of the conventional finite-temperature MBPT properly accounts for such diagrams, the neglect of which makes it erroneous at the third and higher orders and nonconvergent to the finite-temperature FCI.⁵⁷ The renormalization diagrams may be related to the linked-disconnected diagrams in ΔMP_n .⁷⁵

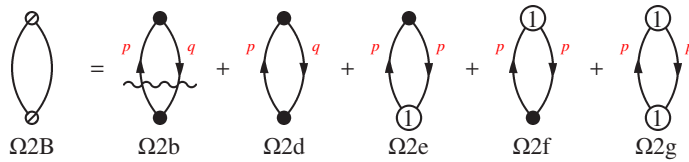
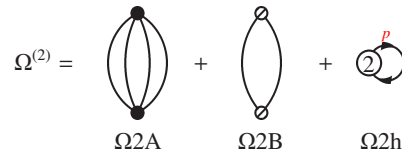
Diagrams Ω_{3a3} , Ω_{3a4} , and Ω_{3a5} are anomalous diagrams of which one or two resolvents are missing. The summation is correspondingly restricted to the cases where the missing denominator factors are zero. For each missing denominator factor, the diagram is divided by $k_B T$ times some integer factor. The presence of these anomalous diagrams is considered well known.^{48,52}

The remaining normal diagrams (Ω_{3x1}) are interpreted algebraically as

$$\Omega_{3b1} = (-1)^{4+2} \left(\frac{1}{2}\right)^3 \times \sum_{p,q,r,s,t,u}^{\text{denom.1} \neq 0, \text{denom.2} \neq 0} \frac{\langle qr||ps \rangle \langle tu||qr \rangle \langle ps||tu \rangle f_p^+ f_q^- f_r^- f_s^+ f_t^- f_u^-}{(\epsilon_q + \epsilon_r - \epsilon_p - \epsilon_s)(\epsilon_t + \epsilon_u - \epsilon_p - \epsilon_s)}, \quad (107)$$

$$\Omega_{3c1} = (-1)^{3+2} \times \sum_{p,q,r,s,t,u}^{\text{denom.1} \neq 0, \text{denom.2} \neq 0} \frac{\langle qs||pr \rangle \langle tr||qu \rangle \langle pu||ts \rangle f_p^+ f_q^- f_r^+ f_s^- f_t^- f_u^+}{(\epsilon_q + \epsilon_s - \epsilon_p - \epsilon_r)(\epsilon_t + \epsilon_s - \epsilon_p - \epsilon_u)}, \quad (108)$$

$$\Omega_{3d1} = (-1)^{2+2} \left(\frac{1}{2}\right)^1 \sum_{p,q,r,s,t}^{\text{denom.1} \neq 0, \text{denom.2} \neq 0} \times \frac{(F_{pq} - \mu^{(1)} \delta_{pq}) \langle qs||rt \rangle \langle rt||ps \rangle f_p^- f_q^+ f_r^+ f_s^- f_t^+}{(\epsilon_p - \epsilon_q)(\epsilon_p + \epsilon_s - \epsilon_r - \epsilon_t)}, \quad (109)$$

FIG. 8. Another skeleton diagram of $\Omega^{(2)}$.FIG. 9. Diagrammatic equation of $\Omega^{(2)}$ in terms of skeleton diagrams.

$$\Omega3e1 = (-1)^{3+2} \left(\frac{1}{2}\right) \sum_{p,q,r,s,t}^{\text{denom.1}\neq 0, \text{denom.2}\neq 0} \times \frac{\langle F_{qp} - \mu^{(1)}\delta_{qp} \rangle \langle rt \parallel qs \rangle \langle ps \parallel rt \rangle f_p^+ f_q^- f_r^- f_s^+ f_t^-}{(\epsilon_q - \epsilon_p)(\epsilon_r + \epsilon_t - \epsilon_p - \epsilon_s)}, \quad (110)$$

$$\Omega3f1 = (-1)^{2+2} \left(\frac{1}{2}\right) \sum_{p,q,r,s,t}^{\text{denom.1}\neq 0, \text{denom.2}\neq 0} \times \frac{\langle pr \parallel qs \rangle \langle F_{st} - \mu^{(1)}\delta_{st} \rangle \langle qt \parallel pr \rangle f_p^- f_q^+ f_r^- f_s^+ f_t^+}{(\epsilon_p + \epsilon_r - \epsilon_q - \epsilon_s)(\epsilon_p + \epsilon_r - \epsilon_q - \epsilon_t)}, \quad (111)$$

$$\Omega3g1 = (-1)^{3+2} \left(\frac{1}{2}\right) \sum_{p,q,r,s,t}^{\text{denom.1}\neq 0, \text{denom.2}\neq 0} \times \frac{\langle qs \parallel pr \rangle \langle F_{ts} - \mu^{(1)}\delta_{ts} \rangle \langle pr \parallel qt \rangle f_p^+ f_q^- f_r^+ f_s^- f_t^-}{(\epsilon_q + \epsilon_s - \epsilon_p - \epsilon_r)(\epsilon_q + \epsilon_t - \epsilon_p - \epsilon_r)}, \quad (112)$$

$$\Omega3h1 = (-1)^{2+1} \sum_{p,q,r,s}^{\text{denom.1}\neq 0, \text{denom.2}\neq 0} \times \frac{\langle F_{qp} - \mu^{(1)}\delta_{qp} \rangle \langle F_{rs} - \mu^{(1)}\delta_{rs} \rangle \langle ps \parallel rq \rangle f_p^+ f_q^- f_r^- f_s^+}{(\epsilon_q - \epsilon_p)(\epsilon_q + \epsilon_r - \epsilon_p - \epsilon_s)}, \quad (113)$$

$$\Omega3i1 = (-1)^{2+1} \sum_{p,q,r,s}^{\text{denom.1}\neq 0, \text{denom.2}\neq 0} \times \frac{\langle F_{pq} - \mu^{(1)}\delta_{pq} \rangle \langle rq \parallel ps \rangle \langle F_{sr} - \mu^{(1)}\delta_{sr} \rangle f_p^- f_q^+ f_r^- f_s^+}{(\epsilon_p - \epsilon_q)(\epsilon_r - \epsilon_s)}, \quad (114)$$

$$\Omega3j1 = (-1)^{1+1} \sum_{p,q,r}^{\text{denom.1}\neq 0, \text{denom.2}\neq 0} \times \frac{\langle F_{pq} - \mu^{(1)}\delta_{pq} \rangle \langle F_{qr} - \mu^{(1)}\delta_{qr} \rangle \langle F_{rp} - \mu^{(1)}\delta_{rp} \rangle f_p^- f_q^+ f_r^+}{(\epsilon_p - \epsilon_q)(\epsilon_p - \epsilon_r)}, \quad (115)$$

and

$$\Omega3k1 = (-1)^{2+1} \sum_{p,q,r}^{\text{denom.1}\neq 0, \text{denom.2}\neq 0} \times \frac{\langle F_{qp} - \mu^{(1)}\delta_{qp} \rangle \langle F_{rq} - \mu^{(1)}\delta_{rq} \rangle \langle F_{pr} - \mu^{(1)}\delta_{pr} \rangle f_p^+ f_q^- f_r^-}{(\epsilon_q - \epsilon_p)(\epsilon_r - \epsilon_p)}. \quad (116)$$

The algebraic formulas for the accompanying renormalization and anomalous diagrams can be inferred from these formulas by a systematic modification of the denominators, summation restrictions, and prefactors. Therefore, despite the numerousness of these third-order diagrams, their algebraic evaluations and computer implementation are not as horrendous as they seem.

In the zero-temperature MBPT, $\Omega3B$ and $\Omega3C$ ($\Omega3E$ and $\Omega3F$ also) are a pair of conjugated diagrams,⁶³ whose values are the complex conjugate of each other. In the finite-temperature formalism, renormalization diagrams destroy such time-reversal symmetry at a diagram level (not at the whole theory level), and we need to evaluate $\Omega3B$ and $\Omega3C$ separately, for they have values that are not simply related to each other.

The last three diagrams of Fig. 12 are interpreted as

$$\Omega3m = (-1)^{1+1} \frac{(-\beta)}{2!} \sum_p \langle F_{pp} - \mu^{(1)} \rangle \langle -\mu^{(2)} \rangle f_p^- f_p^+, \quad (117)$$

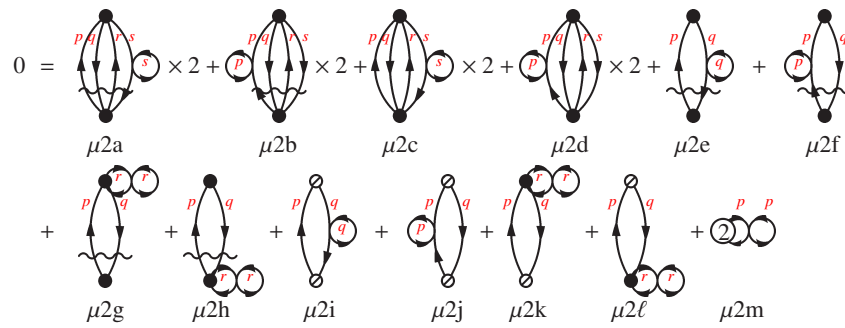
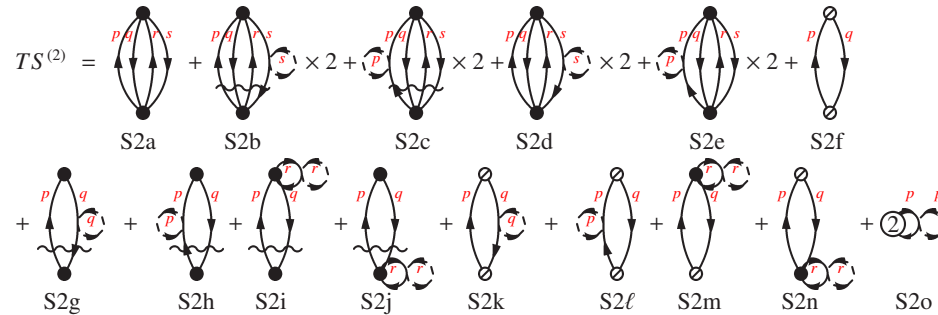
$$\Omega3o = (-1)^{1+1} \sum_p \langle -\mu^{(3)} \rangle f_p^- = -\mu^{(3)} \bar{N}. \quad (118)$$

Diagrams $\Omega3m$ and $\Omega3n$ are a pair of conjugate diagrams (since they are not renormalization diagrams), and the algebraic formula of the latter is the same as Eq. (117).

D. Fourth order

At the fourth order, enumerating and interpreting diagrams manually is no longer practicable and a computerized scheme⁷⁶ may be necessary (not pursued in this study). Here, we focus on how to generate renormalization diagrams, which may be the least trivial step of the diagram enumeration. The n th-order anomalous diagrams are straightforwardly spawned by simply eliminating resolvents in all $2^{n-1} - 1$ ways.

Figure 19 illustrates how all renormalization diagrams are generated systematically from a normal diagram. The latter has exactly one resolvent line in between every pair of adjacent vertexes. The corresponding renormalization diagrams

FIG. 10. Diagrammatic equation of $\mu^{(2)}$.FIG. 11. Diagrammatic equation of $S^{(2)}$.

are obtained by shifting one or more (up to $n - 2$) resolvent lines upwards in all distinct ways. However, it may be safer to use the method of the Brueckner brackets,^{66,70} which enumerates all renormalization terms by indicating how various operators are Wick contracted in such a way that the result is unlinked (in the case of MPPT). In our case, many reference states are degenerate and these brackets are not necessarily unlinked, as emphasized earlier.

For instance, the first renormalization diagram (the second diagram) in the figure corresponds to the Brueckner bracket,

$$\begin{aligned} \langle VRVR \langle V \rangle RV \rangle &= \langle \overline{VR} \overline{VR} \langle V \rangle \overline{RV} \rangle \\ &= \langle \overline{VR} \overline{RR} \overline{VPV} \rangle, \end{aligned} \quad (119)$$

where V stands for \hat{V} , P for \hat{P}_I , R for \hat{R}_I , and $\langle \dots \rangle$ is a thermal average, i.e., $\langle \langle I | \dots | I \rangle \rangle$. Associating V 's from left to right with the vertices from top to bottom, Eq. (119) is the diagram in which there is one resolvent in between the first (top) and second vertexes, two in between the second and third, and none in between the third and fourth (bottom). In other words, the bottom resolvent has been shifted up to the middle. The parity associated with this bracket is (-1) because there is one insertion (one inner bracket),^{63,70} and this factor is properly accounted for by Rule 13 of Table II. The fourth diagram in Fig. 19 is an example of double insertions,^{63,70} whose parity is $(-1)^2$. Generally, an n -tuple insertion or n -fold nested insertion carries a factor of $(-1)^n$.

There should also be anomalous-renormalization diagrams.

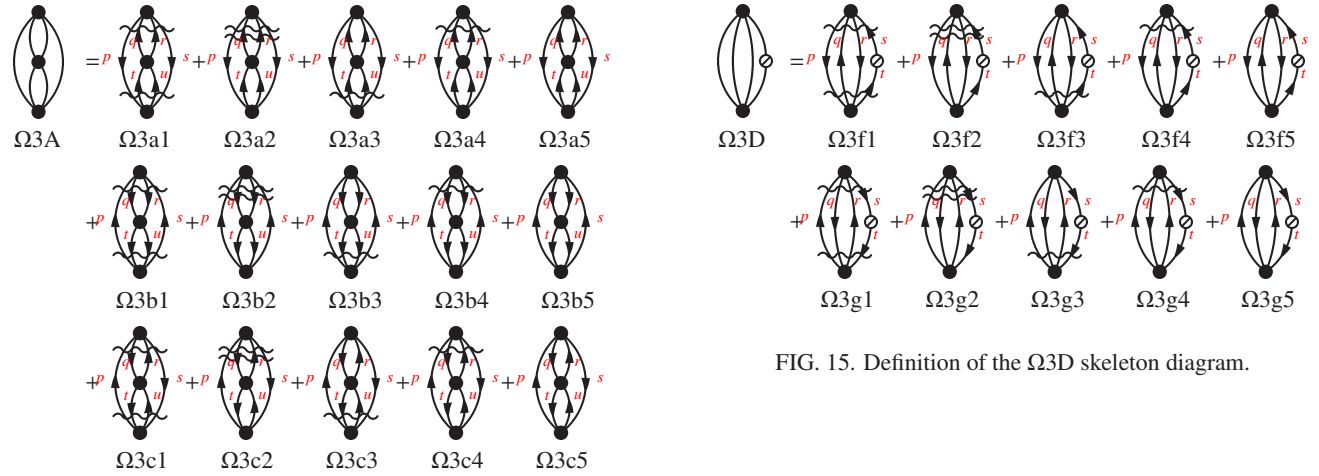
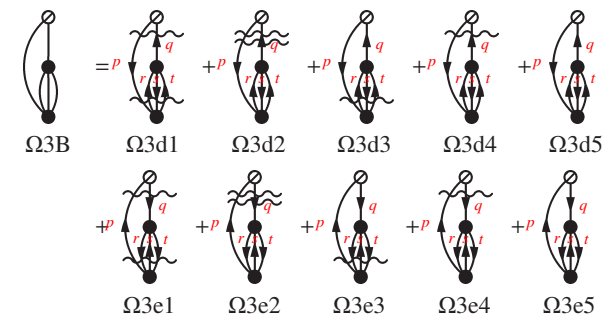
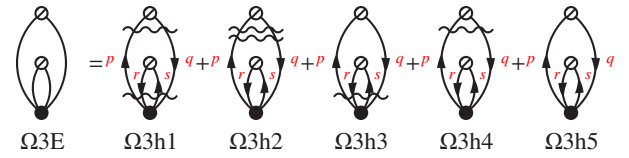
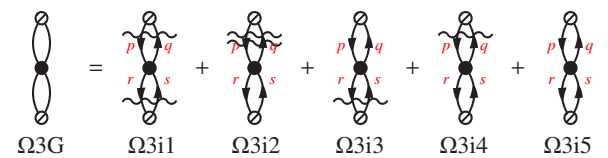
V. LINKED-DIAGRAM THEOREM

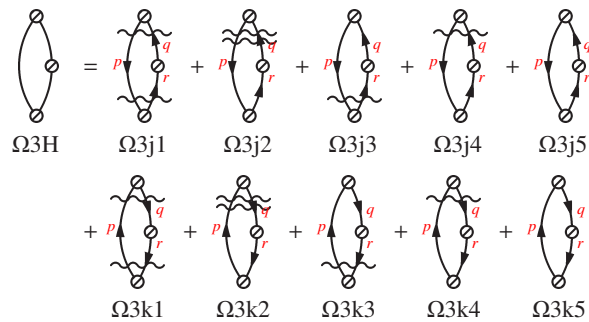
We have established in Eqs. (50) and (62) that $\Omega^{(1)}$ and $\Omega^{(2)}$ are diagrammatically linked and thus size-consistent. We may summarize this as

$$\Omega^{(1)} = \langle D_I^{(1)} \rangle = \langle D_I^{(1)} \rangle_L, \quad (120)$$

$$\begin{aligned} \Omega^{(2)} &= \langle D_I^{(2)} \rangle + \frac{(-\beta)}{2!} (\langle D_I^{(1)} D_I^{(1)} \rangle - \Omega^{(1)} \Omega^{(1)}) \\ &= \langle D_I^{(2)} \rangle_L + \frac{(-\beta)}{2!} (\langle D_I^{(1)} D_I^{(1)} \rangle - \langle D_I^{(1)} \rangle_L \langle D_I^{(1)} \rangle_L) \\ &= \langle D_I^{(2)} \rangle_L + \frac{(-\beta)}{2!} \langle D_I^{(1)} D_I^{(1)} \rangle_L, \end{aligned} \quad (121)$$

$$\Omega^{(3)} = \Omega_{3A} + \Omega_{3B} + \Omega_{3C} + \Omega_{3D} + \Omega_{3E} + \Omega_{3F} + \Omega_{3G} + \Omega_{3H} + \Omega_{3m} + \Omega_{3n} + \Omega_{3o}$$

FIG. 12. Diagrammatic equation of $\Omega^{(3)}$.FIG. 15. Definition of the Ω_{3D} skeleton diagram.FIG. 13. Definition of the Ω_{3A} skeleton diagram.FIG. 14. Definition of the Ω_{3B} skeleton diagram.FIG. 16. Definition of the Ω_{3E} skeleton diagram.FIG. 17. Definition of the Ω_{3G} skeleton diagram.

FIG. 18. Definition of the Ω_{3H} skeleton diagram.

where subscript L means linked. These can be used to show that $\Omega^{(3)}$ is also linked:

$$\begin{aligned} \Omega^{(3)} &= \langle D_I^{(3)} \rangle + \frac{(-\beta)}{2!} (\langle D_I^{(1)} D_I^{(2)} \rangle - \Omega^{(1)} \Omega^{(2)}) \\ &\quad + \frac{(-\beta)}{2!} (\langle D_I^{(2)} D_I^{(1)} \rangle - \Omega^{(2)} \Omega^{(1)}) \\ &\quad + \frac{(-\beta)^2}{3!} (\langle D_I^{(1)} D_I^{(1)} D_I^{(1)} \rangle - \Omega^{(1)} \Omega^{(1)} \Omega^{(1)}) \end{aligned} \quad (122)$$

$$\begin{aligned} &= \langle D_I^{(3)} \rangle_L + \frac{(-\beta)}{2!} (\langle D_I^{(1)} D_I^{(2)} \rangle - \langle D_I^{(1)} \rangle_L \langle D_I^{(2)} \rangle_L) \\ &\quad + \frac{(-\beta)}{2!} (\langle D_I^{(2)} D_I^{(1)} \rangle - \langle D_I^{(2)} \rangle_L \langle D_I^{(1)} \rangle_L) \\ &\quad + \frac{(-\beta)^2}{3!} (\langle D_I^{(1)} D_I^{(1)} D_I^{(1)} \rangle - 3 \langle D_I^{(1)} \rangle_L \langle D_I^{(1)} D_I^{(1)} \rangle_L \\ &\quad - \langle D_I^{(1)} \rangle_L \langle D_I^{(1)} \rangle_L \langle D_I^{(1)} \rangle_L) \end{aligned} \quad (123)$$

$$\begin{aligned} &= \langle D_I^{(3)} \rangle_L + \frac{(-\beta)}{2!} \langle D_I^{(1)} D_I^{(2)} \rangle_L + \frac{(-\beta)}{2!} \langle D_I^{(2)} D_I^{(1)} \rangle_L \\ &\quad + \frac{(-\beta)^2}{3!} \langle D_I^{(1)} D_I^{(1)} D_I^{(1)} \rangle_L. \end{aligned} \quad (124)$$

They lead us to speculate that the recursion of $\Omega^{(n)}$ [Eq. (15)] is always reducible to a linked form:

$$\begin{aligned} \Omega^{(n)} &= \langle D_I^{(n)} \rangle + \frac{(-\beta)}{2!} \sum_{i=1}^{n-1} (\langle D_I^{(i)} D_I^{(n-i)} \rangle - \Omega^{(i)} \Omega^{(n-i)}) \\ &\quad + \frac{(-\beta)^2}{3!} \sum_{i=1}^{n-2} \sum_{j=1}^{n-i-1} (\langle D_I^{(i)} D_I^{(j)} D_I^{(n-i-j)} \rangle - \Omega^{(i)} \Omega^{(j)} \Omega^{(n-i-j)}) \\ &\quad + \dots + \frac{(-\beta)^{n-1}}{n!} (\langle (D_I^{(1)})^n \rangle - (\Omega^{(1)})^n) \end{aligned} \quad (125)$$

$$\begin{aligned} &= \langle D_I^{(n)} \rangle_L + \frac{(-\beta)}{2!} \sum_{i=1}^{n-1} \langle D_I^{(i)} D_I^{(n-i)} \rangle_L \\ &\quad + \frac{(-\beta)^2}{3!} \sum_{i=1}^{n-2} \sum_{j=1}^{n-i-1} \langle D_I^{(i)} D_I^{(j)} D_I^{(n-i-j)} \rangle_L \\ &\quad + \dots + \frac{(-\beta)^{n-1}}{n!} \langle (D_I^{(1)})^n \rangle_L. \end{aligned} \quad (126)$$

This is indeed the case, and has already been implicit in the diagrammatic rules presented in Sec. IV. A proof of this assertion is given here as the linked-diagram theorem at finite temperature.

The proof consists of two parts: First, we show that $\langle D^{(n)} \rangle$ is always linked by relying heavily on the linked-diagram theorem at zero temperature.^{63,65–71} Second, we prove that the unlinked terms in the subsequent sums in Eq. (125) are cancelled out exactly. Note that the cancellation does not complete within each parenthesis, and we have to consider the recursion holistically.

Using the $\langle E^{(n)} \rangle$ recursion in Sec. II C, we can rewrite $\langle D^{(n)} \rangle$ as

$$\langle D^{(n)} \rangle = \langle E^{(n)} \rangle - \mu^{(n)} \bar{N} \quad (127)$$

$$= \langle \langle \Phi_I^{(0)} | \hat{V} | \Phi_I^{(n-1)} \rangle \rangle - (\mu^{(n)} \bar{N})_L \quad (128)$$

$$= \langle \langle \Phi_I^{(0)} | \hat{V} \hat{R}_I \hat{V} | \Phi_I^{(n-2)} \rangle \rangle$$

$$- \sum_{i=1}^{n-2} \langle \sum_J \langle \Phi_I^{(0)} | \hat{V} \hat{R}_I | \Phi_J^{(n-1-i)} \rangle E_{JI}^{(i)} \rangle - (\mu^{(n)} \bar{N})_L, \quad (129)$$

where $\mu^{(n)} \bar{N}$ is linked despite the fact that it is a product of two scalars. This is because $\mu^{(n)}$ is intensive.⁶⁴

As emphasized, at finite temperature the second term (the renormalization term) consists of both unlinked and linked contributions. Factors $E_{JI}^{(i)}$ and $\langle \Phi_I^{(0)} | \hat{V} \hat{R}_I | \Phi_J^{(n-1-i)} \rangle$ are proven by induction (see below) to be individually linked, but not necessarily to each other. The unlinked contribution comes from the diagonal elements $E_{II}^{(i)}$, making the corresponding summand a product of two extensive scalars. Its off-diagonal elements $E_{JI}^{(i)}$ ($J \neq I$) are linked to the $\langle \Phi_I^{(0)} | \hat{V} \hat{R}_I | \Phi_J^{(n-1-i)} \rangle$ part via J , which is degenerate with but distinct from I .

Therefore, we can further rewrite the salient portion of the right-hand side of Eq. (129) as

$$\begin{aligned} &\langle \langle \Phi_I^{(0)} | \hat{V} \hat{R}_I \hat{V} | \Phi_I^{(n-2)} \rangle \rangle - \sum_{i=1}^{n-2} \langle \sum_J \langle \Phi_I^{(0)} | \hat{V} \hat{R}_I | \Phi_J^{(n-1-i)} \rangle E_{JI}^{(i)} \rangle \\ &= \langle \langle \Phi_I^{(0)} | \hat{V} \hat{R}_I \hat{V} | \Phi_I^{(n-2)} \rangle \rangle_L - \sum_{i=1}^{n-2} \langle \sum_J \langle \Phi_I^{(0)} | \hat{V} \hat{R}_I | \Phi_J^{(n-1-i)} \rangle E_{JI}^{(i)} \rangle_L \\ &\quad + \langle \langle \Phi_I^{(0)} | \hat{V} \hat{R}_I \hat{V} | \Phi_I^{(n-2)} \rangle \rangle_U - \sum_{i=1}^{n-2} \langle \sum_J \langle \Phi_I^{(0)} | \hat{V} \hat{R}_I | \Phi_J^{(n-1-i)} \rangle E_{JI}^{(i)} \rangle_U \\ &= \langle \langle \Phi_I^{(0)} | \hat{V} \hat{R}_I \hat{V} | \Phi_I^{(n-2)} \rangle \rangle_L - \sum_{i=1}^{n-2} \langle \sum_{J \neq I} \langle \Phi_I^{(0)} | \hat{V} \hat{R}_I | \Phi_J^{(n-1-i)} \rangle E_{JI}^{(i)} \rangle_L \\ &\quad + \langle \langle \Phi_I^{(0)} | \hat{V} \hat{R}_I \hat{V} | \Phi_I^{(n-2)} \rangle \rangle_U - \sum_{i=1}^{n-2} \langle \langle \Phi_I^{(0)} | \hat{V} \hat{R}_I | \Phi_I^{(n-1-i)} \rangle E_{II}^{(i)} \rangle_U, \end{aligned} \quad (130)$$

where subscript U means unlinked. The identical line of logic proving the linked-diagram theorem at zero temperature can be used to show that the last two terms cancel each other out,

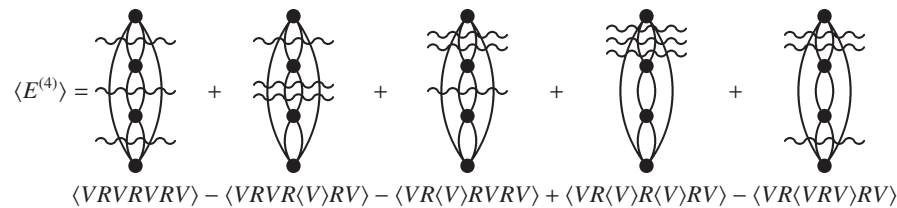


FIG. 19. A normal diagram (the leftmost) and its renormalization diagrams in $\langle E_I^{(4)} \rangle$ and their corresponding Brueckner brackets. Each wiggly line represents a resolvent. Line directions and line labels are suppressed. Signs in front of the Brueckner brackets are absorbed in the algebraic interpretations of the respective diagrams.

leaving only the linked contributions, i.e.,

$$\begin{aligned}
 & \langle \langle \Phi_I^{(0)} | \hat{V} \hat{R}_I \hat{V} | \Phi_I^{(n-2)} \rangle \rangle - \sum_{i=1}^{n-2} \langle \sum_J \langle \Phi_I^{(0)} | \hat{V} \hat{R}_I | \Phi_J^{(n-1-i)} \rangle E_{JI}^{(i)} \rangle \\
 & = \langle \langle \Phi_I^{(0)} | \hat{V} \hat{R}_I \hat{V} | \Phi_I^{(n-2)} \rangle \rangle_L - \sum_{i=1}^{n-2} \langle \sum_{J \neq I} \langle \Phi_I^{(0)} | \hat{V} \hat{R}_I | \Phi_J^{(n-1-i)} \rangle E_{JI}^{(i)} \rangle_L.
 \end{aligned} \tag{131}$$

The reader is referred to Chapter 6 of Shavitt and Bartlett⁶³ or Manne⁷⁰ for the time-independent proof of the linked-diagram theorem of the zero-temperature MBPT, which can be easily seen to be applicable to the thermal averages with no modification.

Next, we prove that the second and subsequent terms in Eq. (125) are linked by virtue of a systematic cancellation of all unlinked terms between $\langle D_I^{(i_1)} \dots D_I^{(i_k)} \rangle$ ($2 \leq k \leq m$) and the products of $\Omega^{(i)}$'s. We borrow equations in Appendix B only for notational clarity.

Let us define $A^{(n)}$ and $B^{(n)}$ by

$$\begin{aligned}
 A^{(n)} & = (-\beta) \Omega^{(n)}, \\
 B^{(n)} & = (-\beta) \langle D_I^{(n)} \rangle + \frac{(-\beta)^2}{2!} \sum_{i=1}^{n-1} \langle D_I^{(i)} D_I^{(n-i)} \rangle \\
 & \quad + \frac{(-\beta)^3}{3!} \sum_{i=1}^{n-2} \sum_{j=1}^{n-i-1} \langle D_I^{(i)} D_I^{(j)} D_I^{(n-i-j)} \rangle \\
 & \quad + \dots + \frac{(-\beta)^n}{n!} \langle (D_I^{(1)})^n \rangle.
 \end{aligned} \tag{132}$$

Equation (125) can then be identified as Eq. (B2) with these definitions of $A^{(n)}$ and $B^{(n)}$. Furthermore, if we divide $B^{(n)}$ into the linked and unlinked parts,

$$B^{(n)} = (B^{(n)})_L + (B^{(n)})_U, \tag{134}$$

the unlinked part is a sum of products of the linked part, having the following exponential structure:⁷⁷

$$\begin{aligned}
 (B^{(n)})_U & = \frac{1}{2!} \sum_{i=1}^{n-1} (B^{(i)})_L (B^{(n-i)})_L \\
 & \quad + \frac{1}{3!} \sum_{i=1}^{n-2} \sum_{j=1}^{n-i-1} (B^{(i)})_L (B^{(j)})_L (B^{(n-i-j)})_L \\
 & \quad + \dots + \frac{1}{n!} (B^{(1)})_L^n.
 \end{aligned} \tag{135}$$

This means

$$\begin{aligned}
 B^{(n)} & = (B^{(n)})_L + \frac{1}{2!} \sum_{i=1}^{n-1} (B^{(i)})_L (B^{(n-i)})_L \\
 & \quad + \frac{1}{3!} \sum_{i=1}^{n-2} \sum_{j=1}^{n-i-1} (B^{(i)})_L (B^{(j)})_L (B^{(n-i-j)})_L \\
 & \quad + \dots + \frac{1}{n!} (B^{(1)})_L^n.
 \end{aligned} \tag{136}$$

Comparing this with Eq. (B3), we immediately surmise $A^{(n)} = (B^{(n)})_L$, proving the linkedness of $\Omega^{(n)}$.

VI. NUMERICAL BENCHMARKS

A. General-order algorithms

The recursion relationships for the grand canonical ensemble in Sec. II and those for the canonical ensemble in Appendix A have been implemented in a determinant-based FCI program. The algorithms are literal translations of those equations. They enable calculations of $\mu^{(n)}$, $\Omega^{(n)}$, and $U^{(n)}$ in the grand canonical ensemble and $F^{(n)}$ and $U^{(n)}$ in the canonical ensemble for an ideal gas of the smallest molecules at any arbitrary perturbation order, while $S^{(n)}$ can be inferred from them. These calculations are more expensive than FCI itself and are not intended for realistic applications. Instead, they are meant to furnish benchmark data^{53,59,78–83} to assess the validity of the theories and the correctness of more efficient algorithms^{84–88} based on reduced analytical formulas to be developed in the future. The latter algorithms should have the same cost scaling as their respective zero-temperature counterparts, and be applicable to solids in the grand canonical ensemble.^{89,90} Practical utility of the canonical ensemble, which does not lend itself to reduced analytical formulas, is doubtful at this point.

We have also implemented the reduced analytical formulas of $\Omega^{(n)}$, $\mu^{(n)}$, $U^{(n)}$, and $S^{(n)}$ in the grand canonical ensemble in the range of $0 \leq n \leq 3$. We already implemented the analytical formulas for $n \leq 2$ in our previous studies.^{54,55} That of $\Omega^{(3)}$ derived in Sec. IV C has been manually implemented. The analytical formulas for $\mu^{(3)}$, $U^{(3)}$, and $S^{(3)}$ have then been directly computer-programmed by systematic modifications of the $\Omega^{(3)}$ code. The derivations at higher n would be extremely tedious and need to be computerized.⁷⁶

We have repeated the λ -variation calculations in both ensembles up to a higher order than previously reported.^{53,62} A λ -variation calculation^{53,59} determines the several lowest-order perturbation corrections by numerical differentiation with respect to λ of the thermodynamic functions obtained by the finite-temperature FCI (Ref. 57) with a perturbation-scaled Hamiltonian, $\hat{H} = \hat{H}_0 + \lambda\hat{V}$. The lower-order data already reported in our previous studies are reproduced by the present calculations. The new data at higher orders are not necessarily precise because of the round-off and finite-difference errors, which have been detected by the disagreements among different finite-difference formulas (not shown).

B. Grand canonical ensemble

Tables III, IV, and V compile the thermodynamic functions in the grand canonical ensemble at $T = 10^5$, 10^6 , and 10^7 K, respectively, of an ideal gas of the identical hydrogen fluoride molecules (0.9168 Å) in the STO-3G basis set.^{53,57,62} The gas consists of infinitely many nonrotating rigid hydrogen fluoride molecules that are not interacting with one another except to exchange electrons. The system and temperatures considered are unrealistic, only serving as a convenient test case for formalisms and computer codes, although a similar atomic calculation might be relevant to the Saha ionization equation.^{91,92} The zero-temperature canonical HF wave function for the singlet ground state has been used as the reference.

In all cases, $\Omega^{(n)}$, $\mu^{(n)}$, and $U^{(n)}$ computed by the sum-over-states (recursion) and sum-over-orbitals (reduced analytical) formulas agree with each other for at least ten decimal places, verifying the formulas and computer programs mutually.

At $T = 10^5$ K, they display a clear sign of divergence. This may not be surprising in light of the fact that HCPT for many states are already divergent.⁵⁹ This is a different type of divergence than discovered by Kohn and Luttinger⁴⁸ and analyzed by us.⁵⁶ The latter is concerned with the zero-temperature limit, at which the radius of convergence is zero under some circumstances,⁵⁶ whereas the former should have a finite radius of convergence, the rate of which may be accelerated by, e.g., the Padé approximant.^{79,93-95} At lower temperatures (not shown), $U^{(n)}$ reproduces $E^{(n)}$ for the reference state computed by the zero-temperature MBPT, and is much less prone to divergence (see, however, Ref. 96). At $T = 10^6$ and 10^7 K, the thermodynamic functions are rapidly convergent at the respective finite-temperature FCI values. At 10^7 K, the tenth-order approximations are within $10^{-7} E_h$ of FCI, testifying that the finite-temperature MBPT presented here is a converging series of approximation towards exactness. This would not be the case if the renormalization diagrams were overlooked or neglected.

At $T = 10^5$ K, the λ -variation method turns out to be surprisingly accurate. It remains somewhat useful up to the fifth order. At $T = 10^6$ and 10^7 K, it breaks down at lower orders, hardly serving as a benchmark even for the second-order corrections. The stability of the λ -variation method may be anticorrelated with the convergence of the perturbation series. At lower temperatures (not shown), the finite-

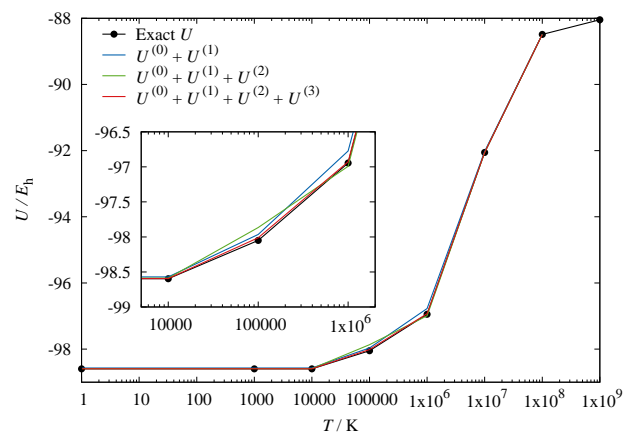


FIG. 20. $U^{(0)} + \dots + U^{(n)}$ ($1 \leq n \leq 3$) as a function of temperature for the same system as Table III.

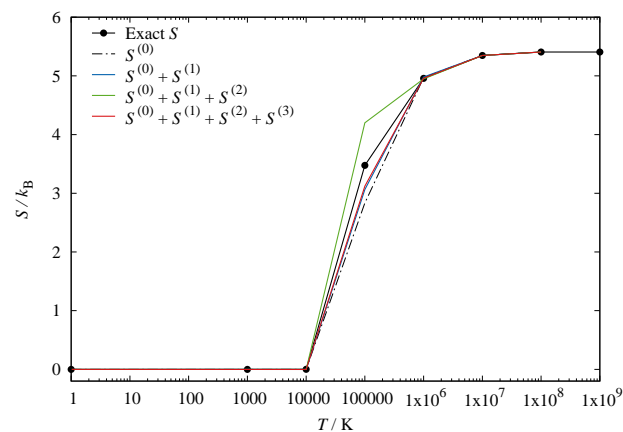


FIG. 21. $S^{(0)} + \dots + S^{(n)}$ ($0 \leq n \leq 3$) as a function of temperature for the same system as Table III.

temperature FCI (and hence the λ -variation also) becomes unstable because of the inherent difficulty of precisely determining μ . At $T = 0$, any value of μ falling in between the highest-occupied (HOMO) and lowest-unoccupied molecular orbital (LUMO) energies satisfies the electroneutrality condition, making it increasingly difficult for μ to reach the correct zero-temperature limit,^{56,57} which is the midpoint of HOMO and LUMO. Nevertheless, for the temperatures used in these tables, analytical results and the λ -variation benchmarks are in reasonable agreement.

Figures 20 and 21 plot the perturbation approximations to U and S and their FCI values as a function of temperature. It can be seen that the perturbation approximations are so accurate that they are indiscernible from the FCI curves at both low and high temperatures. Only at mid-temperatures ($10^4 \leq T/K \leq 10^6$) are the differences noticeable. This is the same temperature domain where these thermodynamic functions exhibit strong temperature dependence and the perturbation series tend to diverge. Still, low-order perturbation theories seem to work well, correcting the vast majority of the discrepancies between the zeroth-order (Fermi-Dirac) theory

TABLE III. Perturbation corrections to the thermodynamic functions of an ideal gas of the hydrogen fluoride molecules (0.9168 Å in STO-3G) in the grand canonical ensemble at $T = 10^5$ K.

n	$\Omega^{(n)} / E_h$			$\mu^{(n)} / E_h$			$U^{(n)} / E_h$		
	Recursion ^a	Analytical ^b	λ -variation ^c	Recursion ^a	Analytical ^b	λ -variation ^c	Recursion ^a	Analytical ^b	λ -variation ^c
0	-55.63656	-55.63656	-55.63656	0.27224	0.27224	0.27224	-52.01659	-52.01659	-52.01659
1	-45.26843	-45.26843	-45.26843	-0.07519	-0.07519	-0.07519	-45.94786	-45.94786	-45.94786
2	-2.58148	-2.58148	-2.58147	0.23198	0.23198	0.23198	0.09841	0.09841	0.09841
3	4.41331	4.41331	4.41356	-0.42177	-0.42177	-0.42180	-0.14604	-0.14604	-0.14602
4	-9.72934		-9.73864	0.92740		0.92833	-0.17127		-0.17196
5	22.27604		22.18099	-2.13089		-2.12063	0.72367		0.71965
6	-53.38526			5.11603			-2.94946		
7	129.97820			-12.46129			10.60352		
8	-311.27100			29.81298			-38.		
9	713.88281			-67.96933			121.		
10	-1661.6			147.87702			3888.		
\sum_0^{10}	-1268.9			101.17918			3881.		
FCI ^d	-102.10659			0.29568			-98.04938		

^a MBPT(n) recursions. The entries with fewer significant figures suffer from large round-off errors.

^b MBPT(n) reduced analytical formulas.

^c Central seven-point formula with $\Delta\lambda = 0.01$. See also Ref. 53

^d Finite-temperature full configuration interaction. See also Ref. 57

TABLE IV. Same as Table III but at $T = 10^6$ K.

n	$\Omega^{(n)} / E_h$			$\mu^{(n)} / E_h$			$U^{(n)} / E_h$		
	Recursion ^a	Analytical ^b	λ -variation ^c	Recursion ^a	Analytical ^b	λ -variation ^c	Recursion ^a	Analytical ^b	λ -variation ^c
0	-105.94753	-105.94753	-105.94753	3.96130	3.96130	3.96130	-50.59635	-50.59635	-50.59635
1	-44.52564	-44.52564	-44.52564	-0.16896	-0.16896	-0.16896	-46.17665	-46.17665	-46.17665
2	-0.96431	-0.96431	-0.96425	0.08509	0.08509	0.08509	-0.21984	-0.21984	-0.21983
3	0.24939	0.24939	0.25774	-0.02270	-0.02270	-0.02353	0.06464	0.06464	0.06648
4	-0.07381		-0.45286	0.00676		0.04467	-0.02389		-0.10720
5	0.02296		-15.64135	-0.00210		1.56433	0.00945		-3.44242
6	-0.00699			0.00063			-0.00373		
7	0.00187			-0.00017			0.00140		
8	-0.00032			0.00003			-0.00048		
9	-0.00005			0.00001			0.00014		
10	0.00009			-0.00001			-0.00002		
\sum_0^{10}	-151.24436			3.85989			-96.94533		
FCI ^d	-151.24440			3.85990			-96.94534		

^a MBPT(n) recursions.

^b MBPT(n) reduced analytical formulas.

^c Central seven-point formula with $\Delta\lambda = 0.01$. See also Ref. 53

^d Finite-temperature full configuration interaction. See also Ref. 57

and FCI in U ($U^{(0)}$ is not shown in Fig. 20 because it is far outside the graph). For S , the first-order approximation over-corrects the errors in $S^{(0)}$ in this temperature domain, while the second- and third-order approximations roughly halve the errors. Given the divergence of the underlying perturbation series at these temperatures, the lower-order perturbation theories are promising.

C. Canonical ensemble

Thermodynamic functions in the canonical ensemble have been calculated for the same system as Sec. VI B. The results at $T = 10^5$, 10^6 , and 10^7 K are summarized in Tables VI, VII,

and VIII, respectively. Only the sum-over-states (recursion) formulas and λ -variation method are available for this ensemble.

Owing to the much fewer number of states involved in the canonical ensemble, the thermodynamic functions are less prone to divergence and the λ -variation method tends to be more accurate. At $T = 10^6$ and 10^7 K, the tenth-order perturbation theory agrees with FCI for five and ten decimal places, respectively, which attests to the convergence of the perturbation series to exactness at any temperature unless they diverge.

TABLE V. Same as Table III but at $T = 10^7$ K.

n	$\Omega^{(n)} / E_h$			$\mu^{(n)} / E_h$			$U^{(n)} / E_h$		
	Recursion ^a	Analytical ^b	λ -variation ^c	Recursion ^a	Analytical ^b	λ -variation ^c	Recursion ^a	Analytical ^b	λ -variation ^c
0	-686.70814	-686.70814	-686.70814	47.15012	47.15012	47.15012	-45.78911	-45.78911	-45.78911
1	-43.19911	-43.19911	-43.19911	-0.29811	-0.29811	-0.29811	-46.23554	-46.23554	-46.23554
2	-0.19696	-0.19696	-0.19691	0.01774	0.01774	0.01774	-0.03260	-0.03260	-0.03258
3	0.00951	0.00951	0.05365	-0.00088	-0.00088	-0.00529	0.00179	0.00179	0.01333
4	-0.00053		1.45717	0.00005		-0.14572	-0.00013		0.38065
5	0.00003		-44.48327	-0.00000		4.44833	0.00001		-11.63101
6	-0.00000			0.00000			-0.00000		
7	0.00000			-0.00000			0.00000		
8	-0.00000			0.00000			-0.00000		
9	0.00000			-0.00000			0.00000		
10	-0.00000			0.00000			-0.00000		
\sum_0^{10}	-730.09519			46.86892			-92.05557		
FCI ^d	-730.09519			46.86892			-92.05557		

^a MBPT(n) recursions.^b MBPT(n) reduced analytical formulas.^c Central seven-point formula with $\Delta\lambda = 0.01$. See also Ref. 53^d Finite-temperature full configuration interaction. See also Ref. 57TABLE VI. Perturbation corrections to the thermodynamic functions of an ideal gas of the hydrogen fluoride molecules (0.9168 Å in STO-3G) in the canonical ensemble at $T = 10^5$ K.

n	$F^{(n)} / E_h$		$U^{(n)} / E_h$	
	Recursion ^a	λ -variation ^b	Recursion ^a	λ -variation ^b
0	-52.67166	-52.67166	-52.26452	-52.26452
1	-46.16315	-46.16315	-45.69442	-45.69442
2	-0.14657	-0.14657	-0.02151	-0.02151
3	-0.05239	-0.05239	-0.16648	-0.16648
4	0.00162	0.00162	-0.08826	-0.08826
5	0.01117	0.01121	0.01989	0.02029
6	0.00359		0.05664	
7	-0.00346		-0.5	
8	0.04590		16.	
9	-0.39063		-562.	
10	-36.6		22464.	
\sum_0^{10}	-136.0		21820.	
FCI ^c	-99.02043		-98.17836	

^a MBPT(n) recursions. The entries with fewer significant figures suffer from large round-off errors.^b Central seven-point formula with $\Delta\lambda = 0.01$. See also Ref. 62.^c Finite-temperature full configuration interaction. See also Ref. 57.

VII. CONCLUSIONS

We have fully developed the finite-temperature MBPT that expands all thermodynamic functions in uniform perturbation series. Both grand canonical and canonical ensembles are considered, although only the former lends itself to more drastic mathematical simplifications, making it useful for condensed-matter applications. The Rayleigh–Schrödinger-like algebraic recursions have been obtained for both, yielding their sum-over-states analytical formulas of all thermodynamic functions at any arbitrary order.

For the grand canonical ensemble, the sum-over-states for-

TABLE VII. Same as Table VI but at $T = 10^6$ K.

n	$F^{(n)} / E_h$		$U^{(n)} / E_h$	
	Recursion ^a	λ -variation ^b	Recursion ^a	λ -variation ^b
0	-62.55550	-62.55550	-50.62284	-50.62284
1	-46.77859	-46.77859	-46.71663	-46.71663
2	-0.01647	-0.01647	-0.03420	-0.03420
3	0.00030	0.00030	0.00090	0.00090
4	0.00000	0.00000	0.00000	0.00000
5	-0.00000	0.00001	-0.00000	0.00002
6	0.00000		0.00000	
7	0.00000		-0.00000	
8	-0.00000		0.00000	
9	-0.00000		-0.00000	
10	0.00000		-0.00000	
\sum_0^{10}	-109.35026		-97.37278	
FCI ^c	-109.35026		-97.37278	

^a MBPT(n) recursions.^b Central seven-point formula with $\Delta\lambda = 0.01$. See also Ref. 62.^c Finite-temperature full configuration interaction. See also Ref. 57.

mulas have been transformed to sum-over-orbitals analytical formulas by the method of normal-ordered second quantization at finite temperature. The rules of Wick contractions and various operators in the normal-ordered form have been derived (as opposed to postulated) and how they are practically applied to integral and thermal-average evaluations has been illustrated. Feynman diagrammatic rules are then introduced as a straightforward graphical representation of Wick contractions as lines and of molecular integrals as vertexes. Nowhere in this formulation do we resort to time-dependent logic^{46–51} or human intuitions to exhaustively enumerate all valid diagrams, which include the renormalization, anomalous, and anomalous-renormalization diagrams.

Normal ordering regroups the Hamiltonian operator into the finite-temperature HF energy, finite-temperature Fock matrix

TABLE VIII. Same as Table VI but at $T = 10^7$ K.

n	$F^{(n)} / E_h$		$U^{(n)} / E_h$	
	Recursion ^a	λ -variation ^b	Recursion ^a	λ -variation ^b
0	-176.80350	-176.80350	-46.00278	-46.00278
1	-46.85743	-46.85743	-46.84516	-46.84516
2	-0.00243	-0.00243	-0.00371	-0.00371
3	0.00003	0.00003	0.00005	0.00005
4	-0.00000	-0.00000	-0.00000	-0.00000
5	0.00000	0.00001	0.00000	0.00001
6	-0.00000		-0.00000	
7	0.00000		0.00000	
8	0.00000		0.00000	
9	0.00000		0.00000	
10	0.00000		0.00000	
\sum_0^{10}	-223.66334		-92.85159	
FCI ^c	-223.66334		-92.85159	

^a MBPT(n) recursions.^b Central seven-point formula with $\Delta\lambda = 0.01$. See also Ref. 62.^c Finite-temperature full configuration interaction. See also Ref. 57.

elements times one-electron operators, and two-electron integrals times two-electron operators. This natural partitioning underscores the significance of the finite-temperature HF theory as the foundation of all converging finite-temperature electron-correlation theories. Its energy expression is identified with $\langle E_I^{(0)} \rangle + \langle E_I^{(1)} \rangle$, which differs from either $U^{(0)} + U^{(1)}$ or $\Omega^{(0)} + \Omega^{(1)}$ at $T > 0$.

In the nondegenerate, the zero-temperature MBPT, the renormalization terms cancel exactly the unlinked contribution of the equal magnitudes in the parent terms, ensuring the size-consistency of MBPT at any order, as proven by the linked-diagram theorem.^{65–70} In the finite-temperature MBPT, which sums over all possible states many of which are degenerate, the renormalization terms consist of both linked and unlinked contributions. The unlinked contributions cancel the same in the parent terms, restoring the linkedness of the perturbation corrections at any order, while nonzero linked renormalization terms persist. They correspond to diagrams whose resolvent lines are displaced upwards in all possible ways, in which there are two or more resolvents in between some pairs of adjacent vertexes and none in between others. These renormalization diagrams are distinguished from the well-known anomalous diagrams whose resolvent lines are deleted. They both are essential numerically, and had it not for them, the perturbation series would not converge at the finite-temperature FCI limit. It is unclear whether the conventional time-dependent, diagrammatic formulation^{46–51} or density-matrix derivation⁵² are aware of such diagrams.

We have proven the linked-diagram theorem of the finite-temperature MBPT. The theorem is based on the linked-diagram theorem at zero temperature^{65–70} and the systematic cancellation of unlinked anomalous diagrams.

We have derived reduced analytical formulas for the perturbation corrections to the thermodynamic functions in the grand canonical ensemble up to the third order. We have also implemented general-order algorithms in both ensemble, and calculated the benchmark perturbation corrections up to the

tenth order. At intermediate temperatures, where thermodynamic functions vary with temperature considerably, the perturbation series tend to diverge, but elsewhere they converge rapidly towards the finite-temperature FCI limits, establishing the correctness of the theory.

In a separate study,⁵⁶ we showed that the finite-temperature MBPT at the first and second orders does not converge at the correct zero-temperature limit when the reference wave function is qualitatively different from the exact one, confirming Kohn and Luttinger.⁴⁸ This originates from the nonanalyticity of the Boltzmann factor and is therefore expected to plague most any finite-temperature MBPT, e.g., the one in the canonical ensemble also.⁶² Nonconvergence should persist at third and all higher orders under the same condition.

This study and another reported in Ref. 59 have been conducted to lay a firm mathematical foundation of perturbation theories,^{97,98} which continue to be a workhorse for efficient, size-consistent,^{64,99} converging *ab initio* electronic structure calculations^{100–112} for large complex molecules and solids.¹¹³ Unlike time-dependent, diagrammatic expositions,^{42–45} which are often incomplete and/or intractable, our derivations follow the transparent, linear, time-independent, algebraic logic, involving only elementary calculus and combinatorial identities. They justify the second-quantized and diagrammatic rules just as tools for expediency rather than rely on them as a graphical method of derivations that are often based on human intuitions detached from mathematics. Our derivation strategy can therefore be universally applied to any perturbation theory insofar as the exact limit is known, reliably leading to recursions, order-by-order analytical formulas, and general-order algorithms.

VIII. DATA AVAILABILITY STATEMENT

The data that supports the findings of this study are available within the article.

ACKNOWLEDGMENTS

The author thanks Professor Rodney J. Bartlett for teaching him the quantum-field-theoretical techniques used in this study. This work was supported by the Center for Scalable, Predictive methods for Excitation and Correlated phenomena (SPEC), which is funded by the U.S. Department of Energy, Office of Science, Office of Basic Energy Sciences, Chemical Sciences, Geosciences, and Biosciences Division, as a part of the Computational Chemical Sciences Program and also by the U.S. Department of Energy, Office of Science, Office of Basic Energy Sciences under Grant No. DE-SC0006028.

Appendix A: Recursions in the canonical ensemble

Thermodynamic functions in the canonical ensemble considered are the canonical partition function (Z), Helmholtz en-

ergy (F), internal energy (U), and entropy (S), which are related to one another by

$$Z = \sum_I e^{-\beta E_I}, \quad (\text{A1})$$

$$F = -\frac{1}{\beta} \ln Z, \quad (\text{A2})$$

$$U = -\frac{\partial}{\partial \beta} \ln Z, \quad (\text{A3})$$

and

$$F = U - TS, \quad (\text{A4})$$

where the I -summation goes over all spin states with a fixed total number (\bar{N}) of electrons. The recursion for $Z^{(n)}$ is given by

$$\begin{aligned} \frac{Z^{(n)}}{Z^{(0)}} &= (-\beta) \langle E^{(n)} \rangle + \frac{(-\beta)^2}{2!} \sum_{i=1}^{n-1} \langle E^{(i)} E^{(n-i)} \rangle \\ &+ \frac{(-\beta)^3}{3!} \sum_{i=1}^{n-2} \sum_{j=1}^{n-i-1} \langle E^{(i)} E^{(j)} E^{(n-i-j)} \rangle \\ &+ \dots + \frac{(-\beta)^n}{n!} \langle (E^{(1)})^n \rangle, \end{aligned} \quad (\text{A5})$$

where $\langle \dots \rangle$ is defined differently from Eq. (12) only in this appendix as

$$\langle X_I \rangle \equiv \frac{\sum_I X_I e^{-\beta E_I^{(0)}}}{\sum_I e^{-\beta E_I^{(0)}}}. \quad (\text{A6})$$

The recursion for $F^{(n)}$ is inferred from Eq. (15) as

$$\begin{aligned} F^{(n)} &= \langle E^{(n)} \rangle + \frac{(-\beta)}{2!} \sum_{i=1}^{n-1} (\langle E^{(i)} E^{(n-i)} \rangle - F^{(i)} F^{(n-i)}) \\ &+ \frac{(-\beta)^2}{3!} \sum_{i=1}^{n-2} \sum_{j=1}^{n-i-1} (\langle E^{(i)} E^{(j)} E^{(n-i-j)} \rangle - F^{(i)} F^{(j)} F^{(n-i-j)}) \\ &+ \dots + \frac{(-\beta)^{n-1}}{n!} \{ \langle (E^{(1)})^n \rangle - (F^{(1)})^n \}. \end{aligned} \quad (\text{A7})$$

Likewise, $U^{(n)}$ is defined recursively by

$$\begin{aligned} U^{(n)} &= \langle E_I^{(n)} \rangle + (-\beta) \sum_{i=1}^n \langle E_I^{(i)} E_I^{(n-i)} \rangle - (-\beta) \sum_{i=1}^n F^{(i)} U^{(n-i)} \\ &+ \frac{(-\beta)^2}{2!} \sum_{i=1}^{n-1} \sum_{j=1}^{n-i} \langle E_I^{(i)} E_I^{(j)} E_I^{(n-i-j)} \rangle \\ &- \frac{(-\beta)^2}{2!} \sum_{i=1}^{n-1} \sum_{j=1}^{n-i} F^{(i)} F^{(j)} U^{(n-i-j)} \\ &+ \dots + \frac{(-\beta)^n}{n!} \langle (E_I^{(1)})^n E_I^{(0)} \rangle - \frac{(-\beta)^n}{n!} (F^{(1)})^n U^{(0)}, \end{aligned} \quad (\text{A8})$$

which implies the recursion for $S^{(n)} = k_B \beta (U^{(n)} - F^{(n)})$.

These have been obtained by restricting the summations to \bar{N} -electron states and setting $\mu^{(n)} = 0$ for all n in the corresponding recursions for the grand canonical ensemble.

Appendix B: A proof of equivalence of Eqs. (13) and (14)

Generally, we prove the equivalence of two recursions,

$$\begin{aligned} A^{(n)} &= B^{(n)} - \frac{1}{2} \sum_{i=1}^{n-1} B^{(i)} B^{(n-i)} \\ &+ \frac{1}{3} \sum_{i=1}^{n-2} \sum_{j=1}^{n-i-1} B^{(i)} B^{(j)} B^{(n-i-j)} \\ &- \dots - \frac{(-1)^n}{n} (B^{(1)})^n, \end{aligned} \quad (\text{B1})$$

and

$$\begin{aligned} A^{(n)} &= B^{(n)} - \frac{1}{2!} \sum_{i=1}^{n-1} A^{(i)} A^{(n-i)} \\ &- \frac{1}{3!} \sum_{i=1}^{n-2} \sum_{j=1}^{n-i-1} A^{(i)} A^{(j)} A^{(n-i-j)} \\ &- \dots - \frac{1}{n!} (A^{(1)})^n. \end{aligned} \quad (\text{B2})$$

Equations (13) and (14) are a special case of these in which $A^{(n)} = -\beta \Omega^{(n)}$ and $B^{(n)} = \Xi^{(n)} / \Xi^{(0)}$. We can rewrite the second equation as

$$\begin{aligned} B^{(n)} &= A^{(n)} + \frac{1}{2!} \sum_{i=1}^{n-1} A^{(i)} A^{(n-i)} \\ &+ \frac{1}{3!} \sum_{i=1}^{n-2} \sum_{j=1}^{n-i-1} A^{(i)} A^{(j)} A^{(n-i-j)} \\ &+ \dots + \frac{1}{n!} (A^{(1)})^n. \end{aligned} \quad (\text{B3})$$

Substituting this into the right-hand side of Eq. (B1), we can convert it into a form expressed entirely in terms of $A^{(i)}$ as

$$\begin{aligned} A^{(n)} &= C_{A^{(n)}} A^{(n)} + \sum_{i=1}^{n-1} C_{A^{(i)} A^{(n-i)}} A^{(i)} A^{(n-i)} \\ &+ \sum_{i=1}^{n-2} \sum_{j=1}^{n-i-1} C_{A^{(i)} A^{(j)} A^{(n-i-j)}} A^{(i)} A^{(j)} A^{(n-i-j)} \\ &+ \dots + C_{(A^{(1)})^n} (A^{(1)})^n. \end{aligned} \quad (\text{B4})$$

We shall show that $C_{A^{(n)}} = 1$ and $C_{A^{(i_1)} A^{(i_2)} \dots A^{(i_m)}} = 0$ ($m \geq 2$).

By inspection, we find $C_{A^{(n)}} = 1$, $C_{A^{(i)} A^{(n-i)}} = 1/2! - 1/2 = 0$, and $C_{A^{(i)} A^{(j)} A^{(n-i-j)}} = 1/3! - (1/2)(1/2!) - (1/2)(1/2!) + 1/3 = 0$. In general, the coefficient multiplying $A^{(i_1)} A^{(i_2)} \dots A^{(i_m)}$ ($m \geq 2$) is given as

$$\begin{aligned} &C_{A^{(i_1)} A^{(i_2)} \dots A^{(i_m)}} \\ &= \frac{1}{m!} - \frac{1}{2} \sum_{i=1}^{m-1} \frac{1}{i!(m-i)!} + \frac{1}{3} \sum_{i=1}^{m-2} \sum_{j=1}^{m-i-1} \frac{1}{i! j!(m-i-j)!} \\ &+ \dots - \frac{(-1)^m}{m} \left(\frac{1}{1!} \right)^m \\ &= \frac{1}{m!} \left(\frac{1!}{1} \binom{m}{1} - \frac{2!}{2} \binom{m}{2} + \frac{3!}{3} \binom{m}{3} + \dots - \frac{(-1)^m m!}{m} \binom{m}{m} \right), \end{aligned} \quad (\text{B5})$$

where $\left\{ \begin{matrix} m \\ k \end{matrix} \right\}$ is the Stirling number of the second kind (the number of ways m objects are partitioned into k nonempty sets).¹¹⁴ It is defined as

$$\left\{ \begin{matrix} m \\ k \end{matrix} \right\} = \frac{1}{k!} \sum_{m_1, \dots, m_k} \frac{m!}{\prod_{i=1}^k m_i!}, \quad (\text{B6})$$

where the summation goes over all natural numbers m_1, \dots, m_k that satisfy $m_1 + \dots + m_k = m$. There is an identity involving the Stirling number, which reads

$$\sum_{k=1}^m (-1)^k (k-1)! \left\{ \begin{matrix} m \\ k \end{matrix} \right\} = 0, \quad (\text{B7})$$

which implies $C_{A^{(i)}A^{(2)}\dots A^{(m)}} = 0$ ($m \geq 2$), proving the equivalence.

The identity (B7) can in turn be proven by induction using the recursion:

$$\left\{ \begin{matrix} n+1 \\ k \end{matrix} \right\} = k \left\{ \begin{matrix} n \\ k \end{matrix} \right\} + \left\{ \begin{matrix} n \\ k-1 \end{matrix} \right\}. \quad (\text{B8})$$

Equation (B7) is true for $m = 2$. If it is true for $m = 2, \dots, n$, it also holds true for $m = n + 1$ and therefore for any $m \geq 2$ because

$$\begin{aligned} & \sum_{k=1}^{n+1} (-1)^k (k-1)! \left\{ \begin{matrix} n+1 \\ k \end{matrix} \right\} \\ &= \sum_{k=1}^{n+1} (-1)^k k! \left\{ \begin{matrix} n \\ k \end{matrix} \right\} + \sum_{k=1}^{n+1} (-1)^k (k-1)! \left\{ \begin{matrix} n \\ k-1 \end{matrix} \right\} \\ &= \sum_{k=1}^{n+1} (-1)^k k! \left\{ \begin{matrix} n \\ k \end{matrix} \right\} + \sum_{k=0}^n (-1)^{k+1} k! \left\{ \begin{matrix} n \\ k \end{matrix} \right\} \\ &= \sum_{k=1}^n (-1)^k k! \left\{ \begin{matrix} n \\ k \end{matrix} \right\} + \sum_{k=1}^n (-1)^{k+1} k! \left\{ \begin{matrix} n \\ k \end{matrix} \right\} = 0, \end{aligned} \quad (\text{B9})$$

where we used $\left\{ \begin{matrix} n \\ 0 \end{matrix} \right\} = \left\{ \begin{matrix} n \\ n+1 \end{matrix} \right\} = 0$.

Finally, the recursion for the Stirling number [Eq. (B8)] can be justified as follows: The left-hand side counts the number of ways $n + 1$ objects are partitioned into k nonempty sets. The first term in the right-hand side is the number of ways in which the $(n + 1)$ th object is absorbed into one of the existing k nonempty sets of the first n objects. The second term is the number of ways in which the $(n + 1)$ th object forms a new (k)th set containing only it and the first n objects are partitioned into $k - 1$ nonempty sets.

One may view Maclaurin series of the right-hand sides of the following equations as a mnemonic for Eqs. (B1) and (B3), respectively:

$$A^{(n)} = \ln(B^{(n)} + 1), \quad (\text{B10})$$

$$B^{(n)} = \exp(A^{(n)}) - 1, \quad (\text{B11})$$

which, however, may not be taken literally.

Appendix C: Normal-ordered second quantization at finite temperature

In this appendix, we fully develop the normal-ordered second quantization at finite temperature^{28,42} within the time-independent framework in a transparent and pedagogical manner. It serves as a basis of the diagrammatic derivation and the linked-diagram theorem. The reader is referred to Shavitt and Bartlett⁶³ for normal-ordered second quantization at zero temperature and to March, Young, and Sampanthar⁴² for an abridged exposition of its finite-temperature counterpart. The following expounds on the latter with enough details to be actually used in deriving the second-order formulas in Sec. III.

1. Normal ordering at finite temperature

A product of creation (\hat{p}^\dagger) and annihilation (\hat{p}) operators in the normal order (denoted by $\{ \dots \}$) is defined [cf. Eq. (9.3.2) of Ref. 42] as

$$\{\hat{p}^\dagger \hat{p}\} \equiv f_p^+ \hat{p}^\dagger \hat{p} - f_p^- \hat{p} \hat{p}^\dagger, \quad (\text{C1})$$

$$\{\hat{p} \hat{p}^\dagger\} \equiv f_p^- \hat{p} \hat{p}^\dagger - f_p^+ \hat{p}^\dagger \hat{p}, \quad (\text{C2})$$

where f_p^- and f_p^+ are the Fermi–Dirac distribution functions given by Eqs. (43) and (44). When $p \neq q$,

$$\{\hat{p}^\dagger \hat{q}\} \equiv \hat{p}^\dagger \hat{q}, \quad (\text{C3})$$

$$\{\hat{p} \hat{q}^\dagger\} \equiv \hat{p} \hat{q}^\dagger. \quad (\text{C4})$$

A normal-ordered product of two creation operators or of two annihilation operators is also the same as the original order.

In analogy to the zero-temperature case, the normal ordering at finite temperature is designed so that the thermal average of a normal-ordered product is always zero. Using Einstein's convention of implied summations of repeated spin-orbital indexes, we confirm

$$\begin{aligned} \langle \langle I | x_{pq} \{\hat{p}^\dagger \hat{q}\} | I \rangle \rangle & \equiv \frac{\sum_I \langle I | x_{pq} \{\hat{p}^\dagger \hat{q}\} | I \rangle e^{-\beta D_I^{(0)}}}{\sum_I e^{-\beta D_I^{(0)}}} \\ &= \frac{\sum_I \langle I | x_{pp} \{\hat{p}^\dagger \hat{p}\} | I \rangle e^{-\beta D_I^{(0)}}}{\sum_I e^{-\beta D_I^{(0)}}} \\ &= \frac{\sum_I \langle I | x_{pp} f_p^+ \hat{p}^\dagger \hat{p} | I \rangle e^{-\beta D_I^{(0)}}}{\sum_I e^{-\beta D_I^{(0)}}} \\ & \quad - \frac{\sum_I \langle I | x_{pp} f_p^- \hat{p} \hat{p}^\dagger | I \rangle e^{-\beta D_I^{(0)}}}{\sum_I e^{-\beta D_I^{(0)}}} \\ &= \sum_p x_{pp} f_p^+ f_p^- - \sum_p x_{pp} f_p^- f_p^+ \\ &= 0, \end{aligned} \quad (\text{C5})$$

where we used the Boltzmann sum identities I and V of Ref. 55 in the penultimate equality.

Next, we define a Wick contraction (denoted by a staple symbol) as the difference between the operator product and

its normal-ordered counterpart.

$$\overline{\hat{p}^\dagger \hat{p}} \equiv \hat{p}^\dagger \hat{p} - \{\hat{p}^\dagger \hat{p}\} = f_p^- (\hat{p}^\dagger \hat{p} + \hat{p} \hat{p}^\dagger) = f_p^-, \quad (\text{C6})$$

$$\overline{\hat{p} \hat{p}^\dagger} \equiv \hat{p} \hat{p}^\dagger - \{\hat{p} \hat{p}^\dagger\} = f_p^+ (\hat{p} \hat{p}^\dagger + \hat{p}^\dagger \hat{p}) = f_p^+, \quad (\text{C7})$$

where we used the anticommutation rules of fermion creation and annihilation operators. When $p \neq q$,

$$\overline{\hat{p}^\dagger \hat{q}} \equiv \hat{p}^\dagger \hat{q} - \{\hat{p}^\dagger \hat{q}\} = 0, \quad (\text{C8})$$

$$\overline{\hat{p} \hat{q}^\dagger} \equiv \hat{p} \hat{q}^\dagger - \{\hat{p} \hat{q}^\dagger\} = 0. \quad (\text{C9})$$

A Wick contraction of two creation or of two annihilation operators is also zero.

The concept of the normal ordering can be generalized to any even number of operators. For instance, a product of four operators in the normal order is defined as ($p \neq q$),

$$\{\hat{p}^\dagger \hat{q}^\dagger \hat{q} \hat{p}\} = -\{\hat{p}^\dagger \hat{q}^\dagger \hat{p} \hat{q}\} = \{\hat{p}^\dagger \hat{p} \hat{q}^\dagger \hat{q}\} \quad (\text{C10})$$

$$\equiv (f_p^+ \hat{p}^\dagger \hat{p} - f_p^- \hat{p} \hat{p}^\dagger) (f_q^+ \hat{q}^\dagger \hat{q} - f_q^- \hat{q} \hat{q}^\dagger) \quad (\text{C11})$$

$$\equiv f_p^+ f_q^+ \hat{p}^\dagger \hat{q}^\dagger \hat{q} \hat{p} - f_p^+ f_q^- \hat{p}^\dagger \hat{q} \hat{q}^\dagger \hat{p} - f_p^- f_q^+ \hat{p} \hat{q}^\dagger \hat{q} \hat{p}^\dagger + f_p^- f_q^- \hat{p} \hat{q} \hat{q}^\dagger \hat{p}^\dagger. \quad (\text{C12})$$

When $pq \neq rs$ or $pq \neq sr$,

$$\{\hat{p}^\dagger \hat{q}^\dagger \hat{r} \hat{s}\} \equiv \hat{p}^\dagger \hat{q}^\dagger \hat{r} \hat{s}. \quad (\text{C13})$$

The thermal average of a normal-ordered product of any number of operators is also always zero by construction. This can be verified for the above product as follows:

$$\begin{aligned} & \langle\langle I | x_{pqrs} \{\hat{p}^\dagger \hat{q}^\dagger \hat{q} \hat{p}\} | I \rangle\rangle \\ &= \langle\langle I | x_{pqrs} f_p^+ f_q^+ \hat{p}^\dagger \hat{q}^\dagger \hat{q} \hat{p} | I \rangle\rangle - \langle\langle I | x_{pqrs} f_p^+ f_q^- \hat{p}^\dagger \hat{q} \hat{q}^\dagger \hat{p} | I \rangle\rangle \\ & \quad - \langle\langle I | x_{pqrs} f_p^- f_q^+ \hat{p} \hat{q}^\dagger \hat{q} \hat{p}^\dagger | I \rangle\rangle + \langle\langle I | x_{pqrs} f_p^- f_q^- \hat{p} \hat{q} \hat{q}^\dagger \hat{p}^\dagger | I \rangle\rangle \\ &= \sum_{p,q} x_{pqrs} f_p^+ f_q^+ f_p^- f_q^- - \sum_{p,q} x_{pqrs} f_p^+ f_q^- f_p^- f_q^+ \\ & \quad - \sum_{p,q} x_{pqrs} f_p^- f_q^+ f_p^+ f_q^- + \sum_{p,q} x_{pqrs} f_p^- f_q^- f_p^+ f_q^+ \\ &= 0, \end{aligned} \quad (\text{C14})$$

where Boltzmann sum identities III, V, and IX of Ref. 55 were used.

For a product of more than two operators, there are two types of contractions: partial and full contractions. Together, they are defined as

$$\{\dots \overline{\hat{p}^\dagger \hat{q}^\dagger} \dots \overline{\hat{p} \hat{q}^\dagger} \dots\} = (-1)^P \overline{\hat{p}^\dagger \hat{p}} \overline{\hat{q} \hat{q}^\dagger} \{\dots\}, \quad (\text{C15})$$

where $\{\dots\}$ in the right-hand side gathers the uncontracted operators (kept in the original order), and P is the number of permutations necessary to reorder the whole operator sequence from the left- to right-hand side. If there are no operators left in $\{\dots\}$, it is a full contraction; otherwise it is a partial contraction. A full contraction is a real number, while a partial contraction is a normal-ordered operator multiplied by a real number. The parity of a full contraction is $+1$ (-1) for an even (odd) number of intersections of the staple symbols of Wick contractions.⁶³

2. Wick's theorem at finite temperature

Wick's theorem states that a product of operators is the sum of its normal-ordered product and all of its partial and full contractions.⁶³ This holds true at zero and nonzero temperatures. For a product of two operators, the theorem is just a restatement of the definitions of Wick contractions:

$$\overline{\hat{p}^\dagger \hat{q}} = \{\hat{p}^\dagger \hat{q}\} + \overline{\hat{p}^\dagger \hat{q}}, \quad (\text{C16})$$

$$\overline{\hat{p} \hat{q}^\dagger} = \{\hat{p} \hat{q}^\dagger\} + \overline{\hat{p} \hat{q}^\dagger}. \quad (\text{C17})$$

For a product of four operators, the theorem asserts

$$\begin{aligned} \overline{\hat{p}^\dagger \hat{q} \hat{r}^\dagger \hat{s}} &= \{\hat{p}^\dagger \hat{q} \hat{r}^\dagger \hat{s}\} + \overline{\{\hat{p}^\dagger \hat{q} \hat{r}^\dagger \hat{s}\}} + \overline{\{\hat{p}^\dagger \hat{q} \hat{r}^\dagger \hat{s}\}} + \overline{\{\hat{p}^\dagger \hat{q} \hat{r}^\dagger \hat{s}\}} \\ & \quad + \overline{\{\hat{p}^\dagger \hat{q} \hat{r}^\dagger \hat{s}\}} + \overline{\{\hat{p}^\dagger \hat{q} \hat{r}^\dagger \hat{s}\}} + \overline{\{\hat{p}^\dagger \hat{q} \hat{r}^\dagger \hat{s}\}}. \end{aligned} \quad (\text{C18})$$

We can verify this for the following simpler, but nontrivial case by inspection:

$$\begin{aligned} \overline{\hat{p}^\dagger \hat{q}^\dagger \hat{q} \hat{p}} &= \{\hat{p}^\dagger \hat{q}^\dagger \hat{q} \hat{p}\} + \overline{\{\hat{p}^\dagger \hat{q}^\dagger \hat{q} \hat{p}\}} + \overline{\{\hat{p}^\dagger \hat{q}^\dagger \hat{q} \hat{p}\}} \\ & \quad + \overline{\{\hat{p}^\dagger \hat{q}^\dagger \hat{q} \hat{p}\}} \end{aligned} \quad (\text{C19})$$

$$\begin{aligned} &= \{\hat{p}^\dagger \hat{q}^\dagger \hat{q} \hat{p}\} + \overline{\hat{p}^\dagger \hat{p}} \{\hat{q}^\dagger \hat{q}\} + \overline{\hat{q}^\dagger \hat{q}} \{\hat{p}^\dagger \hat{p}\} \\ & \quad + \overline{\hat{p}^\dagger \hat{p}} \overline{\hat{q}^\dagger \hat{q}} \end{aligned} \quad (\text{C20})$$

$$\begin{aligned} &= f_p^+ f_q^+ \hat{p}^\dagger \hat{q}^\dagger \hat{q} \hat{p} - f_p^+ f_q^- \hat{p}^\dagger \hat{q} \hat{q}^\dagger \hat{p} - f_p^- f_q^+ \hat{p} \hat{q}^\dagger \hat{q} \hat{p}^\dagger \\ & \quad + f_p^- f_q^- \hat{p} \hat{q} \hat{q}^\dagger \hat{p}^\dagger + f_p^- (f_q^+ \hat{q}^\dagger \hat{q} - f_q^- \hat{q} \hat{q}^\dagger) \\ & \quad + f_q^- (f_p^+ \hat{p}^\dagger \hat{p} - f_p^- \hat{p} \hat{p}^\dagger) + f_p^- f_q^- \end{aligned} \quad (\text{C21})$$

$$\begin{aligned} &= f_p^+ f_q^+ \hat{p}^\dagger \hat{q}^\dagger \hat{q} \hat{p} - f_p^+ f_q^- \hat{p}^\dagger (1 - \hat{q}^\dagger \hat{q}) \hat{p} \\ & \quad - f_p^- f_q^+ \hat{q}^\dagger (1 - \hat{p}^\dagger \hat{p}) \hat{q} + f_p^- f_q^- (1 - \hat{p}^\dagger \hat{p}) (1 - \hat{q}^\dagger \hat{q}) \\ & \quad + f_p^- (f_q^+ \hat{q}^\dagger \hat{q} - f_q^- \hat{q} \hat{q}^\dagger) + f_q^- (f_p^+ \hat{p}^\dagger \hat{p} - f_p^- \hat{p} \hat{p}^\dagger) \\ & \quad + f_p^- f_q^- \end{aligned} \quad (\text{C22})$$

$$\begin{aligned} &= (f_p^+ f_q^+ + f_p^+ f_q^- + f_p^- f_q^+ + f_p^- f_q^-) \hat{p}^\dagger \hat{q}^\dagger \hat{q} \hat{p} \\ & \quad + f_p^- f_q^- - f_p^- f_q^- (\hat{p}^\dagger \hat{p} + \hat{p} \hat{p}^\dagger) \\ & \quad - f_p^- f_q^- (\hat{q}^\dagger \hat{q} + \hat{q} \hat{q}^\dagger) + f_p^- f_q^- \end{aligned} \quad (\text{C23})$$

$$= \hat{p}^\dagger \hat{q}^\dagger \hat{q} \hat{p}. \quad (\text{C24})$$

When $pq \neq rs$ or $pq \neq sr$, Eq. (C13) embodies the theorem. In general situations, the theorem can be proven by induction. See Ref. 63 for an outline of the proof for the zero-temperature case.

Since the thermal average of any normal-ordered product of operators vanishes, a nonzero thermal average arises solely from full contractions, e.g.,

$$\begin{aligned} \langle\langle I | x_{pqrs} \overline{\hat{p}^\dagger \hat{q} \hat{r}^\dagger \hat{s}} | I \rangle\rangle &= x_{pqrs} \overline{\{\hat{p}^\dagger \hat{q} \hat{r}^\dagger \hat{s}\}} + x_{pqrs} \overline{\{\hat{p}^\dagger \hat{q} \hat{r}^\dagger \hat{s}\}} \\ &= \sum_{p,q} x_{pqrs} f_p^- f_q^+ + \sum_{p,r} x_{pqrs} f_p^- f_r^- \end{aligned} \quad (\text{C25})$$

However, more frequently, we need to evaluate the thermal average of a product of two or more normal-ordered products. We show that such a product is the sum of concatenated

normal-ordered product plus all of its partial and full contractions excluding internal contractions. An internal contraction is the one that involves at least one contraction within an original normal-ordered product. The following is an illustration of this rule:

$$\{\hat{p}^\dagger \hat{q}\} \{\hat{r}^\dagger \hat{s}\} = \{\hat{p}^\dagger \hat{q} \hat{r}^\dagger \hat{s}\} + \overline{\{\hat{p}^\dagger \hat{q} \hat{r}^\dagger \hat{s}\}} + \{\hat{p}^\dagger \hat{q} \overline{\hat{r}^\dagger \hat{s}}\} + \overline{\{\hat{p}^\dagger \hat{q} \overline{\hat{r}^\dagger \hat{s}}\}}. \quad (\text{C26})$$

Internal contractions in this example are the ones that contract \hat{p}^\dagger with \hat{q} and/or \hat{r}^\dagger with \hat{s} , which are therefore excluded from the right-hand side. This rule can be justified by comparing Eq. (C18) with

$$\begin{aligned} \hat{p}^\dagger \hat{q} \hat{r}^\dagger \hat{s} &= (\hat{p}^\dagger \hat{q}) (\hat{r}^\dagger \hat{s}) \\ &= (\{\hat{p}^\dagger \hat{q}\} + \overline{\hat{p}^\dagger \hat{q}}) + (\{\hat{r}^\dagger \hat{s}\} + \overline{\hat{r}^\dagger \hat{s}}) \\ &= \{\hat{p}^\dagger \hat{q}\} \{\hat{r}^\dagger \hat{s}\} + \{\hat{p}^\dagger \hat{q}\} \overline{\hat{r}^\dagger \hat{s}} + \overline{\hat{p}^\dagger \hat{q}} \{\hat{r}^\dagger \hat{s}\} + \overline{\hat{p}^\dagger \hat{q}} \overline{\hat{r}^\dagger \hat{s}}. \end{aligned} \quad (\text{C27})$$

The last three terms are internal contractions, which cancel out the same in Eq. (C18) when equated with the above. Therefore, the thermal average of a product of normal-ordered products comes solely from its full contractions excluding internal contractions, e.g.,

$$\begin{aligned} \langle \langle I | x_{pq} y_{rs} \{\hat{p}^\dagger \hat{q}\} \{\hat{r}^\dagger \hat{s}\} | I \rangle \rangle &= \langle \langle I | x_{pq} y_{rs} \overline{\{\hat{p}^\dagger \hat{q}\} \{\hat{r}^\dagger \hat{s}\}} | I \rangle \rangle \\ &= \sum_{p,q} x_{pq} y_{qp} f_p^- f_q^+. \end{aligned} \quad (\text{C28})$$

3. Hamiltonian and number operators

Let us express the number operator in the normal-ordered second quantization at finite temperature.

$$\begin{aligned} \hat{N} &\equiv \sum_p \hat{p}^\dagger \hat{p} \\ &= \sum_p (\{\hat{p}^\dagger \hat{p}\} + \overline{\hat{p}^\dagger \hat{p}}) \\ &= \sum_p \{\hat{p}^\dagger \hat{p}\} + \sum_p f_p^- \\ &= \sum_p \{\hat{p}^\dagger \hat{p}\} + \bar{N}, \end{aligned} \quad (\text{C29})$$

where we used the zeroth-order electroneutrality condition [Eq. (45)] in the last equality. Taking the thermal average of the above equation, we immediately find $\langle \hat{N} \rangle = \bar{N}$.

The Hamiltonian operator in second quantization is written as^{63,74}

$$\hat{H} = E_{\text{nuc.}} + \sum_{p,q} h_{pq} \hat{p}^\dagger \hat{q} + \frac{1}{4} \sum_{p,q,r,s} \langle pq || rs \rangle \hat{p}^\dagger \hat{q}^\dagger \hat{s} \hat{r}, \quad (\text{C30})$$

where $E_{\text{nuc.}}$ is the nucleus-nucleus repulsion energy, h_{pq} is the integral of the one-electron part of the Hamiltonian operator,

and $\langle pq || rs \rangle$ is the antisymmetrized two-electron integral. This can be finite-temperature normal ordered as

$$\begin{aligned} \hat{H} &= E_{\text{nuc.}} + \sum_{p,q} h_{pq} (\{\hat{p}^\dagger \hat{q}\} + \overline{\hat{p}^\dagger \hat{q}}) \\ &\quad + \frac{1}{4} \sum_{p,q,r,s} \langle pq || rs \rangle (\{\hat{p}^\dagger \hat{q}^\dagger \hat{s} \hat{r}\} + \overline{\{\hat{p}^\dagger \hat{q}^\dagger \hat{s} \hat{r}\}} + \{\hat{p}^\dagger \hat{q}^\dagger \overline{\hat{s} \hat{r}}\} \\ &\quad + \{\hat{p}^\dagger \hat{q}^\dagger \overline{\hat{s} \hat{r}}\} + \{\hat{p}^\dagger \overline{\hat{q}^\dagger \hat{s}} \hat{r}\} + \overline{\{\hat{p}^\dagger \overline{\hat{q}^\dagger \hat{s}} \hat{r}\}} + \overline{\{\hat{p}^\dagger \overline{\hat{q}^\dagger \hat{s}} \hat{r}\}}) \\ &= E_{\text{HF}}(T) + \sum_{p,q} f_{pq}(T) \{\hat{p}^\dagger \hat{q}\} + \frac{1}{4} \sum_{p,q,r,s} \langle pq || rs \rangle \{\hat{p}^\dagger \hat{q}^\dagger \hat{s} \hat{r}\}, \end{aligned} \quad (\text{C31})$$

where $E_{\text{HF}}(T)$ and $f_{pq}(T)$ are the finite-temperature Hartree-Fock energy and Fock matrix element,⁵⁸ defined by

$$E_{\text{HF}}(T) = E_{\text{nuc.}} + \sum_p h_{pp} f_p^- + \frac{1}{2} \sum_{p,q} \langle pq || pq \rangle f_p^- f_q^-, \quad (\text{C32})$$

$$f_{pq}(T) = h_{pq} + \sum_r \langle pr || qr \rangle f_r^-. \quad (\text{C33})$$

Therefore, $E_{\text{HF}}(T)$ is identified as the following sum,

$$E_{\text{HF}}(T) = \langle E_I^{(0)} \rangle + \langle E_I^{(1)} \rangle, \quad (\text{C34})$$

where the thermal averages of the zeroth- and first-order energy corrections^{54,55} are given by

$$\langle E_I^{(0)} \rangle = E_{\text{nuc.}} + \sum_p \epsilon_p f_p^-, \quad (\text{C35})$$

$$\langle E_I^{(1)} \rangle = \sum_p F_{pp} f_p^- - \frac{1}{2} \sum_{p,q} \langle pq || pq \rangle f_p^- f_q^- \quad (\text{C36})$$

with F_{pq} being the difference between the finite-temperature Fock and diagonal zero-temperature Fock matrix elements,

$$F_{pq} = f_{pq}(T) - \epsilon_p \delta_{pq}. \quad (\text{C37})$$

Equation (C34) mirrors the well-known identity⁷⁴ in the zero-temperature case, $E_{\text{HF}} = E^{(0)} + E^{(1)}$, but it does not agree with either $U^{(0)} + U^{(1)}$ or $\Omega^{(0)} + \Omega^{(1)}$ at $T > 0$. They are instead related to one another by^{54,55}

$$\begin{aligned} U^{(0)} + U^{(1)} &= E_{\text{nuc.}} + \sum_p \epsilon_p f_p^- + \sum_p F_{pp} f_p^- \\ &\quad - \frac{1}{2} \sum_{p,q} \langle pq || pq \rangle f_p^- f_q^- - \beta \sum_p (F_{pp} - \mu^{(1)}) \epsilon_p f_p^- f_p^+ \\ &= E_{\text{HF}}(T) + TS^{(1)}, \end{aligned} \quad (\text{C38})$$

$$\begin{aligned} \Omega^{(0)} + \Omega^{(1)} &= E_{\text{nuc.}} + \frac{1}{\beta} \sum_p \ln f_p^+ + \sum_p F_{pp} f_p^- \\ &\quad - \frac{1}{2} \sum_{p,q} \langle pq || pq \rangle f_p^- f_q^- - \mu^{(1)} \bar{N} \\ &= E_{\text{HF}}(T) - (\mu^{(0)} + \mu^{(1)}) \bar{N} - TS^{(0)}. \end{aligned} \quad (\text{C39})$$

We employ the Møller–Plesset partitioning⁷² of the Hamiltonian. The zeroth-order Hamiltonian and perturbation operators are then written in the normal-ordered form as

$$\hat{H}_0 \equiv E_{\text{nuc.}} + \sum_p \epsilon_p \hat{p}^\dagger \hat{p} = \langle E_I^{(0)} \rangle + \sum_p \epsilon_p \{\hat{p}^\dagger \hat{p}\}, \quad (\text{C40})$$

$$\hat{V} \equiv \langle E_I^{(1)} \rangle + \sum_{p,q} F_{pq} \{\hat{p}^\dagger \hat{q}\} + \frac{1}{4} \sum_{p,q,r,s} \langle pq||rs \rangle \{\hat{p}^\dagger \hat{q}^\dagger \hat{s} \hat{r}\}. \quad (\text{C41})$$

4. Projector and resolvent operator

In order to understand the second-quantization rule for the resolvent operator, let us first examine the effect of inserting the resolution-of-the-identity in Eq. (C28). Using Einstein's implied summation of repeated spinorbital and state indexes, we can rewrite Eq. (C28) as

$$\begin{aligned} & \langle \langle I | x_{pq} y_{rs} \{ \hat{p}^\dagger \hat{q} \} \{ \hat{r}^\dagger \hat{s} \} | I \rangle \rangle \\ &= \langle \langle I | x_{pq} \{ \hat{p}^\dagger \hat{q} \} | Q \rangle \langle Q | \{ \hat{r}^\dagger \hat{s} \} y_{rs} | I \rangle \rangle \\ &= \langle \langle I | x_{pq} \{ \hat{p}^\dagger \hat{q} \} \{ \hat{t}^\dagger \hat{u} \} | I \rangle \langle I | \{ \hat{u}^\dagger \hat{t} \} \{ \hat{r}^\dagger \hat{s} \} y_{rs} | I \rangle \rangle \\ &= \sum_{p,q} x_{pq} y_{qp} f_p^- f_q^+, \end{aligned} \quad (\text{C42})$$

where Q runs over all determinants, and hence $\sum |Q\rangle\langle Q| = 1$. In the second equality, we wrote $|Q\rangle = \{ \hat{t}^\dagger \hat{u} \} | I \rangle$. For the last equality to hold, we should regard a chain of contractions, p - u - s or q - t - r , as a single contraction evaluated as f_p^- or f_q^+ , respectively, rather than view each as three consecutive contractions evaluated as $f_p^- f_p^+ f_p^-$ or $f_q^+ f_q^- f_q^+$, which is erroneous.

Then, the rule for evaluating thermal averages involving a resolvent operator is essentially the same. To explain the rule by a similar example, we may consider

$$\begin{aligned} & \langle \langle I | x_{pq} y_{rs} \{ \hat{p}^\dagger \hat{q} \} \hat{R}_I \{ \hat{r}^\dagger \hat{s} \} | I \rangle \rangle \\ &= \langle \langle I | x_{pq} \{ \hat{p}^\dagger \hat{q} \} | A \rangle \langle E_I^{(0)} - E_A^{(0)} \rangle^{-1} \langle A | \{ \hat{r}^\dagger \hat{s} \} y_{rs} | I \rangle \rangle \\ &= \langle \langle I | x_{pq} \{ \hat{p}^\dagger \hat{q} \} \{ \hat{t}^\dagger \hat{u} \} | I \rangle \langle \epsilon_u - \epsilon_t \rangle^{-1} \langle I | \{ \hat{u}^\dagger \hat{t} \} \{ \hat{r}^\dagger \hat{s} \} y_{rs} | I \rangle \rangle \\ &= \sum_{p,q}^{\text{denom.} \neq 0} \frac{x_{pq} y_{qp} f_p^- f_q^+}{\epsilon_p - \epsilon_q}, \end{aligned} \quad (\text{C43})$$

where A stands for a determinant outside the degenerate subspace of I , which explains why the summations over p and q must be restricted (“denom. $\neq 0$ ”) to nonzero denominators. In other words, \hat{R}_I acts as an outer projector.

Let us define inner projector $\hat{P}_I = \sum |J\rangle\langle J|$, where J runs over only those determinants that are degenerate with I .

$$\begin{aligned} & \langle \langle I | x_{pq} y_{rs} \{ \hat{p}^\dagger \hat{q} \} \hat{P}_I \{ \hat{r}^\dagger \hat{s} \} | I \rangle \rangle \\ &= \langle \langle I | x_{pq} \{ \hat{p}^\dagger \hat{q} \} | J \rangle \langle J | \{ \hat{r}^\dagger \hat{s} \} y_{rs} | I \rangle \rangle \\ &= \langle \langle I | x_{pq} \{ \hat{p}^\dagger \hat{q} \} \{ \hat{t}^\dagger \hat{u} \} | I \rangle \langle I | \{ \hat{u}^\dagger \hat{t} \} \{ \hat{r}^\dagger \hat{s} \} y_{rs} | I \rangle \rangle \\ &= \sum_{p,q}^{\text{denom.}=0} x_{pq} y_{qp} f_p^- f_q^+, \end{aligned} \quad (\text{C44})$$

where the summations over p and q are now restricted (“denom. = 0”) to the cases whose fictitious denominator ($\epsilon_p - \epsilon_q$) is zero.

- ¹Y. Kurashige and T. Yanai, *J. Chem. Phys.* **130**, 234114 (2009).
- ²D. Zgid and G. K.-L. Chan, *J. Chem. Phys.* **134**, 094115 (2011).
- ³G. H. Booth, D. Cleland, A. J. W. Thom, and A. Alavi, *J. Chem. Phys.* **135**, 084104 (2011).
- ⁴J. K. Ellis, R. L. Martin, and G. E. Scuseria, *J. Chem. Theory Comput.* **9**, 2857 (2013).
- ⁵L. Bytautas, G. E. Scuseria, and K. Ruedenberg, *J. Chem. Phys.* **143**, 094105 (2015).
- ⁶Y. Ohtsuka and S. Ten-no, *J. Chem. Phys.* **143**, 144116 (2015).
- ⁷G. K.-L. Chan, A. Keselman, N. Nakatani, Z. D. Li, and S. R. White, *J. Chem. Phys.* **145**, 014102 (2016).
- ⁸A. A. Holmes, N. M. Tubman, and C. J. Umrigar, *J. Chem. Theory Comput.* **12**, 3674 (2016).
- ⁹Y. Y. He, M. P. Qin, H. Shi, Z. Y. Lu, and S. W. Zhang, *Phys. Rev. B* **99**, 045108 (2019).
- ¹⁰A. Baiardi and M. Reiher, *J. Chem. Phys.* **152**, 040903 (2020).
- ¹¹N. H. Stair and F. A. Evangelista, *J. Chem. Phys.* **153**, 104108 (2020).
- ¹²Z. H. Cui, T. Y. Zhu, and G. K.-L. Chan, *J. Chem. Theory Comput.* **16**, 119 (2020).
- ¹³J. E. Deustua, J. Shen, and P. Piecuch, *J. Chem. Phys.* **154**, 124103 (2021).
- ¹⁴M. Motta, D. M. Ceperley, G. K.-L. Chan, J. A. Gomez, E. Gull, S. Guo, C. A. Jiménez-Hoyos, T. N. Lan, J. Li, F. J. Ma, A. J. Millis, N. V. Prokof'ev, U. Ray, G. E. Scuseria, S. Sorella, E. M. Stoudenmire, Q. M. Sun, I. S. Tupitsyn, S. R. White, D. Zgid, and S. W. Zhang, *Phys. Rev. X* **7**, 031059 (2017).
- ¹⁵K. T. Williams, Y. Yao, J. Li, L. Chen, H. Shi, M. Motta, C. Y. Niu, U. Ray, S. Guo, R. J. Anderson, J. H. Li, L. N. Tran, C. N. Yeh, B. Mussard, S. Sharma, F. Bruneval, M. van Schilfgaarde, G. H. Booth, G. K.-L. Chan, S. W. Zhang, E. Gull, D. Zgid, A. Millis, C. J. Umrigar, and L. K. Wagner, *Phys. Rev. X* **10**, 011041 (2020).
- ¹⁶P. A. Lee, N. Nagaosa, and X. G. Wen, *Rev. Mod. Phys.* **78**, 17 (2006).
- ¹⁷P. Phillips, T. P. Choy, and R. G. Leigh, *Rep. Prog. Phys.* **72**, 036501 (2009).
- ¹⁸W. P. Su, J. R. Schrieffer, and A. J. Heeger, *Phys. Rev. Lett.* **42**, 1698 (1979).
- ¹⁹A. J. Heeger, S. Kivelson, J. R. Schrieffer, and W. P. Su, *Rev. Mod. Phys.* **60**, 781 (1988).
- ²⁰P. W. Anderson, *Phys. Rev. Lett.* **64**, 1839 (1990).
- ²¹C. Kittel, *Quantum Theory of Solids*, 2nd ed. (Wiley, Delhi, 1987).
- ²²M. Tinkham, *Introduction to Superconductivity*, 2nd ed. (Dover, New York, 1996).
- ²³V. Z. Kresin, H. Morawitz, and S. A. Wolf, *Superconducting State: Mechanisms and Properties* (Oxford University Press, Oxford, 2014).
- ²⁴A. W. Overhauser, *Phys. Rev. Lett.* **4**, 462 (1960).
- ²⁵A. W. Overhauser, *Phys. Rev.* **128**, 1437 (1962).
- ²⁶J. Čížek and J. Paldus, *J. Chem. Phys.* **47**, 3976 (1967).
- ²⁷T. Yamada and S. Hirata, *J. Chem. Phys.* **143**, 114112 (2015).
- ²⁸G. Sanyal, S. H. Mandal, S. Guha, and D. Mukherjee, *Phys. Rev. E* **48**, 3373 (1993).
- ²⁹S. H. Mandal, R. Ghosh, and D. Mukherjee, *Chem. Phys. Lett.* **335**, 281 (2001).
- ³⁰S. H. Mandal, R. Ghosh, G. Sanyal, and D. Mukherjee, in *Recent Progress in Many-Body Theories*, edited by R. Bishop, T. Brandes, K. A. Gernoth, N. R. Walet, and Y. Xian (World Scientific, Singapore, 2002) pp. 383–392.
- ³¹F. D. Malone, N. S. Blunt, E. W. Brown, D. K. K. Lee, J. S. Spencer, W. M. C. Foulkes, and J. J. Shepherd, *Phys. Rev. Lett.* **117**, 115701 (2016).
- ³²A. A. Rusakov and D. Zgid, *J. Chem. Phys.* **144**, 054106 (2016).
- ³³A. R. Welden, A. A. Rusakov, and D. Zgid, *J. Chem. Phys.* **145**, 204106 (2016).
- ³⁴A. F. White and G. K.-L. Chan, *J. Chem. Theory Comput.* **14**, 5690 (2018).
- ³⁵G. Harsha, T. M. Henderson, and G. E. Scuseria, *J. Chem. Phys.* **150**, 154109 (2019).
- ³⁶G. Harsha, T. M. Henderson, and G. E. Scuseria, *J. Chem. Theory Comput.* **15**, 6127 (2019).
- ³⁷Y. Liu, T. Shen, H. Zhang, and B. Rubenstein, *J. Chem. Theory Comput.* **16**, 4298 (2020).

This is the author's peer reviewed, accepted manuscript. However, the online version of record will be different from this version once it has been copyedited and typeset.
PLEASE CITE THIS ARTICLE AS DOI:10.1063/1.50061384

- ³⁸G. Harsha, T. M. Henderson, and G. E. Scuseria, *J. Chem. Phys.* **153**, 124115 (2020).
- ³⁹H. Barghathi, J. Yu, and A. Del Maestro, *Phys. Rev. Research* **2**, 043206 (2020).
- ⁴⁰C. Sun, U. Ray, Z. H. Cui, M. Stoudenmire, M. Ferrero, and G. K.-L. Chan, *Phys. Rev. B* **101**, 075131 (2020).
- ⁴¹J. Lee, M. A. Morales, and F. D. Malone, *J. Chem. Phys.* **154**, 064109 (2021).
- ⁴²N. H. March, W. H. Young, and S. Sampanthar, *The Many-Body Problem in Quantum Mechanics* (Cambridge University Press, Cambridge, 1967).
- ⁴³D. J. Thouless, *The Quantum Mechanics of Many-Body Systems*, 2nd ed. (Dover, New York, 1990).
- ⁴⁴R. D. Mattuck, *A Guide to Feynman Diagrams in the Many-Body Problem* (Dover, New York, 1992).
- ⁴⁵A. L. Fetter and J. D. Walecka, *Quantum Theory of Many-Particle Systems* (Dover, New York, 2003).
- ⁴⁶T. Matsubara, *Prog. Theor. Phys.* **14**, 351 (1955).
- ⁴⁷C. Bloch and C. De Dominicis, *Nucl. Phys.* **7**, 459 (1958).
- ⁴⁸W. Kohn and J. M. Luttinger, *Phys. Rev.* **118**, 41 (1960).
- ⁴⁹J. M. Luttinger and J. C. Ward, *Phys. Rev.* **118**, 1417 (1960).
- ⁵⁰R. Balian, C. Bloch, and C. De Dominicis, *Nucl. Phys.* **25**, 529 (1961).
- ⁵¹C. Bloch, in *Studies in Statistical Mechanics*, edited by J. De Boer and G. E. Uhlenbeck (North Holland, Amsterdam, 1965) pp. 3–211.
- ⁵²R. Santra and J. Schirmer, *Chem. Phys.* **482**, 355 (2017).
- ⁵³P. K. Jha and S. Hirata, *Annu. Rep. Comput. Chem.* **15**, 3 (2019).
- ⁵⁴S. Hirata and P. K. Jha, *Annu. Rep. Comput. Chem.* **15**, 17 (2019).
- ⁵⁵S. Hirata and P. K. Jha, *J. Chem. Phys.* **153**, 014103 (2020).
- ⁵⁶S. Hirata, *Phys. Rev. A* **103**, 012223 (2021).
- ⁵⁷Z. Kou and S. Hirata, *Theor. Chem. Acc.* **133**, 1487 (2014).
- ⁵⁸N. D. Mermin, *Ann. Phys.* **21**, 99 (1963).
- ⁵⁹S. Hirata, A. E. Doran, P. J. Knowles, and J. V. Ortiz, *J. Chem. Phys.* **147**, 044108 (2017).
- ⁶⁰J. C. Pain, *J. Phys. B: At. Mol. Opt.* **44**, 145001 (2011).
- ⁶¹J. O. Hirschfelder and P. R. Certain, *J. Chem. Phys.* **60**, 1118 (1974).
- ⁶²P. K. Jha and S. Hirata, *Phys. Rev. E* **101**, 022106 (2020).
- ⁶³I. Shavitt and R. J. Bartlett, *Many-Body Methods in Chemistry and Physics* (Cambridge University Press, Cambridge, 2009).
- ⁶⁴S. Hirata, *Theor. Chem. Acc.* **129**, 727 (2011).
- ⁶⁵M. Gell-Mann and F. Low, *Phys. Rev.* **84**, 350 (1951).
- ⁶⁶K. A. Brueckner, *Phys. Rev.* **100**, 36 (1955).
- ⁶⁷J. Goldstone, *Proc. Roy. Soc. A (London)* **239**, 267 (1957).
- ⁶⁸N. M. Hugenholtz, *Physica* **23**, 481 (1957).
- ⁶⁹L. M. Frantz and R. L. Mills, *Nucl. Phys.* **15**, 16 (1960).
- ⁷⁰R. Manne, *Int. J. Quantum Chem. Symp.* **11**, 175 (1977).
- ⁷¹F. E. Harris, H. J. Monkhorst, and D. L. Freeman, *Algebraic and Diagrammatic Methods in Many-Fermion Theory* (Oxford University Press, Oxford, 1992).
- ⁷²C. Møller and M. S. Plesset, *Phys. Rev.* **46**, 618 (1934).
- ⁷³D. J. Klein, *J. Chem. Phys.* **61**, 786 (1974).
- ⁷⁴A. Szabo and N. S. Ostlund, *Modern Quantum Chemistry* (MacMillan, New York, 1982).
- ⁷⁵S. Hirata, M. R. Hermes, J. Simons, and J. V. Ortiz, *J. Chem. Theory Comput.* **11**, 1595 (2015).
- ⁷⁶S. Hirata, *J. Phys. Chem. A* **107**, 9887 (2003).
- ⁷⁷R. J. Bartlett and J. Noga, *Chem. Phys. Lett.* **150**, 29 (1988).
- ⁷⁸P. J. Knowles, K. Somasundram, N. C. Handy, and K. Hirao, *Chem. Phys. Lett.* **113**, 8 (1985).
- ⁷⁹S. Hirata and R. J. Bartlett, *Chem. Phys. Lett.* **321**, 216 (2000).
- ⁸⁰M. Kállay and P. R. Surján, *J. Chem. Phys.* **113**, 1359 (2000).
- ⁸¹J. Olsen, *J. Chem. Phys.* **113**, 7140 (2000).
- ⁸²S. Hirata, M. Nooijen, and R. J. Bartlett, *Chem. Phys. Lett.* **326**, 255 (2000).
- ⁸³S. Hirata, M. Nooijen, and R. J. Bartlett, *Chem. Phys. Lett.* **328**, 459 (2000).
- ⁸⁴T. Shimazaki and S. Hirata, *Int. J. Quantum Chem.* **109**, 2953 (2009).
- ⁸⁵S. Hirata and T. Shimazaki, *Phys. Rev. B* **80**, 085118 (2009).
- ⁸⁶Y.-y. Ohnishi and S. Hirata, *J. Chem. Phys.* **133**, 034106 (2010).
- ⁸⁷Y.-y. Ohnishi and S. Hirata, *J. Chem. Phys.* **135**, 094108 (2011).
- ⁸⁸S. Y. Willow, K. S. Kim, and S. Hirata, *Phys. Rev. B* **90**, 201110(R) (2014).
- ⁸⁹X. He, S. Ryu, and S. Hirata, *J. Chem. Phys.* **140**, 024702 (2014).
- ⁹⁰M. R. Hermes and S. Hirata, *J. Chem. Phys.* **143**, 102818 (2015).
- ⁹¹M. N. Saha, *Philos. Mag.* **40**, 472 (1920).
- ⁹²M. N. Saha, *Proc. Roy. Soc. (London) A* **99**, 135 (1921).
- ⁹³E. J. Brändas and R. J. Bartlett, *Chem. Phys. Lett.* **8**, 153 (1971).
- ⁹⁴C. M. Bender and S. A. Orszag, *Advanced Mathematical Methods for Scientist and Engineers I: Asymptotic Methods and Perturbation Theory* (McGraw-Hill, New York, 1978).
- ⁹⁵W. D. Laidig, G. Fitzgerald, and R. J. Bartlett, *Chem. Phys. Lett.* **113**, 151 (1985).
- ⁹⁶J. Olsen, O. Christiansen, H. Koch, and P. Jørgensen, *J. Chem. Phys.* **105**, 5082 (1996).
- ⁹⁷R. J. Bartlett, *Annu. Rev. Phys. Chem.* **32**, 359 (1981).
- ⁹⁸S. Hirata, X. He, M. R. Hermes, and S. Y. Willow, *J. Phys. Chem. A* **118**, 655 (2014).
- ⁹⁹S. Hirata and I. Grabowski, *Theor. Chem. Acc.* **133**, 1440 (2014).
- ¹⁰⁰S. Y. Willow, K. S. Kim, and S. Hirata, *J. Chem. Phys.* **137**, 204122 (2012).
- ¹⁰¹S. Y. Willow, K. S. Kim, and S. Hirata, *J. Chem. Phys.* **138**, 164111 (2013).
- ¹⁰²S. Y. Willow, M. R. Hermes, K. S. Kim, and S. Hirata, *J. Chem. Theory Comput.* **9**, 4396 (2013).
- ¹⁰³S. Y. Willow and S. Hirata, *J. Chem. Phys.* **140**, 024111 (2014).
- ¹⁰⁴S. Y. Willow, K. S. Kim, and S. Hirata, *Phys. Rev. B* **90**, 201110 (2014).
- ¹⁰⁵S. Y. Willow, J. Zhang, E. F. Valeev, and S. Hirata, *J. Chem. Phys.* **140**, 031101 (2014).
- ¹⁰⁶A. E. Doran and S. Hirata, *J. Chem. Theory Comput.* **12**, 4821 (2016).
- ¹⁰⁷C. M. Johnson, A. E. Doran, J. Zhang, E. F. Valeev, and S. Hirata, *J. Chem. Phys.* **145**, 154115 (2016).
- ¹⁰⁸C. M. Johnson, A. E. Doran, S. L. Ten-no, and S. Hirata, *J. Chem. Phys.* **149**, 174112 (2018).
- ¹⁰⁹A. E. Doran and S. Hirata, *J. Chem. Theory Comput.* **15**, 6097 (2019).
- ¹¹⁰A. E. Doran and S. Hirata, *J. Chem. Phys.* **153**, 094108 (2020).
- ¹¹¹A. E. Doran and S. Hirata, *J. Chem. Phys.* **153**, 104112 (2020).
- ¹¹²A. E. Doran and S. Hirata, *J. Chem. Phys.* **154**, 134114 (2021).
- ¹¹³A. Grüneis, S. Hirata, Y.-y. Ohnishi, and S. Ten-no, *J. Chem. Phys.* **146**, 080901 (2017).
- ¹¹⁴R. C. Kao and L. H. Zetterberg, *Amer. Math. Monthly* **64**, 96 (1957).

Diagrammatic equation for the Fock matrix element F_{pq} :

$$F_{pq} = h_{pq} - \epsilon_p \delta_{pq} + \sum_r \langle pr || qr \rangle f_r^-$$

The diagrammatic representation shows a vertex (black dot) with two external lines labeled p and q . This is equal to the sum of two terms:


- A hole-line diagram (white circle) with two external lines labeled p and q .
- A ring diagram (black circle) with two external lines labeled p and q , and a ring labeled r .

$$\begin{array}{ccccccc}
 & p & p & p & & p & q & q & & p & p & q & & p & p \\
 0 & = & \text{diagram } \mu 1a & + & \text{diagram } \mu 1b & + & \text{diagram } \mu 1c & + & \text{diagram } \mu 1d
 \end{array}$$


The image shows an equation where the left side is a vertical oval labeled '0'. The right side is a sum of four terms, each consisting of a diagram of three circles and a label below it.

- Diagram $\mu 1a$:** Three circles in a horizontal line. The leftmost circle is smaller than the other two. The top and bottom arcs of the leftmost circle are connected to the top and bottom arcs of the middle circle, respectively. The top and bottom arcs of the middle circle are connected to the top and bottom arcs of the rightmost circle, respectively.
- Diagram $\mu 1b$:** Three circles in a horizontal line. The middle circle is shaded black. The top and bottom arcs of the leftmost circle are connected to the top and bottom arcs of the middle circle, respectively. The top and bottom arcs of the middle circle are connected to the top and bottom arcs of the rightmost circle, respectively.
- Diagram $\mu 1c$:** Three circles in a horizontal line. The rightmost circle is shaded black. The top and bottom arcs of the leftmost circle are connected to the top and bottom arcs of the middle circle, respectively. The top and bottom arcs of the middle circle are connected to the top and bottom arcs of the rightmost circle, respectively.
- Diagram $\mu 1d$:** Three circles in a horizontal line. The leftmost circle is shaded black and contains the number '1'. The top and bottom arcs of the leftmost circle are connected to the top and bottom arcs of the middle circle, respectively. The top and bottom arcs of the middle circle are connected to the top and bottom arcs of the rightmost circle, respectively.


$$TS^{(1)} = \overset{p}{\circ} \overset{p}{\circ} \overset{p}{\circ} + \overset{p}{\circ} \overset{q}{\circ} \overset{q}{\circ} + \overset{p}{\circ} \overset{p}{\circ} \overset{q}{\circ} + \overset{p}{\circ} \overset{p}{\circ} \overset{q}{\circ}$$




S1a



S1b



S1c



S1d

$$\Omega^{(2)} = \Omega_{2a} + \Omega_{2b} + \Omega_{2c} + \Omega_{2d} + \Omega_{2e} + \Omega_{2f} + \Omega_{2g} + \Omega_{2h}$$

$\Omega^{(2)}$ is equal to the sum of eight diagrams:

- Ω_{2a} : Two vertices with four external lines labeled p, q, r, s and a wavy loop.
- Ω_{2b} : Two vertices with two external lines labeled p, q and a wavy loop.
- Ω_{2c} : Two vertices with four external lines labeled p, q, r, s and a loop.
- Ω_{2d} : Two vertices with two external lines labeled p, q and a loop.
- Ω_{2e} : Two vertices with two external lines labeled p, p and a loop labeled 1.
- Ω_{2f} : Two vertices with two external lines labeled p, p and a loop labeled 1.
- Ω_{2g} : Two vertices with two external lines labeled p, p and a loop labeled 1.
- Ω_{2h} : A loop with two external lines labeled p, p and a loop labeled 2.

Diagrammatic equation showing the dressed propagator \tilde{F}_{pq} (left) equal to the sum of the bare propagator F_{pq} (middle) and a term involving the self-energy $\mu^{(1)}$ (right).

The diagram on the left shows a fermion line with a self-energy loop (circle with slash) and external momenta q and p .

The diagram in the middle shows a bare fermion line (black dot) with external momenta q and p .

The diagram on the right shows a fermion line with a self-energy loop (circle with '1') and external momenta q and p .

$$\tilde{F}_{pq} = F_{pq} + \mu^{(1)} \delta_{pq}$$

 $\Omega 2A$ $=$  $\Omega 2a$ $+$  $\Omega 2c$

$\Omega_{2B} = \Omega_{2b} + \Omega_{2d} + \Omega_{2e} + \Omega_{2f} + \Omega_{2g}$

The diagrammatic equation shows the decomposition of a loop with two external lines (labeled Ω_{2B}) into five terms:

- Ω_{2b} : A loop with two external lines (labeled p and q) and a wavy line connecting the two vertices.
- Ω_{2d} : A loop with two external lines (labeled p and q) and two vertices.
- Ω_{2e} : A loop with one external line (labeled p) and one vertex (labeled 1).
- Ω_{2f} : A loop with one external line (labeled p) and one vertex (labeled 1).
- Ω_{2g} : A loop with two external lines (labeled p) and two vertices (labeled 1).

$$\Omega^{(2)} = \Omega_{2A} + \Omega_{2B} + \Omega_{2h}$$

The diagram illustrates the decomposition of the second-order correlation function $\Omega^{(2)}$ into three components:

- Ω_{2A} : A diagram with two solid black vertices at the top and bottom. Two curved lines connect the top vertex to the bottom vertex, and a third curved line connects them directly, forming a lens-like shape.
- Ω_{2B} : A diagram with two vertices at the top and bottom, each marked with a diagonal slash. Two curved lines connect the top vertex to the bottom vertex, forming a lens-like shape.
- Ω_{2h} : A diagram showing a circular loop with a double arrow indicating a path. The number '2' is written inside the loop, and a red letter 'p' is written above the loop.

$$\begin{aligned}
0 = & \mu2a \times 2 + \mu2b \times 2 + \mu2c \times 2 + \mu2d \times 2 + \mu2e + \mu2f \\
& + \mu2g + \mu2h + \mu2i + \mu2j + \mu2k + \mu2l + \mu2m
\end{aligned}$$

The image displays 13 Feynman diagrams, labeled $\mu2a$ through $\mu2m$, arranged in two rows. The first row contains $\mu2a$, $\mu2b$, $\mu2c$, $\mu2d$, $\mu2e$, and $\mu2f$. The second row contains $\mu2g$, $\mu2h$, $\mu2i$, $\mu2j$, $\mu2k$, $\mu2l$, and $\mu2m$. Each diagram shows a two-loop structure with vertices (black dots) and internal lines (solid and wavy). External lines are labeled with momenta p , q , r , and s . Diagrams $\mu2a$, $\mu2b$, $\mu2c$, and $\mu2d$ are each multiplied by 2. Diagrams $\mu2e$ and $\mu2f$ are added once. Diagrams $\mu2g$ through $\mu2m$ are added once. The diagrams represent various two-loop topologies, including self-energy loops on vertices and various internal line configurations.

$$\begin{aligned}
 TS^{(2)} = & \text{S2a} + \text{S2b} \times 2 + \text{S2c} \times 2 + \text{S2d} \times 2 + \text{S2e} \times 2 + \text{S2f} \\
 & + \text{S2g} + \text{S2h} + \text{S2i} + \text{S2j} + \text{S2k} + \text{S2l} + \text{S2m} + \text{S2n} + \text{S2o}
 \end{aligned}$$

The diagram illustrates the expansion of $TS^{(2)}$ into 15 terms, labeled S2a through S2o. Each term is represented by a graph with two vertices (top and bottom) and various internal connections and loops.

- S2a:** A graph with two vertices and four directed edges forming two loops. Edges are labeled p, q, r, s in red.
- S2b:** Similar to S2a, but with a wavy line between the vertices and a loop labeled s on the right.
- S2c:** Similar to S2a, but with a loop labeled p on the left and a wavy line between the vertices.
- S2d:** Similar to S2a, but with a loop labeled s on the right and a wavy line between the vertices.
- S2e:** Similar to S2a, but with a loop labeled p on the left and a wavy line between the vertices.
- S2f:** A graph with two vertices and two directed edges forming a loop. Edges are labeled p, q in red.
- S2g:** Similar to S2f, but with a wavy line between the vertices and a loop labeled q on the right.
- S2h:** Similar to S2f, but with a loop labeled p on the left and a wavy line between the vertices.
- S2i:** Similar to S2f, but with a wavy line between the vertices and two loops labeled r at the top vertex.
- S2j:** Similar to S2f, but with a wavy line between the vertices and two loops labeled r at the bottom vertex.
- S2k:** Similar to S2f, but with a loop labeled q on the right.
- S2l:** Similar to S2f, but with a loop labeled p on the left.
- S2m:** Similar to S2f, but with a wavy line between the vertices and two loops labeled r at the top vertex.
- S2n:** Similar to S2f, but with a wavy line between the vertices and two loops labeled r at the bottom vertex.
- S2o:** A graph with two vertices and two directed edges forming a loop, with a circled number 2 and two loops labeled p on the left.

$$\Omega^{(3)} = \Omega_{3A} + \Omega_{3B} + \Omega_{3C} + \Omega_{3D} + \Omega_{3E} + \Omega_{3F} + \Omega_{3G} + \Omega_{3H} + \Omega_{3m} + \Omega_{3n} + \Omega_{3o}$$

$\Omega^{(3)}$ is equal to the sum of the following diagrams:

- Ω_{3A} : Three vertices (black dots) in a vertical line. Two external lines connect the top and bottom vertices, and two internal lines connect the top and bottom vertices through the middle vertex.
- Ω_{3B} : Three vertices (black dots) in a vertical line. Two external lines connect the top and bottom vertices, and two internal lines connect the top and bottom vertices through the middle vertex, with a different internal structure than Ω_{3A} .
- Ω_{3C} : Three vertices (black dots) in a vertical line. Two external lines connect the top and bottom vertices, and two internal lines connect the top and bottom vertices through the middle vertex.
- Ω_{3D} : Three vertices (black dots) in a vertical line. Two external lines connect the top and bottom vertices, and two internal lines connect the top and bottom vertices through the middle vertex.
- Ω_{3E} : Three vertices (black dots) in a vertical line. Two external lines connect the top and bottom vertices, and two internal lines connect the top and bottom vertices through the middle vertex.
- Ω_{3F} : Three vertices (black dots) in a vertical line. Two external lines connect the top and bottom vertices, and two internal lines connect the top and bottom vertices through the middle vertex.
- Ω_{3G} : Three vertices (black dots) in a vertical line. Two external lines connect the top and bottom vertices, and two internal lines connect the top and bottom vertices through the middle vertex.
- Ω_{3H} : Three vertices (black dots) in a vertical line. Two external lines connect the top and bottom vertices, and two internal lines connect the top and bottom vertices through the middle vertex.
- Ω_{3m} : Two vertices (circles labeled 2) in a vertical line. Two external lines connect the top and bottom vertices, and two internal lines connect the top and bottom vertices through the middle vertex. Red arrows and momentum labels p are shown on the external lines.
- Ω_{3n} : Two vertices (circles labeled 2) in a vertical line. Two external lines connect the top and bottom vertices, and two internal lines connect the top and bottom vertices through the middle vertex. Red arrows and momentum labels p are shown on the external lines.
- Ω_{3o} : Three vertices (circles labeled 3) in a vertical line. Two external lines connect the top and bottom vertices, and two internal lines connect the top and bottom vertices through the middle vertex. Red arrows and momentum labels p are shown on the external lines.

Diagrammatic expansion of $\Omega 3A$ into $\Omega 3a1$ through $\Omega 3a5$. The diagram $\Omega 3A$ is a vertical oval with three black dots (top, middle, bottom) and two curved lines connecting them. It is equal to the sum of five diagrams, each with a coefficient:

$\Omega 3A = p \Omega 3a1 + (s+p) \Omega 3a2 + (s+p) \Omega 3a3 + (s+p) \Omega 3a4 + (s+p) \Omega 3a5$

The diagrams $\Omega 3a1$ through $\Omega 3a5$ are variations of $\Omega 3A$ with internal lines labeled q , r , t , and u . In $\Omega 3a1$, q and r are wavy lines, while t and u are straight lines with arrows. In $\Omega 3a2$, q and r are straight lines with arrows, while t and u are wavy lines. In $\Omega 3a3$, q and r are straight lines with arrows, while t and u are straight lines with arrows. In $\Omega 3a4$, q and r are wavy lines, while t and u are straight lines with arrows. In $\Omega 3a5$, q and r are straight lines with arrows, while t and u are straight lines with arrows.

Diagrammatic expansion of $\Omega 3b1$ through $\Omega 3b5$. Each diagram is a variation of $\Omega 3A$ with internal lines labeled q , r , t , and u . The expansion is:

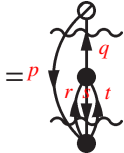
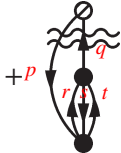
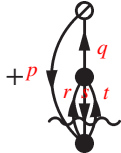
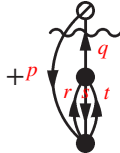
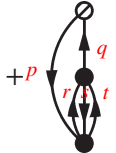
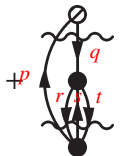
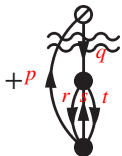
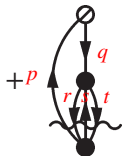
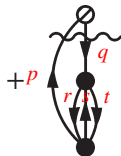
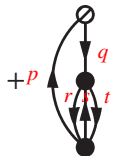
$+p \Omega 3b1 + (s+p) \Omega 3b2 + (s+p) \Omega 3b3 + (s+p) \Omega 3b4 + (s+p) \Omega 3b5$

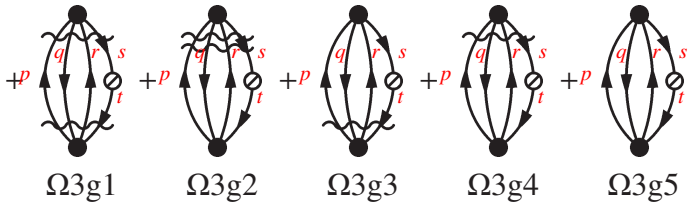
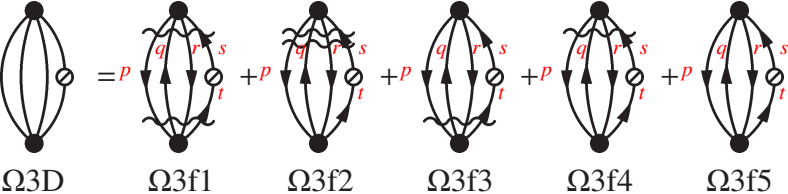
The diagrams $\Omega 3b1$ through $\Omega 3b5$ are variations of $\Omega 3A$ with internal lines labeled q , r , t , and u . In $\Omega 3b1$, q and r are straight lines with arrows, while t and u are wavy lines. In $\Omega 3b2$, q and r are wavy lines, while t and u are straight lines with arrows. In $\Omega 3b3$, q and r are straight lines with arrows, while t and u are straight lines with arrows. In $\Omega 3b4$, q and r are wavy lines, while t and u are straight lines with arrows. In $\Omega 3b5$, q and r are straight lines with arrows, while t and u are straight lines with arrows.

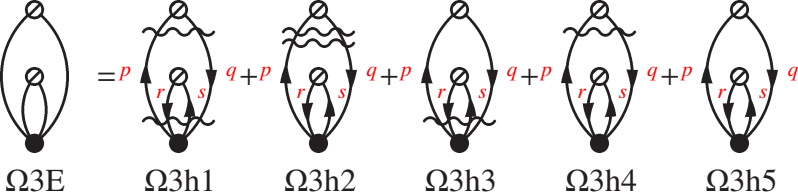
Diagrammatic expansion of $\Omega 3c1$ through $\Omega 3c5$. Each diagram is a variation of $\Omega 3A$ with internal lines labeled q , r , t , and u . The expansion is:

$+p \Omega 3c1 + (s+p) \Omega 3c2 + (s+p) \Omega 3c3 + (s+p) \Omega 3c4 + (s+p) \Omega 3c5$

The diagrams $\Omega 3c1$ through $\Omega 3c5$ are variations of $\Omega 3A$ with internal lines labeled q , r , t , and u . In $\Omega 3c1$, q and r are straight lines with arrows, while t and u are wavy lines. In $\Omega 3c2$, q and r are wavy lines, while t and u are straight lines with arrows. In $\Omega 3c3$, q and r are straight lines with arrows, while t and u are straight lines with arrows. In $\Omega 3c4$, q and r are wavy lines, while t and u are straight lines with arrows. In $\Omega 3c5$, q and r are straight lines with arrows, while t and u are straight lines with arrows.


 $\Omega 3B$

 $\Omega 3d1$

 $\Omega 3d2$

 $\Omega 3d3$

 $\Omega 3d4$

 $\Omega 3d5$

 $\Omega 3e1$

 $\Omega 3e2$

 $\Omega 3e3$

 $\Omega 3e4$

 $\Omega 3e5$





The diagram illustrates the decomposition of a gluon self-energy diagram, labeled Ω_{3G} , into five ghost diagrams, labeled Ω_{3i1} through Ω_{3i5} . The gluon self-energy diagram consists of a central black vertex connected to two external gluon lines (represented by ovals with diagonal slashes). The ghost diagrams are similar, but the internal lines are wavy, representing ghost loops. The diagrams are summed together, as indicated by the equals sign and plus signs.

$\Omega_{3G} = \Omega_{3i1} + \Omega_{3i2} + \Omega_{3i3} + \Omega_{3i4} + \Omega_{3i5}$

The diagrams are labeled Ω_{3G} , Ω_{3i1} , Ω_{3i2} , Ω_{3i3} , Ω_{3i4} , and Ω_{3i5} from left to right. The ghost diagrams also feature external momenta labeled p , q , r , and s in red.

$\Omega_{3H} = \Omega_{3j1} + \Omega_{3j2} + \Omega_{3j3} + \Omega_{3j4} + \Omega_{3j5}$

Ω_{3H} Ω_{3j1} Ω_{3j2} Ω_{3j3} Ω_{3j4} Ω_{3j5}

$+ \Omega_{3k1} + \Omega_{3k2} + \Omega_{3k3} + \Omega_{3k4} + \Omega_{3k5}$

Ω_{3k1} Ω_{3k2} Ω_{3k3} Ω_{3k4} Ω_{3k5}

$$\langle E^{(4)} \rangle = \text{Diagram 1} + \text{Diagram 2} + \text{Diagram 3} + \text{Diagram 4} + \text{Diagram 5}$$

The diagrams represent the following terms:

$$\langle VRVRVRV \rangle - \langle VRVR \langle V \rangle RV \rangle - \langle VR \langle V \rangle RVRV \rangle + \langle VR \langle V \rangle R \langle V \rangle RV \rangle - \langle VR \langle VRV \rangle RV \rangle$$

